



PERGAMON

Progress in Surface Science 65 (2000) 151–256

www.elsevier.com/locate/progsurf

Progress in
SURFACE
SCIENCE

Structure and growth of self-assembling monolayers

Frank Schreiber^{a,b,*}

^a *Institut für Theoretische und Angewandte Physik, Universität Stuttgart, Pfaffenwaldring 57, 70550 Stuttgart, Germany*

^b *Max-Planck-Institut für Metallforschung, Heisenbergstr. 1, 70569 Stuttgart, Germany*

Abstract

The structural phases and the growth of self-assembled monolayers (SAMs) are reviewed from a surface science perspective, with emphasis on simple model systems. The concept of self-assembly is explained, and different self-assembling materials are briefly discussed. A summary of the techniques used for the study of SAMs is given. Different general scenarios for structures obtained by self-assembly are described. Thiols on Au(1 1 1) surfaces are used as an archetypal system to investigate in detail the structural phase diagram as a function of temperature and coverage, the specific structural features on a molecular level, and the effect of changes of the molecular backbone and the end group on the structure of the SAM. Temperature effects including phase transitions are discussed. Concepts for the preparation of more complex structures such as multi-component SAMs, laterally structured SAMs, and heterostructures, also with inorganic materials, are outlined. The growth and ways to control it are discussed in detail. Solution and gas phase deposition and the impact of various parameters such as temperature, concentration (in solution) or partial pressure (in the gas phase) are described. The kinetics and the energetics of self-assembly are analyzed. Several more complex issues of the film formation process including non-equilibrium issues are discussed. Some general conclusions are drawn concerning the impact of various molecular features on the growth behavior and concerning the relationship between growth and structural phase diagram. Finally, the potential of self-assembly as a route for the preparation of monolayers with pre-designed properties and SAMs as building blocks in heterostructures as well as application strategies are discussed. © 2000 Elsevier Science Ltd. All rights reserved.

Keywords: Self-assembled monolayer; Monolayer structure; Phase transitions; Growth kinetics; Adsorption; Physisorption; Chemisorption; Organics; Thiols; Silanes

* Fax: +49-711-689-1902.

E-mail address: fschreib@dxray.mpi-stuttgart.mpg.de (F. Schreiber).

Nomenclature

AES	Auger electron spectroscopy
AFM	atomic force microscopy
DW	Debye–Waller
ESR	electron spin resonance
GIXD	grazing-incidence X-ray diffraction
HAR	helium atom reflectivity
HREELS	high-resolution electron-energy-loss spectroscopy
IR	infrared
IS	intermediate structures
LB	Langmuir–Blodgett
LEAD	low-energy atom diffraction
LEED	low-energy electron diffraction
ML	monolayer
MMB	4-methyl-4'-mercaptobiphenyl
NEXAFS	near-edge X-ray absorption fine structure (spectroscopy)
NMR	nuclear magnetic resonance
NN	next neighbor
NNN	next-nearest neighbor
OEG	oligo(ethylene glycol)
OMBD	organic molecular beam deposition
OMBE	organic molecular beam epitaxy
OPA	octadecylphosphonic acid
OTS	octadecyltrichlorosilane
PTCDA	3,4,9,10-perylenetetracarboxylic dianhydride
QCM	quartz crystal microbalance
SAM	self-assembled monolayer
SERS	surface-enhanced Raman scattering
SFG	sum frequency generation
SHG	second harmonic generation
SPS	surface plasmon spectroscopy
STM	scanning tunneling microscopy
TFAA	trifluoroacetic anhydride
THF	tetrahydrofuran
TPD	thermally programmed desorption (spectroscopy)
UHV	ultrahigh vacuum
XPS	X-ray photoelectron spectroscopy
XR	X-ray reflectivity
XSW	X-ray standing waves
μCP	micro-contact printing

Contents

1. Introduction	153
1.1. Organic thin films	153
1.2. Concept of self-assembly	156
1.3. Scope of review	157
2. Techniques for study of self-assembled monolayers.	158
2.1. Sample preparation	158
2.2. Characterization techniques	160
3. Structure	162
3.1. Thiols on Au(1 1 1)	164
3.2. An overview of various self-assembling systems and their structures	183
3.3. Temperature-related issues: structural phase transitions, thermal stability, and desorption	189
3.4. More complex structures: lateral structuring, multi-component structures, surface reactions, and heterostructures	197
4. Growth	203
4.1. Growth from solution	204
4.2. Growth from gas phase	213
4.3. Physisorption and chemisorption: energetics and kinetics	227
4.4. Discussion of growth behavior	237
5. Discussion	241
5.1. Relationship of molecular features, structures, and growth	241
5.2. Theoretical models and simulations	243
5.3. Applications of SAMs	245
6. Conclusion	247
Acknowledgements	248
References	248

1. Introduction

1.1. Organic thin films

For a multitude of reasons, organic thin films have attracted considerable attention over the last years, although the subject has fairly old roots. More than 200 years ago, Franklin observed the calming influence of oil on water surfaces [1]. In the 19th century, Pockels prepared monolayers at the air–water interface [2–5], followed by the works of Rayleigh [6], Hardy [7], Devaux [8], and others. Later, monolayers of amphiphilic molecules on the water surface were named after Langmuir [9,10].

On *solid* substrates, Blodgett did the first study on the deposition of long-chain carboxylic acids [11,12]. Around that time, amphiphilic monolayers were already used to control the wetting behavior of metal condenser plates in steam engines [13–15]. Systematic research on systems related to self-assembled monolayers (SAMs) was performed later by Zisman [16] and Blackman and Dewar [17]. For further account of the history of organic thin films, we refer to [18,19].

In these earlier studies, in which structures and processes on the molecular level remained unexplored due to the lack of appropriate tools, much of the interest centered around macroscopic properties such as surface tension and wetting properties. With the microscopic tools available today, one can attempt to correlate macroscopic to microscopic properties, e.g., the change in surface energy to a change in molecular structure. In fact, the field of wetting and surface modification has undergone a revival, and the great potential of organic thin films for wetting control is recognized [20–22].

In addition, these materials often exhibit optical, electrical, optoelectrical, mechanical, chemical, or other properties interesting from the applications point of view, which are not accessible with inorganic materials. Besides applications in “classical” areas of technology, organic thin films can play an important role in interfacing bio-technological devices.

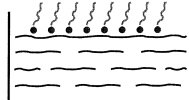
One deeper reason why organic materials are attractive in such diverse fields is probably what might be called the “modular concept of organic chemistry”, i.e., the tunability of the properties of these materials by selectively modifying specific functional groups while leaving the rest of the molecule unchanged. A good example for this is the change from a hydrophobic to a hydrophilic surface by changing just the endgroup of alkylthiol-based monolayers from $-\text{CH}_3$ to $-\text{OH}$.

In view of the several million organic compounds known, and a correspondingly wide variety of molecular properties, it is not surprising that there are different routes for the preparation of organic thin films. For thin polymer films, e.g., spin-coating is a very popular preparation method [23]. For the group of crystalline films of relatively small molecules, Fig. 1 schematically shows the most common methods.

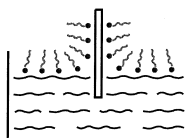
1. Langmuir films consist of amphiphilic molecules spread on a liquid surface like water [18,24]. The hydrophilic headgroup has an affinity to the water while the hydrophobic endgroup sticks out on the other side.
2. Langmuir–Blodgett (LB) films are prepared by transferring Langmuir films onto a solid substrate [19]. Multilayers are prepared by repeated (periodic) dipping of the substrate in appropriate solutions.
3. *Organic molecular beam deposition* (OMBD) or *organic molecular beam epitaxy* (OMBE) is very similar to evaporation techniques in *ultrahigh vacuum* (UHV) for inorganic materials. For example, aromatic molecules such as perylene-derivatives, which form molecular crystals in the bulk, are typical systems for OMBD [25,26]. In OMBD, similar to inorganic MBE, not only the two-dimensional epitaxy of monolayers, but also the behavior along the normal, when thicker films are grown, is an important issue [25,27].

Preparation of Organic Layers

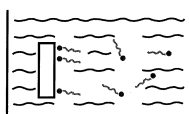
- Langmuir Films
amphiphilic molecules
at liquid/gas interface



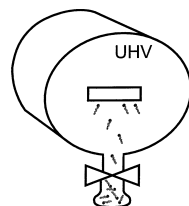
- Langmuir-Blodgett Films
Langmuir films
transferred onto solid substrate



- Self-Assembled Monolayers
grown from solution



- Self-Assembled Monolayers
grown from vapor



- Organic Molecular Beam Epitaxy
similar to inorganic MBE

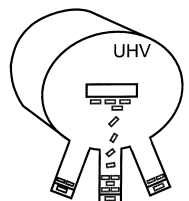


Fig. 1. Overview of various preparation routes of crystalline organic thin films. Langmuir films are formed by spreading amphiphilic molecules on liquid surface. LB films are prepared by transferring Langmuir films onto a solid substrate. OMBD or OMBE uses evaporation techniques in UHV, similar to MBE growth of inorganic materials. Growth of SAMs, which is driven by specific affinity of headgroup to substrate, can be done either in solution or in UHV.

4. SAMs grown from solution or from the gas-phase, represent a further class of organic thin films. The defining feature is the chemisorption (or, generally, strong interaction) of the headgroup with a specific affinity to the substrate (Fig. 2). Since SAMs are the subject of this review, the concept of self-assembly is discussed in more detail in the next section.

We should note that the boundaries between some of these techniques are not rigid. For example, some systems prepared from the gas phase, particularly in the

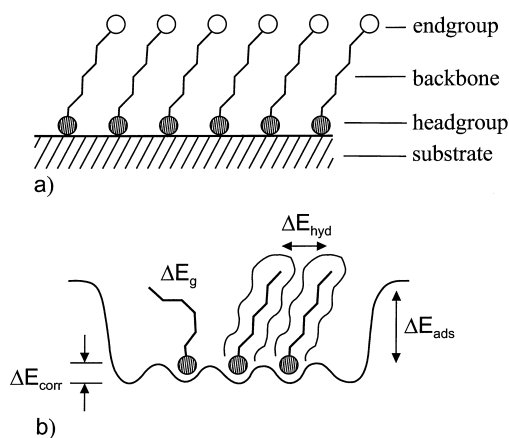


Fig. 2. (a) Schematic of SAM. Shaded circle indicates chemisorbing headgroup and open circle endgroup, which can be chosen from variety of chemical functionalities. (b) Schematic of different energies. ΔE_{ads} stands for adsorption energy, ΔE_{corr} corrugation of substrate potential experienced by molecule, ΔE_{hyd} van der Waals interaction of (hydrocarbon) tails, and ΔE_{g} energy of gauche defect (or, generally, deviation from fully stretched backbone).

monolayer regime, in principle might be considered both as OMBE-systems and as SAMs. Also, one might view the distinction between Langmuir layers and SAMs as not absolutely sharp. Langmuir layers are on liquid surfaces and are typically also weakly bound to the substrate. SAMs as we define them here are on solid substrates and chemisorbed, i.e., strongly bound. An interesting intermediate case would be molecules on a liquid substrate with strong interaction, such as thiols on liquid Hg [28]. Once the temperature is lowered and the substrate frozen, this might be considered as a transition from a Langmuir layer to a SAM.

1.2. Concept of self-assembly

Self-assembly, in a general sense, might be defined as the spontaneous formation of complex hierarchical structures from pre-designed building blocks, typically involving multiple energy scales and multiple degrees of freedom. Self-assembly is also a very general principle in nature, as seen in the formation of, e.g., membranes from lipid molecules, or the living cell as probably the most important paradigm.

Self-assembled monolayers are ordered molecular assemblies that are formed spontaneously by the adsorption of a surfactant with a specific affinity of its headgroup to a substrate. Fig. 2 shows a schematic, including the constituents of a SAM-molecule (headgroup, chain or backbone, endgroup). We will use the headgroup-substrate “pair” to define the individual SAM-systems.

After the historical predecessors, mentioned above, a strong activity in the area of SAMs and progress in the understanding on a microscopic level started in the 1980s.

Around that time, also important experimental tools like scanning probe microscopies and grazing-incidence X-ray diffraction were developed. Thiols (R-SH, where R denotes the rest of the molecule) on Au [29] and silane-based systems on SiO₂ [30] were identified as model systems. The general interest in organic thin films was one reason for these activities. In addition, SAMs are particularly attractive for the following reasons:

1. the ease of preparation;
2. the tunability of surface properties via modification of molecular structure and functions;
3. the use of SAMs as building blocks in more complex structures, e.g., for “docking” additional layers to a surface;
4. the possibility of lateral structuring in the nanometer regime;
5. the applications made possible by these features.

Several fundamental issues in the context of growth and structure require investigation, the understanding of which will also promote the design of new applications. The following questions may serve to illustrate this:

- Which types of structures and phases are formed and which parameters characterize the order?
- In which way does the order appear and disappear (e.g., as a function of coverage or temperature) and what is the nature of the phase transitions?
- In which way do the various degrees of freedom and the different constituents of the molecule (headgroup, chain or backbone, endgroup) have an impact on the growth and the structure?
- What are the driving forces of self-assembly? What determines the growth kinetics and the growth regimes? What are the “internal” (e.g., chain length or substrate orientation) and the “external” (e.g., temperature) control parameters?

1.3. Scope of review

This review is written from a surface science perspective, with the focus on the fundamental principles governing the growth and the structures of self-assembling monolayers. While this naturally puts the emphasis on chemically simple compounds, we outline the rich opportunities in the area of heterostructures using SAMs as building blocks, lateral patterning, chemical functionalization, and some technological applications. Some of the earlier work has already been reviewed [19,31–36], in some cases from a more chemical or technique-oriented perspective.

The paper is organized as follows. In Section 2, the specific techniques employed in the study of self-assembly are briefly reviewed.

Section 3 deals with the structure of SAMs. Its goal is two-fold. One is to provide an overview of various self-assembling systems, attempting to cover the breadth of the field (Section 3.2). It is clear that in this rapidly growing field this goal cannot be reached to full satisfaction, and we apologize for omissions. We try to make sure that every group is quoted at least once, so that the interested reader might obtain a more complete list of references on a given subject by computer search. The second goal is to illustrate typical scenarios and mechanisms by investigating a few systems in more

detail. Particular emphasis is put on the archetypal case of alkanethiols and related compounds on Au(1 1 1) (Section 3.1). Temperature-related issues are the subject of Section 3.3. In Section 3.4, more complex systems such as multi-component SAMs and vertical heterostructures are briefly reviewed, as well as lateral structuring and surface reactions.

Section 4 deals with the growth of SAMs, its energetics, and its kinetics. The role of various growth parameters, the differences and similarities of solution and gas phase deposition as well as ways to control the growth are discussed.

A general discussion is given in Section 5. We try to outline some general principles governing the structure and the growth behavior of SAMs and address the mutual relationship of growth and phase diagram. We also discuss the theoretical approaches existing so far. Finally, we give a brief overview of the applications and conclude with an outlook and some open issues.

2. Techniques for study of self-assembled monolayers

In this section, we will briefly explain the main experimental ingredients needed for the preparation and analysis of SAMs, while keeping the number of references limited. Specific recipes and problems related to the growth are discussed in more detail in Section 4. We also try to give an overview of the different classes of characterization techniques.

2.1. Sample preparation

As indicated in Section 1.2, the general concept of self-assembly, which exploits the preferential, strong binding of one functional group of the molecule to the substrate (e.g., S–Au), allows, in principle, the preparation both from solution and from the gas phase (see Fig. 1), except for those systems, where a precursor reaction is required in the solution. Possible differences between the two preparation routes regarding, e.g., the kinetics will be discussed in Section 4.4. In both cases, of course, great care has to be taken to achieve clean and reproducible conditions, particularly for the growth studies.

2.1.1. Substrates

Besides the chemical nature of the substrate, the choice of which depends on the monolayer to be deposited, the crystalline state and quality need to be considered. Metal single crystals are very frequently used in traditional surface science, and they constitute well-defined substrates. Moreover, they offer the possibility to freely choose the crystallographic orientation.

Particularly for thiols on Au(1 1 1), in many cases evaporated Au films have been employed. However, while these predominantly exhibit (1 1 1)-oriented terraces, as this is the lowest-energy surface of Au, the crystalline quality, the number of non-(1 1 1)-oriented crystallites, the density of defects, etc. can vary substantially depending on the evaporation conditions, the thermal treatment and other

parameters. For structural studies with local probes such as *scanning tunneling microscopy* (STM) this may not be a problem, but it can affect the comparability of the kinetic parameters of the SAM growth, as determined with spatially averaging techniques.

For the cleaning of metal surfaces, the classical recipe employs ion sputtering and annealing. This is typically done in UHV-based studies with single crystals. For Au(111), the clean surface is not only identified by the lack of surface contaminations, but also by the well-known ($22 \times \sqrt{3}$) reconstruction [37]. Alternatively, Au surfaces can also be cleaned by flame annealing.

A very popular substrate for silane-based SAMs is silicon with its native oxide layer. In this case, the comparability of the structure and morphology is less a problem, since the native oxide layer is non-crystalline but usually very smooth. As with all other systems, however, a specific cleaning procedure has to be applied. For the removal of possible organic contaminants from the substrate as well as the glassware used for solution deposition, “piranha solution” (7:3 concentrated H_2SO_4 /30% H_2O_2) is frequently employed.

We should note that for some systems not only surface cleaning in a conventional sense, but a specific treatment is required. An example for this is the preparation of SAMs starting with H-terminated Si surfaces [38] (see Section 3.2.4).

2.1.2. Solution deposition

The ease of preparation and the low costs of solution deposition are one important reason for the popularity of SAMs. Provided that the substrate has been properly cleaned, in principle, it simply has to be dipped into the corresponding solution for a certain period of time, and the monolayer will assemble (see Fig. 1 and Section 4.1). A popular example is alkanethiols in ethanolic solution with concentrations in the micromolar to millimolar range.

Of course, it is very important to carefully control the cleanliness of the solution, which can be difficult. In the case of silane-based systems, e.g., the water content turned out to be crucial for the proper preparation of the SAM (see Section 4.1.2). Proper outgassing of the solution is another important issue. Moreover, after completion of the SAM an appropriate rinsing procedure has to be followed.

2.1.3. Gas phase deposition

The principle of gas phase deposition is also very simple. If the substrate is located in a generic surface science UHV chamber, which allows for cleaning of the surface by, e.g., ion sputtering and annealing as done for metal single crystals, only one additional port is needed for attaching a valve, through which the molecules can be dosed with a controllable flux from a little container or glass bulb (Fig. 1). This method has been employed successfully in, e.g., [39–44]. Besides work in UHV it has also been shown that alkanethiols can be deposited using a nitrogen stream [45].

For molecules with a low vapor pressure the container can be heated moderately. We should note that the exact calibration of the partial pressure, P , and, therefore,

the impingement rate on the surface of, e.g., alkanethiols, requires some care due to a nontrivial sensitivity factor of ionization gauges for many-atomic molecules (see Eq. (4.14)) and also the knowledge of the pumping conditions.

While employing a UHV chamber generally is more expensive than growth from solution, the advantages of gas phase deposition in a UHV chamber are the clean environment and the availability of a large number of in situ analytical surface science tools (see below).

2.2. Characterization techniques

Many different thin film characterization techniques have been applied to SAMs. While it is not our goal to review all of these, we try to provide an overview of those techniques, which are more frequently used for investigations of the structure and the growth of SAMs as reviewed in the next sections. More specific information can be found in the technical references given below and in textbooks [19,32,46].

Here we shall organize the techniques in different categories according to their spatial averaging behavior, i.e., local vs. non-local probes. We shall also distinguish direct structural and spectroscopic probes. Generally, due to the sensitivity to different features of the structure and the different averaging behavior, in order to obtain a complete picture the use of several complementary methods is desirable.

2.2.1. Microscopy-based techniques

The obvious strength of STM [36] and *atomic force microscopy* (AFM) [32] is to provide a direct image of the structure, including defects or mixtures of different structures during growth, which has made them irreplaceable tools. At the same time, since they provide local information, it has to be assured that the images are actually representative of the entire surface. Whereas STM usually offers better spatial resolution than AFM, it should be noted that reasonable tunneling currents through (standing-up) hydrocarbon chains can only be obtained for about $n \leq 12$.

2.2.2. Diffraction-based techniques

Low-energy electron diffraction (LEED) [46,47], *grazing-incidence X-ray diffraction* (GIXD) [48–50], and *low-energy atom diffraction* (LEAD) [51,52] have been used for diffraction from the 2D structure of SAMs. Among these techniques, LEED is the oldest. With the screen acting as an area detector, conventional LEED has the advantage of displaying the entire reciprocal lattice (projected in 2D) at once, but the disadvantage of limited resolution (about 100 Å transfer width). LEAD, which provides also only limited resolution, is the most surface-specific and the most gentle probe. GIXD has the best resolution. Compared to LEED and LEAD, an important advantage of X-ray (and neutron) diffraction is the applicability of a simple scattering theory (“kinematic theory”, i.e., negligence of multiple scattering), which allows a very direct analysis of GIXD signals.

Information along the surface normal (e.g., layer thickness, tilt structure) can be obtained using X-rays with so-called *rodscans*, where the momentum transfer along the surface normal, q_z , is varied (Section 3.1).

If the in-plane momentum transfer, $q_{||}$, is zero and the total momentum transfer, q , is entirely along the surface normal ($q = q_z$), this is called specular reflectivity. *X-ray reflectivity* (XR) [53,54] provides information on the electron density profile along the surface normal, i.e. film thicknesses, roughnesses, and (electron) densities. This scattering technique is very useful also for SAM-based multilayered structures (see Section 3.4.5) [55]. Helium atom reflectivity (HAR) [51] gives also information on the roughness. In contrast to XR, HAR sees only the outermost surface, but is extremely sensitive to small changes like the adsorption of a small number of molecules.

2.2.3. Spectroscopy-based techniques

Various spectroscopies, which are different in nature and energy scale, can be exploited to deduce information on the structure and the growth:

1. *Infrared* (IR) spectroscopy [19,56,57]. For simplicity, the term IR should comprise all types of spectroscopies based on IR radiation without distinguishing explicitly different geometries like reflection or transmission.
2. *Second harmonic generation* (SHG) [58,59].
3. *Sum frequency generation* (SFG) [60].
4. *Surface-enhanced Raman scattering* (SERS) [19].
5. *High-resolution electron energy loss spectroscopy* (HREELS) [46,61].
6. *Near-edge X-ray absorption fine structure* (spectroscopy) (NEXAFS) [62].
7. *X-ray photoelectron spectroscopy* (XPS) [19].

IR uses the transition dipoles associated with vibrational modes (and their anisotropy) to draw conclusions on the structure, e.g. the molecular (chain) orientation. In that sense, SFG and NEXAFS fall in a similar category, although they work in different energy ranges. In XPS the deeper energy levels are exploited to deduce the binding state of the headgroup (e.g., S–Au) or simply the mass coverage.

It is important to note that while the diffraction-based and the spectroscopy-based methods are both spatially averaging, the average is performed over different regions with different weight. For instance, if the molecular tilt angle is determined by IR, the average is performed over *all* molecular chains, including the disordered regions like grain boundaries, defect sites, etc., and also molecules which are only physisorbed in a precursor layer. In contrast, the determination of the tilt angle by GIXD (rodscans) includes only the *ordered* (crystalline) regions. This is important when results from different techniques are compared.

2.2.4. Other techniques

Besides the techniques mentioned above, many others have been applied [19], which are not easily categorized. We should mention contact angle measurements [19,22] to determine the surface energies and wetting behavior; *thermally-programmed desorption* (TPD) [46,63,64]; various techniques related to the thickness or coverage determination, such as *surface plasmon spectroscopy* (SPS) [65,66], ellipsometry [67], and the use of a *quartz crystal microbalance* (QCM) [32]; *metastable*

induced electron spectroscopy (MIES) [68]; nuclear magnetic resonance (NMR) [32]; electron spin resonance (ESR) [69]; and X-ray standing waves (XSW) [70–72]. Each of these methods is spatially averaging. Again, we emphasize that this list and the references given are far from being complete.

3. Structure

Several systems have been used to form SAMs. Since the defining feature is the “pair” of the chemisorbing headgroup of the molecule and the substrate (while the rest of the molecule can be almost freely chosen), this “chemisorption pair” is used to classify the specific system in the following. Probably the most popular

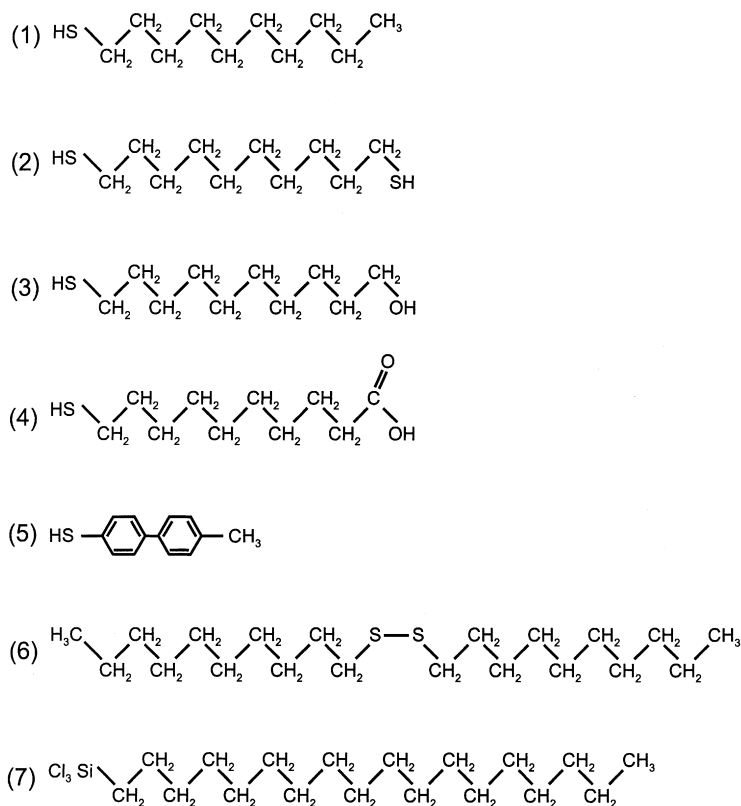


Fig. 3. Some frequently used compounds for SAMs. For purpose of illustration, chain length is specified to $n = 10$ except for case of OTS ($n = 18$). (1) n -alkanethiol: $\text{HS}-(\text{CH}_2)_{n-1}-\text{CH}_3$; (2) α, ω -alkanedithiol: $\text{HS}-(\text{CH}_2)_n-\text{SH}$; (3) ω -mercaptoalkanol: $\text{HS}-(\text{CH}_2)_n-\text{OH}$; (4) ω -mercaptoalkane carboxylic acid: $\text{HS}-(\text{CH}_2)_{n-1}-\text{COOH}$; (5) 4-methyl-4'-mercaptobiphenyl (MMB): $\text{HS}-(\text{C}_6\text{H}_4)_2-\text{CH}_3$; (6) 1, 1'-dialkyl-disulfide: $\text{H}_3\text{C}-(\text{CH}_2)_{n-1}-\text{S}-\text{S}-(\text{CH}_2)_{n-1}-\text{CH}_3$; (7) alkyltrichlorosilane: $\text{Cl}_3\text{Si}-(\text{CH}_2)_{n-1}-\text{CH}_3$ (shown here: octadecyltrichlorosilane (OTS) $\text{Cl}_3\text{Si}-(\text{CH}_2)_{17}-\text{CH}_3$).

SAM system is that of thiols on Au(111). Another popular example is organo-silicon monolayers on hydroxylated surfaces, which, however, typically do not exhibit the degree of long-range order observed for thiols on Au(111). Some frequently-used compounds are shown in Fig. 3. We will use thiols on Au(111) to illustrate the different features characterizing the structure of SAMs, i.e., we will explain:

1. the “2D structure” (i.e., the structure projected onto the surface plane), which describes the type (or absence) of crystalline long-range order, the symmetry, the lattice parameters, the packing in the plane, etc.;
2. the structure of the molecular backbone (see Fig. 4), which includes a possible tilt angle with respect to the surface normal, the tilt direction, the twist angle, etc. Of course, in principle the molecular backbone does not need to be fully extended (e.g., alkane chains might be bent or exhibit gauche-defects), and different backbones have different degrees of freedom to describe their conformational state.

After introducing this terminology (Section 3.1) we will provide an overview of other SAM systems (Section 3.2) and compare these to the example of alkanethiol on

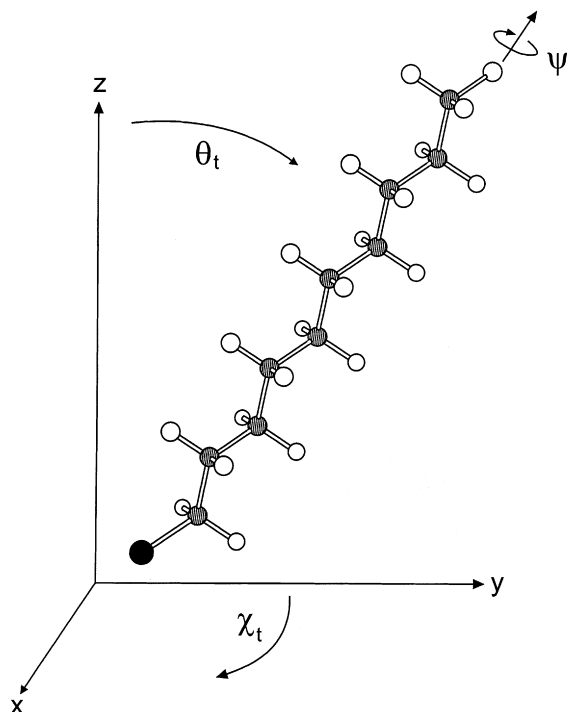


Fig. 4. Schematic of angular degrees of freedom of alkanethiol (bound to substrate via thiol group, with alkyl chain fully stretched). Angle θ_t refers to tilt of molecular axis with respect to substrate surface normal. χ_t defines tilt direction, i.e., it is derived from projection of molecule in substrate plane. χ_t is undefined for $\theta_t = 0$. Twist angle, ψ , describes rotation about axis of molecule.

Au(111). In this section, we limit ourselves solely to the characterization of structures. Their preparation and under which growth conditions they appear will be the subject of Section 4.

We will first concentrate on the phases at ambient temperature. Issues related to changes with temperature, possible high temperature phases, and phase transitions will be discussed in Section 3.3.

Sections 3.1–3.3 will deal mostly with homogeneous one-component SAMs. More complex systems such as multi-component structures, heterostructures, and laterally structured layers are the subject of Section 3.4.

3.1. Thiols on Au(111)

Due to their ease of preparation and well-defined order and also the relative inertness of the substrate, which makes it comparatively easy to clean, thiols on gold have become a model system for SAMs. The (111) surface is the lowest energy surface, which is thus preferred in the growth of thin Au films. Since evaporated Au films are easy to prepare and are more likely to be used in applications than single-crystals, the (111) surface is the most popular one.

3.1.1. Alkanethiols as the archetypal case

Since *n*-alkanethiols are fully saturated and, from a chemical perspective, fairly simple compounds, which still exhibit all necessary features and degrees of freedom typical for SAMs, they are considered the simplest case among the thiols on Au(111) and, thus, the archetypal case. We will first focus on the full-coverage phase and then explain the lower-coverage phases.

3.1.1.1. Full-coverage phase. (i) Overall characteristics. The full-coverage phase, by definition, corresponds to the highest possible packing of the molecules, i.e., the surface is saturated. Early studies of the structure of alkanethiols on Au(111) with molecular-level resolution reported diffraction peaks representative of a $(\sqrt{3} \times \sqrt{3})$ R30° structure (see Fig. 5) relative to the underlying Au(111) substrate [52,73,74]. Ref. [52] was also the first demonstration of the detection of crystalline order on the surface of an organic material with LEAD in general.

The $(\sqrt{3} \times \sqrt{3})$ R30° structure corresponds to a molecule–molecule spacing of ~ 5 Å and an area per molecule of 21.6 Å^2 . For the projection onto the 2D plane one expects an area of 18.4 Å^2 for a straight hydrocarbon chain [75]. Assuming that the molecules are still densely packed, this difference would suggest that the axis of the hydrocarbon chains is tilted away from the normal by about $\theta_t \sim \arccos(18.4/21.6) \sim 32^\circ$, consistent with early IR studies [56,76]. The latter established the molecular orientation of an *average* single chain, with the structure consisting of an all-*trans* zig-zag chain canted by $\sim 34^\circ$ from the surface normal with the plane defined by the *trans* segments rotated by $\sim 55^\circ$ (from the plane established by the chain axis and surface normal vectors).

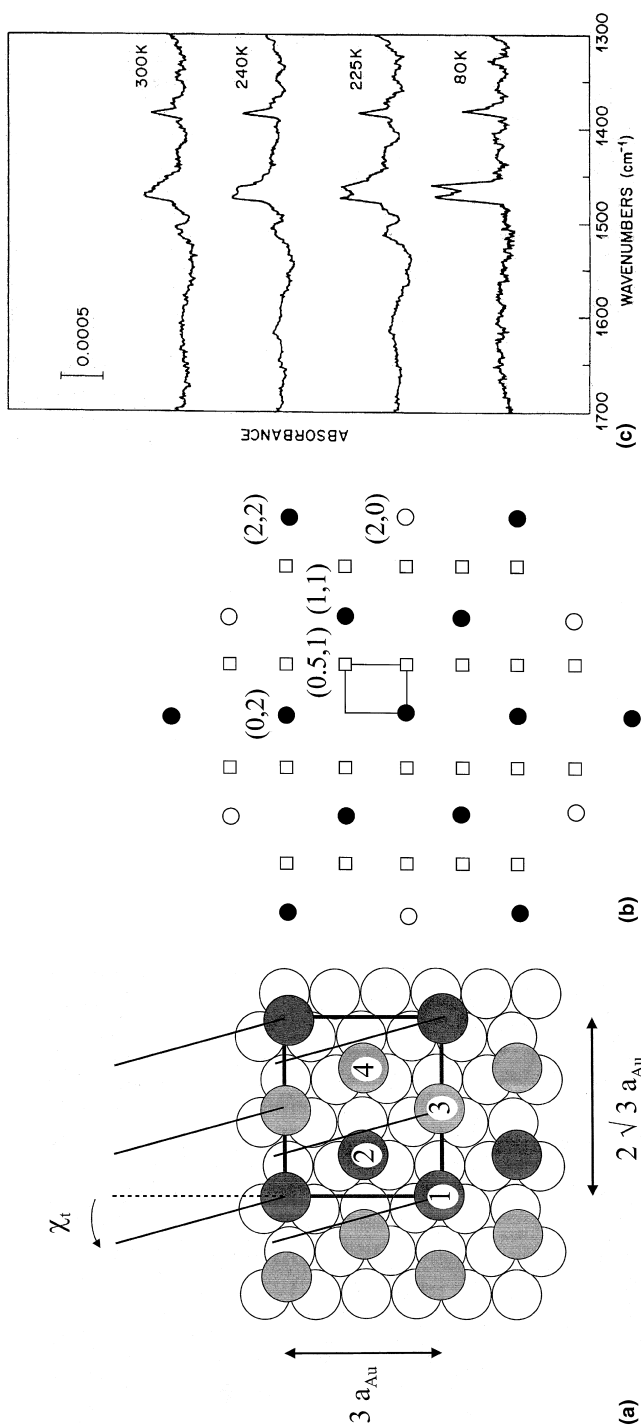


Fig. 5. 2D schematic of real space (a) and reciprocal space (b) picture of $c(4 \times 2)$ structure of decanethiol on Au(111). In (a), χ_t defines tilt direction of hydrocarbon chains (indicated simply by solid lines) projected into 2D plane. Note that notation of this structure as “ $c(4 \times 2)$ ” is somewhat unconventional. More conventional notation would be rectangular ($2\sqrt{3} \times 3$) in units of nearest-neighbor spacing of substrate, a_{Au} , as indicated in the figure (see also Fig. 6). Open circles (2,0), etc.) denote surface diffraction peaks from Au(111) substrate in present surface coordinates. Diffraction peaks at (1,1), (2,2), etc. (full circles) correspond to hexagonal ($\sqrt{3} \times \sqrt{3}$) R30° structure of SAM, while peaks at (0.5,0), (0.5,1), etc. (open squares) are due to “ $c(4 \times 2)$ ” superlattice (note that only one rotational domain is shown). Systematic absence of superlattice peaks (1,0), (1,2), etc.) implies that molecules labeled 1 and 2 (dark circles in (a)) have to be symmetry-equivalent as have to be 3 and 4 (shaded circles). Part (c) shows splitting of methylene (CH_2) scissors mode at 1467 cm^{-1} into two peaks at 1472 and 1463 cm^{-1} upon cooling as observed in IR, which is precisely of same character as factor group splitting seen in monoclinic or orthorhombic phases of crystalline *n*-alkanes, and led to suggestion of model with *nwo* (inequivalent) chains per unit cell. Part (c) is from [76].

We first discuss the features of the 2D structure in detail, and then analyze the tilt structure. Finally, we review the results on the interface structure.

(ii) $c(4 \times 2)$ *superlattice*. Closer inspection of the IR spectra showed a splitting of the methylene (CH_2) scissors mode at 1467 cm^{-1} into two peaks at 1472 cm^{-1} and at 1463 cm^{-1} (see Fig. 5(c)), which was resolved upon cooling of docosanethiol SAMs ($n = 22$) [76]. This led to discarding the single-chain model, and a model with *two (inequivalent) chains per unit cell* was suggested.

In fact, the existence of a $c(4 \times 2)$ superlattice of the $(\sqrt{3} \times \sqrt{3})$ $\text{R}30^\circ$ structure (see Fig. 5),¹ was observed by LEAD [77], GIXD [78], and STM (Fig. 6) [79–81]. This rectangular unit cell has the dimensions $9.994 \text{ \AA} \times 8.655 \text{ \AA}$, which is four times larger than that of the $(\sqrt{3} \times \sqrt{3})$ $\text{R}30^\circ$ lattice, i.e., it should contain four molecules.

Whereas the $(\sqrt{3} \times \sqrt{3})$ $\text{R}30^\circ$ structure is intuitively understandable based on packing considerations as explained above, the reason for the formation of the superlattice is less obvious.

Before going into the details of the structure model for the $c(4 \times 2)$, we want to analyze the qualitative features revealed by various complementary methods, which already put severe constraints on the possible structure models. We note that the superlattice was observed for various lengths of the alkyl chain.

(iii) *What produces the superlattice?* First of all, the discovery of the superlattice with LEAD, a method which is sensitive to the outermost part of the molecules, suggests that the terminating methyl groups have different heights and/or orientations. However, with LEAD it is difficult to deduce the reason for this observation, i.e., a possibly different conformation of the chains or headgroups.

The interpretation of the STM data is similarly complicated due to the fact that the tunneling mechanism through the relatively long chain in itself is difficult to understand. The “bright” and “less bright” molecules can be due to a variation of the height (Fig. 6), but from the STM data alone it cannot be determined what exactly gives rise to the superlattice.

One key to understanding the origin of the height modulation are the above-mentioned IR data, which suggest that there should be at least two different types of molecules in the unit cell with different orientations of the molecular backbone (twist angles different by about 90°) [57,76]. Since the band splitting is precisely of the same character as the factor group splitting seen in the monoclinic or orthorhombic phases of crystalline n -alkanes, it can be considered as suggestive of a structure with a similar unit cell and two inequivalent chains (consistent with the results from GIXD; see below). Also, it is important to note that IR and SERS reported few gauche defects in full coverage SAMs compared to bulk samples at the same temperature, at least in the polymethylene portion [56,82]. In other words, the

¹ This notation of a $c(4 \times 2)$ superlattice based on a hexagonal coordinate system may appear somewhat unconventional, since the structure is actually rectangular, and since a hexagonal phase is usually not referred to as centered. A more conventional notation would be $(2\sqrt{3} \times 3)$. However, since historically it has been introduced as $c(4 \times 2)$, we will stay with this notation.

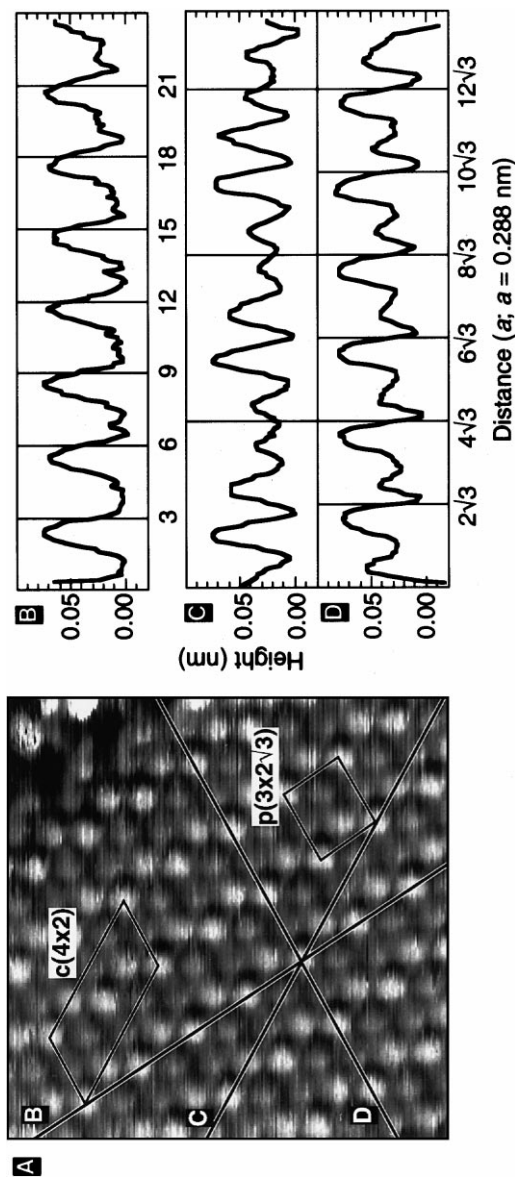


Fig. 6. (A) Constant-current STM image ($60 \text{ \AA} \times 60 \text{ \AA}$) of octanethiol on Au(111) in standing-up phase. The $(2\sqrt{3} \times 3)$ unit mesh and $c(4 \times 2)$ superlattice unit cell are outlined. (B) Plot of cross-section B in (A) running in the Au nearest-neighbor direction. (C and D) Cross-sectional plots running in two of Au NNN directions. From [79].

chains are largely in the all-*trans* configuration. Another interesting finding is that of odd–even chain-length-dependent orientations of the terminating methyl group which provides evidence for a conserved bonding configuration of the headgroup [35].

For a structural analysis of the “interior” of the SAM penetrating structural methods such as X-ray or neutron diffraction or XSW are required. A key feature of the diffraction pattern of the $c(4 \times 2)$ structure (Fig. 5(b); obtained by GIXD) is the systematic absence of superlattice peaks, namely those with $h + k = \text{odd}$, with the rectangular unit cell having dimensions of 9.994 Å ($\equiv 2a$) and 8.655 Å ($\equiv b$). This indicates that there is a symmetry within the unit cell corresponding to a translation of $(a/2, b/2)$. In other words, for every molecule at the position (x, y) there is an equivalent molecule at $(x + a/2, y + b/2)$. With this symmetry, the unit cell contains only two inequivalent molecules, i.e., the molecules labeled 1 and 2 in Fig. 5 are symmetry-equivalent as are 3 and 4.

We note that while some STM studies (see, e.g., [83,84]) have suggested polymorphism, i.e., that there may be more than one molecular arrangement that results in the $c(4 \times 2)$ structure, the diffraction data can rule out any $c(4 \times 2)$ structure that does not exhibit the centered rectangular symmetry shown schematically in Fig. 5.

At this point, with the knowledge of the symmetry features of the unit cell from GIXD and the constraints imposed from other methods including the IR data, it is clear that within the rectangular unit cell with four molecules only two of these (pairwise) can be inequivalent, and that these should differ in the twist angle of the molecular backbone. However, the difference *only* in the twist angle, ψ , of the backbone is *not enough* to explain the $c(4 \times 2)$ structure (since a difference in ψ causes only a small GIXD scattering contrast), and further analysis of the GIXD data, supported by results from SFG [60] and XSW [71,72], suggests that the sulfur headgroups have to contribute to the formation of the superlattice, i.e., they cannot be located in a hexagonal symmetry. Before discussing this complex issue of a detailed structure model which includes also the headgroup (i.e., interface structure), we will first analyze the tilt structure of the hydrocarbon chains.

(iv) *Tilt structure and its chain length dependence.* The tilt structure of the SAM is obtained directly from the analysis of the q_z -dependence of the GIXD scattering intensity (so-called rodscans), $I(q_z)$. If we consider a purely two-dimensional film (e.g., a monolayer of atoms), we would expect the diffraction intensity to be peaked at the Bragg condition for q_{\parallel} in the 2D plane, but flat along q_z , since an object which is essentially a delta-function in real space, will be constant in reciprocal space. A 2D crystal of standing-up molecules with length, L , will have also diffraction intensity peaked at the in-plane Bragg conditions, but along q_z we will find peaks of width $\Delta q_z \sim 2\pi/L$ rather than a flat profile. If the molecules are tilted by an angle θ_t in the direction χ_t (relative to the direction χ_q of the in-plane scattering vector, q_{\parallel}), the q_z position of these peaks (at a given q_{\parallel}) will be related by [85]

$$q_z = q_{\parallel} \tan(\theta_t) \cos(\chi_t - \chi_q). \quad (3.1)$$

For untilted molecules, the maximum of $I(q_z)$ is found at $q_z \rightarrow 0$ (and only “one half” of this peak is measured for $q_z \geq 0$). While (3.1) is useful for a description of the peak locations, for a fit of the entire rod structure factor calculations are required [86].

Fig. 7(a) shows rodscaans of the hexagonal (1,1) rod ($I(q_z)$ with $q_{\parallel} = 1.45 \text{ \AA}^{-1}$ fixed) for different chain lengths. The existence of more than one peak is related to the different projections of multiple tilt domains (with the 60° symmetry of the substrate) on the scattering vector q_{\parallel} along the direction χ_q , which enters $\cos(\chi_t - \chi_q)$ in

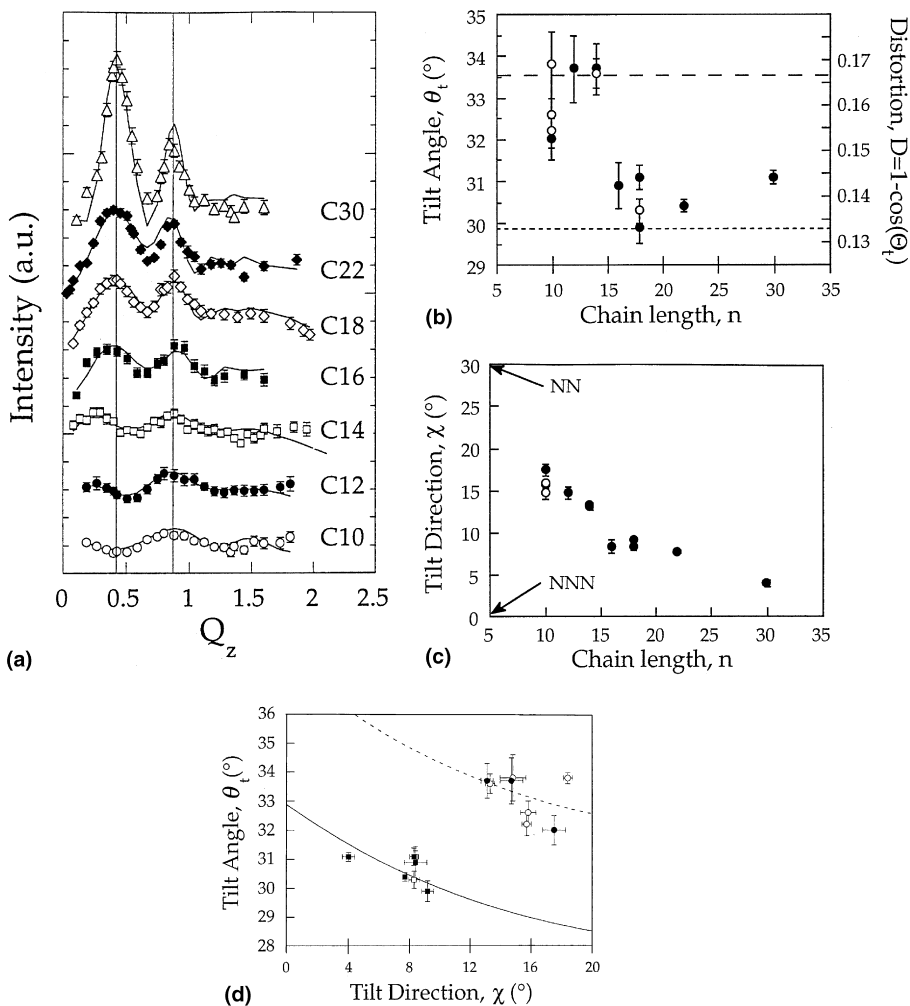


Fig. 7. Tilt structure for alkanethiol on Au(111) in $c(4 \times 2)$ structure as function of chain length, n . (a) Bragg rod profiles measured by X-ray diffraction. (b) Tilt angle vs. n . (c) Tilt direction vs. n . (d) Tilt angle plotted against tilt direction with data from part (b) and (c), which includes n as implicit parameter. For definition of angles see Fig. 4. Data in (d) show that, although changes as function of n in (b) and (c) are small, there are two distinct regimes of tilt structures. From [86].

(3.1). For octadecanethiol (“C18”), the peaks at $q_z = 0.42 \text{ \AA}^{-1}$ and $q_z = 0.87 \text{ \AA}^{-1}$ are related to a tilt angle $\theta_t \sim 30^\circ$ and a tilt direction $\chi_t \sim 8^\circ$ (relative to the direction of the next-nearest neighbor). The error bar for θ_t and χ_t is typically around 0.5° .

Owing to the high sensitivity of the hexagonal rods measured with GIXD for changes in the tilt structure, it was possible to resolve a chain length dependence of θ_t and χ_t . Inspection of Fig. 7(a) shows that the q_z positions of the maxima exhibit a systematic change with chain length. Particularly for shorter chain lengths ($n \leq 14$) the peak positions clearly deviate from the vertical lines marking the peak positions for C18. Fig. 7(b) and (c) display the results of a detailed analysis of θ_t and χ_t as a function of n .

There are two different regimes for the tilt angle, which for $n \leq 14$ is systematically $\sim 3^\circ$ greater than for $n \geq 16$. Furthermore, the tilt direction (which is measured from the next-nearest neighbor (NNN) direction) exhibits a clear trend of shifting away from the NNN direction towards the NN direction for shorter chain lengths.

The existence of two regimes is most obvious in Fig. 7(d), where the tilt angle is plotted against the tilt direction with the data from part (b) and (c). Fig. 7(d) includes the chain length as an implicit parameter.

In an attempt to rationalize these structures, it was pointed out [86] that for $n \geq 16$ the hydrocarbon packing is very similar to that of the bulk orthorhombic phases of n -alkanes of odd chain length, and that for $n \leq 14$ the packing is similar to that of a predicted monoclinic structure, which is not observed experimentally in the bulk [75].

In a broader sense, the chain-length dependence of the tilt structure probes the competition between the different interactions. Namely, the chain–chain interaction is increased, while the headgroup–substrate interaction is nominally fixed. For uncorrugated, i.e., smooth chains, one would expect the impact of the chain length to be small. This should result at most in a slight and continuous variation of the tilt structure with chain length. On the other hand, for the more realistic picture of corrugated chains (due to their zig-zag-like internal structure), certain relative positions of the chains with respect to each other would be preferred. Depending on whether the chain–chain or the headgroup–substrate interaction dominates (“long” vs. “short” chain length regime), this corrugation should give rise to discrete regimes. In this way, the experimental finding of two discrete regimes reflects the non-negligible influence of the chain corrugation. It can also be viewed as an effect of the (“soft”) epitaxy in this system.

(v) *Cases of very short and very long chains.* While the above-described behavior is found in a broad range of chain lengths, for very long chains the headgroup interaction will be less important and deviations will occur. For $n \rightarrow \infty$, gauche-defects and entropic contributions will become increasingly important, but so far a clear transition to a “polymeric regime” has not been established.

Deviations were also reported for very short chains (typically for $n < 8$, but establishing a sharp boundary is difficult) [87–89]. The energy balance is strongly changed, since the chain–chain interaction can no longer compete with the headgroup–substrate interaction.

(vi) *Headgroup structure.* The above analysis was concerned with the “hexagonal” rods. Inspection of the superlattice rods [90] shows that they are essentially

flat, suggesting that the features responsible for the formation of the superlattice (i.e., the deviation from pure hexagonal symmetry) are located in a very thin layer in real space (Δz), which makes the rods flat (features on the rod would be broad in reciprocal space, according to $\Delta q_z \sim 2\pi/\Delta z$). If the backbones (with their possible difference in the twist angle ψ for molecule “1” and “3”) were solely responsible for the superlattice formation, the superlattice rods would have to have a similar q_z -dependence as the hexagonal peaks (reflecting the hydrocarbon tilt structure), but they do not. Moreover, the difference in ψ produces only a very weak scattering contrast in GIXD between the inequivalent molecules (i.e., hydrocarbon chains), which alone cannot account for the observed superlattice intensities.

Consequently, the sulfur positions have to deviate from the hexagonal ($\sqrt{3} \times \sqrt{3}$) $R30^\circ$ symmetry, implying that they cannot all be situated in equivalent sites. This conclusion already follows directly from the qualitative features of the rodscans and does not depend on a particular model. At this point, the question is no longer whether or not the headgroups are moved out of the hexagonal symmetry at all, but only *how far*.

Inspired by the above qualitative characteristics, in [90] a structure model, which fits the entire rods, was presented. Besides the tilt structure and the symmetry shown in Fig. 5, the most prominent feature is the strong deviation of the sulfur atoms from the hexagonal symmetry. The result of the fit, a S–S spacing of only $\sim 2.2 \text{ \AA}$ (instead of 5 \AA for a perfect hexagonal ($\sqrt{3} \times \sqrt{3}$) $R30^\circ$ symmetry), was interpreted in terms of a dimerization, which was subject of much discussion in the literature, although to date no other model consistent with the experimental data has been presented.

Before discussing the structure model in the light of results from other techniques, we should emphasize that, first, the qualitative features outlined above essentially dictate a S–S spacing of the inequivalent molecules in the unit cell smaller than 5 \AA , and, second, that X-ray diffraction is sensitive to distances between atoms, but not directly to chemical bonding states. In that sense, one might call the reduced S–S spacing a “pairing” rather than a dimerization. Note that the observation of disulfides in TPD [91] cannot serve as a proof for this structure, since dimers may be formed upon desorption.

Data consistent with a break of the hexagonal symmetry of the sulfurs were provided in an SFG study by Yeganeh et al. [60]. From the type of symmetry, i.e., the azimuthal dependence of the SFG signal, the authors infer that the sulfurs cannot be situated at sites of a single type, e.g., hollow or bridge, but must be in a mixed arrangement. Based on their analysis of STM data on short-chain alkanethiols, Voets et al. [92], claim support of the sulfur pairing model.

One argument against the “pairing” model might be that sulfur has typically only two valencies, which would rule out a dimerization of alkanethiols chemisorbed on the Au(111) surface. However, for binding on surfaces these rules may not be strictly valid. Furthermore, for the lying-down phase (discussed below), there is also evidence pointing towards a reduced S–S spacing, and it can be argued that if a S–S interaction is possible in the lying-down phase, there should be no fundamental

objections in the standing-up phase. The structure suggested in [90] was confirmed to correspond to an energy minimum in calculations using quantum-mechanics-based force fields [93]. It is also consistent with a recent study employing XSW, in which the two inequivalent sulfur binding sites were determined with high precision [71,72] (see also Section 5.2).

A recent HREELS study of octadecanethiol on Au(1 1 1) revealed an S–S stretch mode (at 530 cm^{-1}), supporting the finding of sulfur pairing on the surface. Since this mode was only detected for layers annealed to 375 K, it was concluded that the formation of the gauche defect required to allow the sulfurs to move to the pairing configuration is associated with an activation barrier [61].

Another issue that requires consideration is related to possible irradiation effects. The GIXD measurements, however, although sensitive to any type of structural changes, only detected weak changes on the time scale of days [50], which is three orders of magnitude above the typical time for the GIXD scans (of the order of minutes). It could also be shown that under the typical experimental conditions used in GIXD (sample in UHV; photon energy about 10 keV, where the inelastic cross-section is small), no changes are observed for exposure times as short as a few seconds. On that time scale, for the GIXD experiments in [90], less than one X-ray photon per 10^4 molecules strikes the surface, and the absorption corresponds to less than one X-ray photon per 10^{10} molecules, making significant damage on a shorter time scale unlikely [50]. In this context, we should note that the inelastic cross-section for X-rays *decreases* with the X-ray energy as $1/E^3$. Moreover, in those studies where radiation damage by X-rays was observed after high exposures, the main effect was due to secondary electrons [94], the interaction cross-section of which also *decreases* with energy in that regime. It should be noted that the GIXD peak width of the superlattice was found to correspond to the same coherence length as the hexagonal structure. If the reported structure were an effect of irradiation, this process would have to produce a highly coherent structure, which appears unlikely.

(vii) *Structural defects.* The growth of a low-symmetry structure on a high-symmetry substrate naturally leads to domain boundaries. In the case of the $c(4 \times 2)$ structure on Au(1 1 1) various types of domain boundaries can be found due to the 12-fold translational and the 3-fold orientational degeneracy of the unit cell and the additional degeneracy due to the different tilt directions. While the occurrence of these defects cannot be avoided, their density, which is inversely related to the size of the domains, can be influenced [40,78,95–97] by annealing or by the appropriate growth conditions (Section 4.2.1).

In addition, pit-like defects 2.5 \AA in depth were observed by several groups employing STM [36]. These were assigned to 2D islands of Au vacancies. Since evidence was found for mobile Au-adatoms during growth, it was suggested that the vacancy islands form by ejection of excess Au atoms when the surface reconstruction is removed. For a detailed discussion on the issue of vacancy islands see [36,98] and references therein.

Furthermore, we should mention molecular vacancies as studied by STM and discussed in [36] and gauche defects of the chain conformation, which are followed, e.g., by IR [35,76]. Their temperature evolution is discussed in Section 3.3.

3.1.1.2. Lower-coverage phases. Besides the full-coverage “standing-up” phase discussed above, at lower coverages other structures and metastable configurations were found (Fig. 26). The preparation, stability, and relevance of various lower-coverage structures for the growth process will be discussed in Section 4. Here, we want to focus on the structural characterization.

Intuitively, it can already be expected that at sufficiently low coverage the molecular backbone is lying down flat on the surface, which is, in fact, the defining feature of the most important low-coverage phase, the “lying-down” phase. It has been observed by Camillone et al. [99] after reducing the coverage of a standing-up phase SAM by thermal desorption. Later it was found that the lying-down phase is also formed in the initial stage of the growth (see Section 4).

Fig. 8 shows the 2D projection of the real-space and the reciprocal space picture schematically. This phase is generally characterized by a $(m \times \sqrt{3})$ unit cell. In [99], for decanethiol m was found to be 11 (corresponding to 31.7 Å), which is close to twice the length of one molecule and which is equivalent to 27% coverage normalized to the standing-up phase.

From the periodicity and the reduced coverage, the nature of the structure as the “lying-down” phase is apparent, which is seen also from the STM data [99,100]. The alkane chains are fully stretched, which is consistent with the chain-length dependence, where an increase of the lattice parameter, m , by about $0.83 \pm$

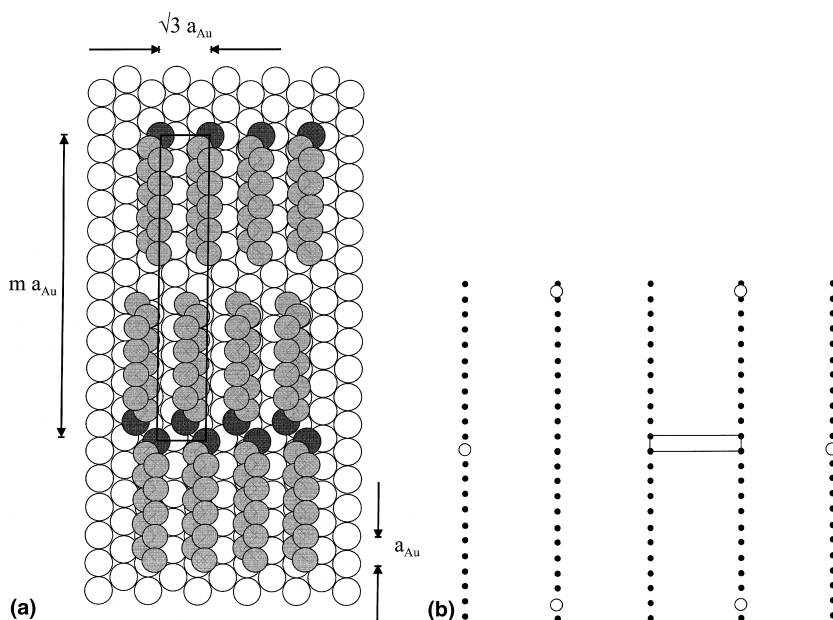


Fig. 8. 2D schematic of real space (a) and reciprocal space (b) picture of striped phase structure of alkanethiol on Au(111). For decanethiol, the unit cell can be described by $p(m \times \sqrt{3})$ unit mesh with $m = 11$. Note that also $c(23 \times \sqrt{3})$ unit mesh has been observed, which is obtained after only small displacement of every second row of stripes (see text).

0.04 (2.4 ± 0.1 Å) per methylene group was found [101]. This is close to what would be expected from twice the projection of the length of a C–C bond along the molecular axis (for two molecules lying head-to-head along the long axis of the unit cell). The zig-zag plane of the C–C–C bonds is parallel to the substrate.

The existence of the lying-down phase was confirmed by several groups for various chain lengths, but two slightly different unit cells were found. Besides the originally reported *primitive* (p) unit cell, a *centered* (c) one with approximately twice the lattice parameter m and two molecules per unit cell was found [43,44,102]. For decanethiol, these structures were labeled p($11 \times \sqrt{3}$) and c($23 \times \sqrt{3}$), for hexanethiol p($8 \times \sqrt{3}$) and c($15 \times \sqrt{3}$), respectively. No evidence for incommensuration was reported. Closer inspection shows that for a change from the primitive to the centered structure, only a small displacement of every second row of stripes in the perpendicular ($\sqrt{3}$) direction is needed [44]. In fact, the two different phases were found within one set of experiments for slightly different preparation conditions and are obviously very similar in terms of area per molecule [44].

Since the molecules are lying down on the surface in a simple, fully stretched configuration, the question arises what the driving force is for the unit cell to contain a head-to-head arrangement of the molecules. The natural interpretation would be the headgroup–headgroup interaction. In fact, it was inferred from the unit cell spacing compared to the length of the molecules, that the distance of the sulfur headgroups of neighboring molecules is consistent with a typical disulfide bond length (about 2.2 Å) [101].

The hypothesis of a small headgroup–headgroup distance, which is suggestive of dimerization, is supported by XSW data, which resulted in an indistinguishable S/Au interface structure in terms of binding sites for the lying-down and the standing-up phase [71,72]. From the analysis of STM images of the lying-down phase of short-chain alkanethiols, Voets et al. [92] report to have found support of the dimer model. Furthermore, the issue of the headgroup configuration and a possible alternative headgroup bonding structure involving different sites is discussed in a recent STM work [100].

In addition, other structures have been reported, most notably one described by a ($5\sqrt{3} \times \sqrt{3}$) R30° unit cell [43,47,101,102]. It corresponds to a coverage of 40% relative to the c(4×2) phase, implying that the molecules can no longer all be lying down on the surface, but also not yet stand upright in a close-packed structure. We note that the ($5\sqrt{3} \times \sqrt{3}$) R30° unit cell (in hexagonal notation) is identical to an oblique ($\sqrt{57} \times \sqrt{3}$) and to a centered rectangular ($15 \times \sqrt{3}$). Since the nomenclature of the ($5\sqrt{3} \times \sqrt{3}$) R30° unit cell was used first in the literature, it will be used here. The appearance of intermediate-coverage structures and their relationship to the growth is discussed in Section 4.2.1.

3.1.2. Unsaturated hydrocarbon thiols and others

Besides the “simple” alkanethiols, several other thiols have been studied. By comparing these different compounds, the impact of changing the balance of the various interactions (see Fig. 2 and Section 4.3) on the structure as well as on the growth (Section 4) can be studied.

3.1.2.1. *n*-Alkenethiols. Including an olefin-termination (i.e., a C=C double bond at the end of the chain), is probably one of the smallest changes one could imagine for alkanethiols. In fact, it was found that the structure of alkenethiol SAMs with different chain lengths ($n = 9, 10, 11, 17,$ and 18) exhibits the same unit cell as the corresponding alkanethiols, i.e., a $c(4 \times 2)$ superlattice of the $(\sqrt{3} \times \sqrt{3})$ R30° structure, and very similar tilt angles of the molecular backbone. It should be noted, however, that minute amounts of impurities can have a strong impact on these SAMs, possibly resulting in a completely different structure [103,104].

3.1.2.2. *Oligophenylthiols.* By studying oligophenylthiols, the role of the molecular backbone can be addressed. Phenyl rings might be expected to introduce stronger interactions (molecule–substrate and molecule–molecule). Also, they are generally more rigid than alkane chains, which can have an impact on structure formation in that it might be more difficult to change between different structures as a function of coverage.

Creager and Steiger studied monolayers of 4-mercaptobenzoic acid on gold, and concluded that the rigidity of the phenyl rings prevented intermolecular H-bonding and the dimerization of the carboxylic groups [105]. In [106], oligophenyl-based thiols were found to provide stable model surfaces for wetting studies. In [107], oligo(phenylethynyl)benzenethiols of different length (with 1, 2, and 3 phenyl rings) were studied by STM. It was found that the degree of order in that series increased with the number of phenyl rings. For the triphenyl compound, SAMs of reproducibly high order are found with standing-up molecules in a herringbone structure.

A good compound for comparison with the above described decanethiols is 4-methyl-4'-mercaptobiphenyl (MMB), since it has both the same methyl endgroup and about the same length, so that possible differences in the structure can be attributed to the difference in the backbone. Previously, 4-mercaptobiphenyl (similar to MMB, but without methyl group) had been investigated [108,109], but without direct structural evidence for an ordered monolayer. In [110], the structure and growth of MMB SAMs was studied by GIXD and LEAD. Similar to the alkanethiols, a low-coverage (“lying-down” or “striped”) and a high-coverage (“standing-up”) phase were found.

The standing-up phase was found to have a hexagonal commensurate $(\sqrt{3} \times \sqrt{3})$ R30° structure, which is similar to that found for the alkanethiols, but without superlattice peaks at the $c(4 \times 2)$ positions (note, however, that generally other types of superlattices cannot be ruled out on the basis of the data) [110]. The absence of a superlattice would imply that also all sulfurs are in the same binding site, i.e., that the structure is not dimerized. The q_z dependence of the hexagonal diffraction peak (rodscan) in GIXD provided an upper limit for the tilt angle θ_t of the molecular backbone ($\theta_t \leq 19^\circ$), i.e., it is smaller than for alkanethiols. Consistent with this, based on IR data Kang et al. [111] found the molecules to stand upright. This smaller tilt angle of MMB reflects the fact that the molecules do not need to tilt strongly in order to maximize their van der Waals interactions when their spacing is

constrained to 5 Å, as a small adjustment of the dihedral angle is sufficient. Comparing the van der Waals dimensions of the molecule (with a cross-sectional area of 21.1 Å² for the phenyl rings) to the area per molecule in the ($\sqrt{3} \times \sqrt{3}$) R30° structure (21.6 Å²) supports this conclusion, since the tilt angle deduced from this comparison is expected to be only about $\theta_t \sim \arccos(21.1/21.6) = 14^\circ$.

It was also reported that the resolution-corrected peak width in LEAD increased with the order of the reflection, which was interpreted in terms of lattice disorder. Since this effect has not been seen with GIXD on MMB, it is suggested that the disorder is related to the top group of the molecule, to which LEAD is solely sensitive. Generally, the hexagonal phase of MMB was difficult to form and its structural quality was rather limited (Section 4.2.2).

For the low-coverage (“lying-down”) phase, a ($8 \times 2\sqrt{3}$) unit cell (corresponding to 23.08 Å × 10 Å with four molecules per unit cell and, therefore, a packing density of 57.7 Å² per molecule) was found, the diffraction pattern of which exhibited systematic absences of certain reflections. The structure proposed in [110] is characterized by a centered rectangular unit cell with the molecules lying in a head-to-head configuration (Fig. 9). If typical van der Waals radii for the groups forming the molecule are assumed, the resulting S–S distance is close to the 2.1 ± 0.2 Å recently reported for 4-mercaptopyridine [112]. In order to fully accommodate the molecules, it was suggested that the molecules tilt partly away from the surface.

To summarize, while the general scenario of the occurrence of a standing-up phase and a lying-down phase is similar to that of alkanethiols, both of these structures exhibit differences to the alkanethiol case. This is also reflected in the growth and the temperature behavior, which will be discussed in Sections 4 and 3.3, respectively.

3.1.2.3. OH-terminated thiols. The change of the endgroup can have an impact on the tilt angle and on possible superstructures (or a complete change of the unit cell) due to steric constraints and endgroup–endgroup interactions. In the case of OH-terminated alkylthiols (SH–(CH₂)₁₆–OH), the tilt structure was determined by Nuzzo et al. [56] using IR, resulting in $\theta_t \sim 28^\circ$ and $\psi_t \sim 50$. This is similar to the results of Bertilsson and Liedberg [113], who found, also using IR, $\theta_t \sim 28^\circ$. Based on NEXAFS data, Himmel et al. [114] concluded that the alkyl chains (of SH–(CH₂)₁₆–OH) are mainly in the *trans* conformation with a homogeneous tilt angle of 44°, which might be in conflict with the maximum packing given by the van-der-Waals radii, if an underlying ($\sqrt{3} \times \sqrt{3}$) lattice is assumed. In [115] $\theta_t = 39.6^\circ$ was derived from NEXAFS data and $\theta_t = 39.6^\circ$ from XPS data for SH–(CH₂)₁₆–OH and a somewhat smaller tilt for SH–(CH₂)₂₂–OH.

The difficult issue of possible superstructures induced by the endgroup–endgroup interactions (hydrogen bonds) was discussed by Sprik et al. [116] for mercapto-undecanol (SH–(CH₂)₁₁–OH) in a combined STM and computer simulation study.

For very short chains, a fairly unconventional structure was found. For mercaptohexanol (SH–(CH₂)₆–OH), Poirier et al. [117] found a commensurate lattice with an oblique primitive unit cell of dimensions $a = 3a_{Au} || [10\bar{1}]$, $b = \sqrt{13}a_{Au} || [341]$,

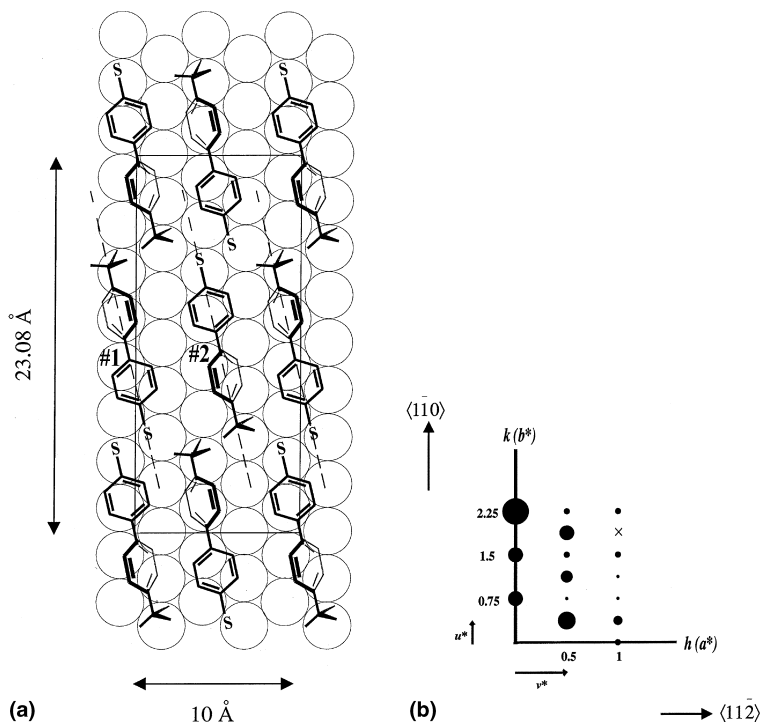


Fig. 9. (a) Proposed structure of lying-down phase of MMB after [110]. The dimensions of the rectangular unit mesh ($23.08 \text{ \AA} \times 10 \text{ \AA}$) are consistent with a $(8 \times 2\sqrt{3})$ lattice. While structure model is not yet refined, main symmetry features (centered rectangular unit cell with molecules labeled 1 and 2 being inequivalent) are implied by relative intensities and systematic absences of peaks in diffraction pattern (b). In (b), size of spots corresponds to intensity of Bragg peak. Cross marks position of peak at noise level. From [110].

$\alpha = \arctan(2\sqrt{3}) = 73.9^\circ$ (with $a_{\text{Au}} = 2.88 \text{ \AA}$ as the Au(111) surface lattice parameter) and a packing density of 21.5 \AA^2 per molecule (identical to alkanethiols on Au(111)), suggesting that the molecules are standing up with some non-zero tilt angle. These SAMs were also reported to be very sensitive to humidity (see Section 3.4.4).

3.1.2.4. COOH-terminated thiols. For the average tilt and the twist angle of COOH-terminated alkythiols, from IR data, Nuzzo et al. [56] reported similar values as for OH-terminated systems, i.e. $\theta_t \sim 32^\circ$ and $\psi_t \sim 55^\circ$. Based on NEXAFS data, it was reported that alkythiols with COOH-termination are largely disordered and exhibit a high density of gauche defects [114,115]. It was speculated that the reason for this is the stronger interaction of the COOH endgroups via hydrogen bonds already in the early stages of the growth which might then prohibit the formation of well-ordered films [115]. Nevertheless, for $\text{SH}-(\text{CH}_2)_{15}-\text{COOH}$ diffraction peaks corresponding to the $(\sqrt{3} \times \sqrt{3})$ R30° structure were found, although with a limited coherence length

of ~ 55 Å (measured by GIXD in contact with solution) [118]. The tilt angle from rodscans was consistent with the IR results.

3.1.2.5. Fluorinated alkanethiols. The fluorination (i.e., the partial or complete substitution of H by F) of *n*-alkanethiols is expected to affect primarily the space requirements of the molecular backbone in the SAM. Ideally, these slightly bulkier molecules might be accommodated by a reduction of the tilt angle and presumably a larger unit cell. In fact, an early AFM study of $\text{CF}_3(\text{CF}_2)_7(\text{CH}_2)_2\text{SH}$ found a lattice parameter of 5.8 ± 0.02 Å, consistent with a commensurate $p(2 \times 2)$ structure with untilted molecules [119]. This picture seemed to be confirmed by GIXD data finding a lattice spacing of 5.780 ± 0.001 Å, consistent with the (2×2) structure within 0.2%. However, it was found independently by AFM and GIXD that the azimuthal orientation of the unit cell was rotated by 30° relative to the expected (2×2) [120]. This implies that the commensurate structure is actually *not* adopted, although the lattice spacing would ideally fit. The preference of the fluorinated molecules to adopt this unexpected azimuthal orientation is accompanied by a high degree of azimuthal disorder, as shown by a large ($\sim 13^\circ$) azimuthal width of the corresponding GIXD peaks [120]. The incommensurate structure also implies that the loss of corrugation energy has to be compensated by some extra energy, in spite of the very small change of the lattice spacing compared to the commensurate $p(2 \times 2)$ structure. The influence of fluorinating just the terminating group (CF_3) on the tilt structure has been discussed by Houssiau et al. [121]. Fluorinated disulfides are discussed further below and in [122].

3.1.2.6. Dithiols. A system, in which the impact of the endgroup is expected to be significant, are dithiols. Moreover, dithiols have attracted considerable attention as a possible anchor to which to attach further building blocks in heterostructures. For instance, electronic transport properties of organic monolayers were investigated by linking Au clusters to a Au(111) surface via α, α' -xylyldithiol and 4,4'-biphenyldithiol [123] and by forming a junction between two Au electrodes via benzene-1,4-dithiol SAMs [124].

The concept of using dithiols as an anchor for, e.g., Au clusters obviously depends critically on the availability of the second thiol functionality at the “surface” of the SAM, i.e., the molecules have to form a “standing-up phase”. This was investigated by a few groups on different compounds, but the findings were not entirely consistent. Tour et al. [125] studied monolayers and multilayers on gold films from a series of conjugated thiols and α, ω -dithiols. Using ellipsometry, XPS, and IR spectroscopy, they find rigid rod α, ω -dithiols to form assemblies in which one thiol group binds to the surface while the second moiety projects upward at the exposed surface of the SAM. Brust et al. [126] reported that structures of copper sandwiched between dithiol molecules can be formed by using 1,6-hexanedithiol ($\text{HS}-(\text{CH}_2)_6-\text{SH}$). Ellipsometry measurements suggested that the molecules attached to the gold surface via only one thiol functionality. Rieley et al. [127] employed XPS for the study of solution-grown 1,8-octanedithiol, finding an “upright” alignment of the hydrocarbon chains. This is in contrast to a combined STM and

IR study of 1,8-octanedithiol ($\text{HS}-(\text{CH}_2)_8-\text{SH}$) grown from solution [128], which found the molecules to be arranged with their axes parallel to the $\text{Au}(111)$ substrate (“lying-down” configuration) and a periodicity of about 15 Å. 1,8-octanedithiol was also found to adopt the lying-down configuration for electrochemical adsorption on $\text{Ag}(111)$ [129]. In [130], 1,6-hexanedithiol on $\text{Au}(111)$ was studied in detail by three complementary structural techniques with molecular resolution (GIXD, LEAD, and STM), revealing a rather sophisticated structural scenario. This is reviewed below.

Fig. 10 gives an overview of the structure for gas phase deposition of 1,6-hexanedithiol on $\text{Au}(111)$ at room temperature [130]. The periodicities along the two lines AB and EF (inclining an angle, γ , of 95°) are about 13.3 and 5 Å. It can also be seen from Fig. 10 that the structural coherence (domain size) is rather limited (~ 100 Å) for room temperature deposition, but this can be significantly improved by high-temperature deposition (see also Section 4.2.2). The elongated bright features in the image correspond to neighboring sulfurs the distance of which was estimated to 2.9 Å, based on the periodicity and the length of the molecule. Closer inspection of

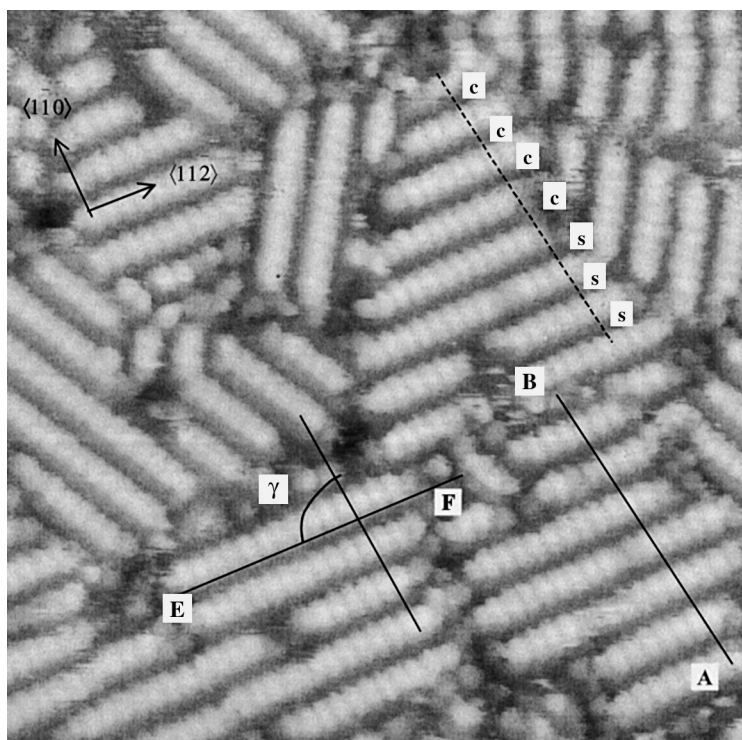


Fig. 10. Constant-current STM image ($220 \text{ \AA} \times 220 \text{ \AA}$) of 1,6-hexanedithiol on $\text{Au}(111)$ prepared at room temperature by gas phase deposition. Periodicities along the two lines AB and EF (inclining an angle, γ , of 95°) are 13.3 and 5 Å. Note that bright features are meandering as explained in text. From [130].

the STM images showed that the sulfur positions do not perfectly line up in rows along the $[1\bar{1}0]$ axis of the substrate, but rather “meander” about these, i.e. they exhibit fluctuations perpendicular to these rows.

The high resolution of GIXD (used on layers prepared at high temperature with a substrate-limited domain size of ~ 2000 Å) revealed that the structure is actually incommensurate along the long axis (see Fig. 11), also after annealing. Two incommensurate phases were found, one with a spacing of 12.23 ± 0.003 Å and another of 12.40 ± 0.01 Å, with the former phase gaining upon annealing at the cost of the latter. We should note that for other chain lengths of alkanedithiols, the structure can nevertheless be commensurate.

LEAD found a structure consistent with GIXD, but with an additional (3×1) superstructure with respect to the GIXD unit cell. In order to understand this difference, one should remember that LEAD scatters mostly from the “outer” electron cloud extending from the surface, whereas GIXD is not as surface-specific and also scatters more from the core electrons, with the heavier elements making a stronger contribution.

After combining the results of these three complementary techniques and taking into account information from related systems, the following structure model was proposed for 1,6-hexanedithiol on Au(111) [130] (see Fig. 12). The molecules are lying flat on the surface with the alkyl chains fully extended and the C–C–C plane parallel to the substrate. In contrast to the lying-down phases of simple alkanedithiols, the structure is incommensurate in the direction of the molecule axis and can be described by $(4.24 \times \sqrt{3})$ (GIXD) or $((3 \times 4.24) \times \sqrt{3})$ (LEAD), respectively. The

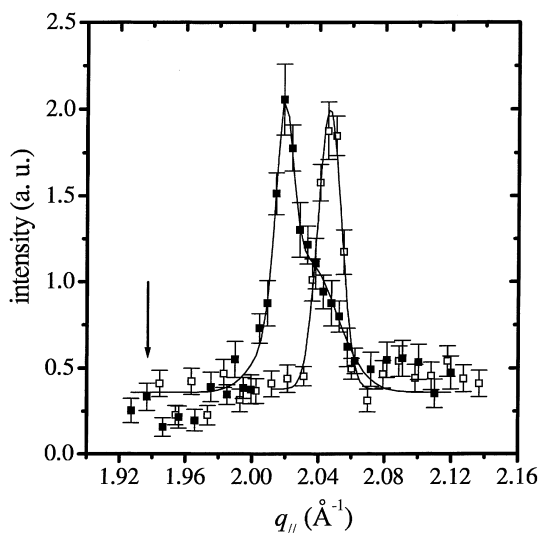


Fig. 11. GIXD radial scan of fourth-order Bragg peak of 1,6-hexanedithiol on Au(111) along $[1\bar{1}0]$ direction of substrate. Arrow marks peak position expected from possible commensurate $(9 \times \sqrt{3})$ lattice. It can be seen that structure is incommensurate, both before (filled squares) and after annealing (open squares). From [130].

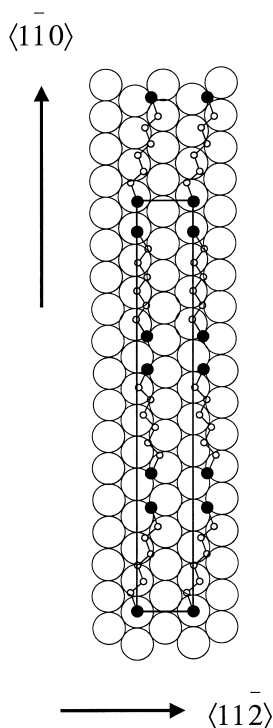


Fig. 12. Structure model proposed for lying-down phase of 1,6-hexanedithiol/Au(111), assuming C–C and C–S bond angles of 112° and C–C and C–S bond lengths of 1.541 and 1.81 Å, respectively. Rectangular highlights unit mesh observed by LEAD. From [130].

difference between GIXD and LEAD can be rationalized as a slight height modulation of the molecules on the surface. The structure is obviously very different from that of the related compound of mercaptohexanol ($\text{SH}-(\text{CH}_2)_6-\text{OH}$) [117] (see above). The binding site of the sulfur atoms, which are inferred to have a distance of ~ 2.9 Å to their neighbors, *cannot* be equivalent for all sulfurs, which is already clear from the incommensurability.

In [130] it was also attempted to analyze the degree of disorder from the width of various diffraction peaks. While with proper preparation at elevated temperatures a substrate-limited domain size of ~ 2000 Å can be reached, *within* these ordered domains there are still some fluctuations of the order. Both lattice disorder effects (fluctuations of the lattice spacing) and orientational disorder (distribution of the molecular axes in the film plane) were found, which is consistent with the observation of “meandering features” in the STM images.

In conclusion, the question concerning the location of the second thiol group leads to apparently conflicting results in the literature. For alkanedithiols the evidence from direct structural methods points towards very stable lying-down arrangements, which have a fairly complex ordering and binding behavior. These

structures with both thiols binding to the substrate are very difficult to overcome when trying to form standing-up structures, which, ultimately, should be the energetically most favorable configuration, at least for long enough hydrocarbon chains (see Sections 4.2.2 and 5). It may be that the standing-up configuration only forms with a very limited in-plane order due to the interacting headgroups. Rigid rod molecules, i.e., compounds with a different molecular backbone might promote a stable standing-up configuration. However, it remains to be checked if these compounds also form well-ordered structures in-plane, i.e., large ordered domains.

3.1.2.7. Alkylthiol SAMs with other terminations. The ability to engineer surface properties by a suitable choice of the endgroup is certainly one reason for the attractiveness of SAMs. Consequently, motivated also by possible technological applications many different systems have been studied. We will not attempt to review all the different endgroups that have been studied. The most common ones (like CH_3 , OH, COOH, etc.) have been discussed above, while for other compounds including those used for building multilayers, we refer to [33,36,56,115,122,131].

As a general trend one might conclude that alkylthiols with various endgroups can form the dense ($\sqrt{3} \times \sqrt{3}$) packing unless this is sterically prohibited or the endgroup–endgroup interaction causes deviations. Of course, as shown by the dithiol example and the discussion in Section 4, the molecules must have a chance to assemble in this structure (i.e., not be hindered by “kinetic traps”), which implies that also the endgroup–substrate or the backbone–substrate interaction should not be too strong, if a ($\sqrt{3} \times \sqrt{3}$) packing is anticipated.

3.1.2.8. Dialkyl disulfides and dialkyl sulfides. Disulfides have been among the first systems studied [29]. For the structure of dialkyl disulfides ($\text{CH}_3(\text{CH}_2)_{n-1}\text{S}-\text{S}-(\text{CH}_2)_{n-1}\text{CH}_3$) the general consensus appears to be that their structure is indistinguishable from that of the corresponding alkanethiols. This was concluded from several studies, employing AFM, XPS, contact angle measurements, and voltammetry [132–134].

In [122], the structures of various long-chain alkyl and perfluoroalkyl esters of bis(2-hydroxyethyl) disulfides (including also asymmetric compounds) were studied by AFM, showing a larger area per molecule than alkanethiols and frequently incommensurability.

Dialkyl sulfides ($\text{CH}_3(\text{CH}_2)_{n-1}\text{S}-(\text{CH}_2)_{n-1}\text{CH}_3$) were reported to be poorly ordered, presumably due to the lack of chemisorption (see [134,135] and discussion therein; see also Section 4.2.2).

Different groups have studied asymmetric dialkyl disulfides (with the second alkyl chain being shorter or fluorinated) in an attempt to clarify if the two chains separate upon adsorption, but the results appear to be not entirely consistent. While Jaschke et al. [122] and Schönherr et al. [136] (after annealing for 17 h at 100°C) do not observe phase separation, Ishida et al. [137] (after annealing for 8 h at 100°C in air), Heister et al. [138], and Noh and Hara [139] do observe deviations from the homogeneous mixture of the two different chains. We should note,

however, that even if the experimental findings were entirely consistent, their implications for the structure of alkanethiols (Section 3.1.1) would be only indirect. If the system does not phase separate, this could mean simply that the mobility of the molecules is not sufficient, but not necessarily that S–S bonds exist. If the asymmetric disulfides do separate, this could mean that the energy gain driving the separation (due to a presumably optimized chain–chain energy in the phase separated domains) exceeds a possible S–S interaction, which on the surface may be weak but non-zero.

3.2. An overview of various self-assembling systems and their structures

After illustrating the principal structural features and degrees of freedom using thiols on Au(1 1 1), we shall now provide an overview of other SAM-systems. Taking the model system of alkanethiols on Au(1 1 1) as a basis for comparison, changes of the molecules (e.g., alkenethiols or biphenylthiols on Au(1 1 1)) as one possible step have already been discussed above. Here, we first discuss other possible changes like the change of the substrate symmetry (Au(1 1 1) vs. Au(0 0 1) and Au(1 1 0)) or the change to another noble metal (Ag and Cu). After that we review results on substrates very different from Au (such as semiconductors, liquid mercury, and Fe). Then the class of silane-based SAMs is reviewed, with which we deal again later in the growth section. Finally, other systems (neither thiol-based nor silane-based) are briefly mentioned.

3.2.1. Thiols on gold surfaces other than (1 1 1)

By changing the Au substrate from (1 1 1) to (0 0 1), not only the symmetry of the monolayer (whose alkyl chains generally tend to prefer a hexagonal coordination) is changed. The more open surface (for an fcc-system like Au), the complex “ 5×20 ” reconstruction of the clean Au(0 0 1) surface, and size considerations (cross-sectional area occupied by one molecule) can have a strong impact. In fact, the study of alkanethiols on Au(0 0 1) revealed a non-trivial situation. While early results from electron diffraction suggested a $c(10 \times 10)$ structure [73], in [47] a $c(2 \times 2)$ -like structure was indicated.

As it was found in a combined LEAD and GIXD study of octadecanethiol on Au(0 0 1), the as-deposited structure can be very different from that of the annealed layer [140]. The equilibrium (annealed) structure of alkanethiol on Au(0 0 1) exhibits a very complex scenario. The LEAD pattern, i.e., the scattering from the topmost part of the SAM, showed a rectangular mesh with lattice spacings of $5.77 \text{ \AA} \times 23.08 \text{ \AA}$, consistent with a commensurate $c(2 \times 8)$ structure [140]. Compared to the LEAD data, GIXD (which is sensitive to the *entire* SAM) showed more diffraction spots. In fact, it was shown that the surface, the hydrocarbon backbone, and the interface all have a different diffraction pattern in terms of size and symmetry of the unit cell. The structure model taking into account all these features includes a $p(1 \times 4)$ array of Au adatoms, with alkanethiol molecules adsorbed both on the adatom array and on the lower-lying Au terraces, as discussed in detail in [50,140]. We note that in an STM study of butanethiol on Au(0 0 1), the same symmetry and

unit mesh size as above was found [141], but with the difference that missing rows of atoms instead of rows of adatoms were suggested. Unfortunately, on the basis of the data shown in [140], this issue (missing rows vs. adatom rows) cannot be resolved. Furthermore, the differences in the two studies (shorter chains and lack of annealing in [141]), limit the comparability.

From rodscans of octadecanethiol on Au(001), the tilt angle was found to be $\theta_t = (33.5 \pm 1.0)^\circ$ [140]. Together with the molecular coverage of $22.2 \text{ \AA}^2/\text{molecule}$ this results in a packing density of the hydrocarbon chains (projected along the hydrocarbon *tilt* axis) of $18.5 \text{ \AA}^2/\text{molecule}$, which corresponds to dense packing.

On Au(110), the LEAD data for alkanethiols (docosyl mercaptan) could be explained by unit mesh parameters $a = b = 4.99 \pm 0.08 \text{ \AA}$ and $\alpha = 109.5^\circ$, consistent with a commensurate $c(2 \times 2)$ lattice (in which the molecules have a quasi-hexagonal coordination) [142].

3.2.2. Thiols on other substrates

3.2.2.1. Thiols on Ag. The system alkanethiols on Ag(111) might be expected to be closest related to alkanethiols on Au(111), since it has the same symmetry, practically the same lattice spacing (4.09 vs. 4.08 \AA), and since Ag and Au are isoelectronic. Instead, as seen in Fig. 13, for alkanethiols on Ag(111) a structure very different from that of Fig. 5 (alkanethiols on Au(111)) was found [50,143]. This SAM is incommensurate with the Ag(111) lattice, forming a quasi-hexagonal structure with lattice spacings $a = 4.85 \text{ \AA}$ and $b = 7.61 \text{ \AA}$ [50], which is very similar to that of the orthorhombic phase of the bulk *n*-alkanes ($a = 4.96 \text{ \AA} \times b = 7.42 \text{ \AA}$). We note that this structure is coincident with a hexagonal ($\sqrt{7} \times \sqrt{7}$) $R10.9^\circ$ unit mesh if the triplets of diffraction peaks are coincident with single peaks [50] (see also Section 3.3).

The high molecular coverage ($18.5 \text{ \AA}^2/\text{molecule}$) implied by this unit cell suggests a smaller tilt angle than for alkanethiol on Au(111) ($21.6 \text{ \AA}^2/\text{molecule}$), which was confirmed by NEXAFS ($\theta_t \sim 10^\circ$ on average [144]), by SPS ($\theta_t \sim 0 \dots 18^\circ$ for $n = 11 \dots 19$ [145]), and by IR ($\theta_t \sim 12 \dots 13^\circ$) [146,147]. Using NEXAFS, the orientation of the S–C bond with respect to the surface normal was probed for octanethiol on Ag(111), resulting in a polar angle of $(39 \pm 4)^\circ$ [148].

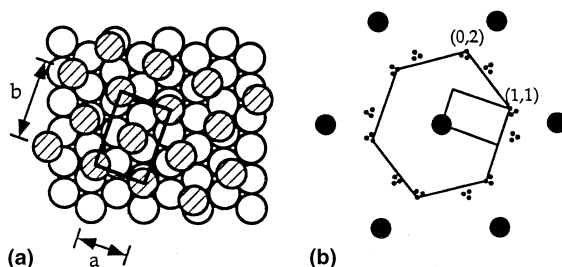


Fig. 13. 2D schematic of real space (a) and reciprocal space (b) picture of full-coverage SAM of alkanethiol on Ag(111). SAM lattice parameters are $a = 4.85$ and $b = 7.61 \text{ \AA}$. Note that, although lattice spacing of Ag is similar to that of Au(111), SAM structure is very different. From [50].

We note that also for 22-mercapto-1-docosanoic acid on Ag(111), an incommensurate monolayer with very small tilt angle ($\theta_t < 5^\circ$) was reported [149]. STM studies of alkanethiol on Ag(111) including an analysis of defects are found in [150,151].

Given that for these apparently very similar systems (alkanethiols on Au(111) and on Ag(111)) the SAM structures are so different, it is obviously a very delicate balance of the chain–chain interaction (which is the same here) and the headgroup–substrate interaction, which determines the structure. The observation of an incommensurate unit cell with higher molecular coverage ($18.5 \text{ \AA}^2/\text{molecule}$ vs. $21.6 \text{ \AA}^2/\text{molecule}$) and a smaller tilt angle suggests that the chain–chain interaction is maximized at the cost of not optimizing the binding site, i.e., at the cost of working against the substrate corrugation. Recent XSW data of octanethiol on Ag(111) report a low coherent fraction for the (11 $\bar{1}$) direction, which is consistent with the model of multiple sulfur binding sites [152]. These results imply that the thiols experience a lower corrugation on Ag(111) compared to Au(111).

3.2.2.2. Thiols on Cu. Cu is also isoelectronic to Au, but the lattice parameter is significantly different from Au (3.61 vs. 4.08 \AA). If the system assumed a ($\sqrt{3} \times \sqrt{3}$) structure, this would lead to an area of 17.0 \AA^2 per molecular site, which appears too small (compared to 18.4 \AA^2 for the cross-section of a straight hydrocarbon chain).

For alkanethiols on Cu(111), the IR spectra were reported to be essentially the same as on Ag(111), suggesting at least a similar tilt structure ($\theta_t \sim 12^\circ$) [146]. This was confirmed in recent studies employing NEXAFS [153,154] for various chain lengths ($n = 6, 8, 12$). However, it could be shown by NEXAFS that the tilt structure of octanethiol on Cu(111) is not exactly identical to that on Ag(111), since the polar angle of the S–C bond with respect to the surface normal is different ($23 \pm 3^\circ$) [148].

In fact, also the headgroup structure should be different for alkanethiols on Cu(111) compared to Ag(111), since the smaller lattice parameter makes a packing with the density of the 7×7 unit mesh sterically impossible. The headgroup structure appears to be complicated, and XSW data for octanethiol on Cu(111) were rationalized by a reconstruction of the Cu surface [154]. A very recent STM study of gas-phase deposited octanethiol on Cu(111) indeed revealed that after initial formation of a “honeycomb” structure a non-trivial higher-density “pseudo-(100)” structure is formed, which requires a significant reconstruction of the substrate. The results on the structure and the growth were interpreted in terms of a stronger interaction and corrugation experienced for the thiol group on Cu(111) compared to Au(111) [356]. Differences in the interaction (S–Cu vs. S–Au) were discussed theoretically by Vargas et al. [357].

Cu surfaces of other symmetry were studied in [155] (Cu(100)) and [156] (Cu(110); see also Section 4.2.2).

3.2.2.3. Alkanethiols on other metal surfaces. The preparation of alkanethiols on Fe and the specific measures to assure a clean surface and to remove the oxide layer were discussed by Stratmann [157,158]. From XPS and AES data it was concluded that the molecules are oriented predominantly perpendicular to the surface. Also the

stability in air and electrolytes was addressed [157]. Delhalle and coworkers discussed alkanethiols on Ni [159].

3.2.2.4. Alkanethiols on semiconductor surfaces. SAMs of alkylthiols with different terminations were prepared on GaAs(100). The IR data indicated a densely packed assembly of rodlike chains with a low degree of gauche defects [160]. Alkanethiol SAMs on InP(100) were described in [161,162]. For hexadecanethiol monolayers on InP(110), based on XANES data a high degree of order in the tilt angle ($\theta_t = 34^\circ$) and in the tilt direction was reported, which could be made plausible based on size considerations on this two-fold surface [163].

3.2.2.5. Thiols on liquid mercury. Liquid mercury is a somewhat exotic choice of a substrate, but it provides an interesting case for comparison. Thiols on mercury are an intermediate case between Langmuir films (weakly bound molecules on the surface of a liquid) and SAMs (strongly bound molecules on the surface of a crystalline solid) in that they experience a strong interaction with a liquid (disordered) substrate (or subphase). Using X-ray reflectivity, Magnussen et al. [28,32] found that alkanethiols of different chain lengths form well-defined monolayers with thicknesses in agreement with the length of fully extended molecules. The electron density ($0.34 \pm 0.02 \text{ e}/\text{\AA}^3$) was close to that found in crystalline alkanes and significantly higher than in the melt. Therefore, in-plane ordering of the molecules might be expected. Despite an exhaustive search with GIXD, no sharp in-plane peaks corresponding to an ordered adlayer structure were found for the monolayer phases of thiol molecules of any of the examined lengths ($n = 8, 12, 16, 18, 22, 30$), implying that the “competition” between the ordering tendency of the chain–chain interactions (as in Langmuir layers) and the disordered substrate is dominated by the latter.

3.2.3. Organosilicon monolayers and related systems on hydroxylated surfaces

Among the most studied systems in this category are alkyltrichlorosilanes, particularly octadecyltrichlorosilane (OTS, $\text{CH}_3-(\text{CH}_2)_{17}-\text{SiCl}_3$), on different hydroxylated surfaces such as oxidized silicon or mica. Also glass can be used as a substrate, as done in one of the first studies of silane-based SAMs [30]. A related popular system is octadecylphosphonic acid (OPA, $\text{CH}_3-(\text{CH}_2)_{17}-\text{PO}(\text{OH})_2$) on mica.

In the frequently assumed bonding scenario for OTS, the chlorines are split off, and the molecules are bound to the surface and to each other by a Si–O–Si network. This is shown schematically in Fig. 14. However, it has been argued [164,165] that this scenario cannot be directly applied to full coverage monolayers. With a typical Si–O bond length of 1.6 Å, the O–O distance has to be 3.2 Å or less (for a O–Si–O bond angle of less than 180°), which would not leave enough space for parallel, upright-standing hydrocarbon chains. The chains would have to be splayed apart, implying that cross-linked headgroups would prevent the formation of a full-coverage layer or, reversely, that a full-coverage layer cannot be

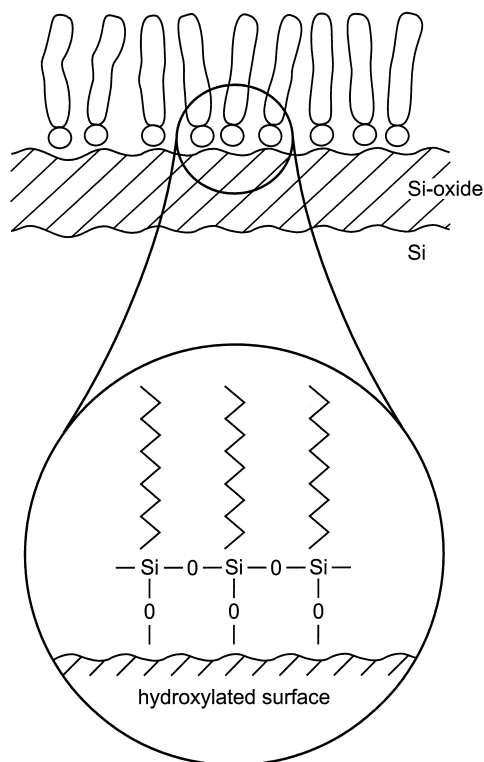


Fig. 14. Schematic of monolayer of *n*-alkyltrichlorosilane ($\text{CH}_3-(\text{CH}_2)_{n-1}-\text{SiCl}_3$) on hydroxylated surface like silicon oxide. Note that layer does not exhibit long-range (crystalline) order. Magnified part shows schematic of cross-linked headgroups, as frequently assumed. However, it has been argued that full cross-linking is sterically hindered [164,165].

fully cross-linked [165]. In this context, a comparison with the recent results by Fontaine et al. [166] for octadecyltrimethoxysilane *on water* is interesting. These imply that the extent of (hexagonal) order is a decreasing function of the number of cross-links. Obviously, the possible cross-linking at partial coverages and the related steric constraints can have a strong impact on the structure and the growth.

For the in-plane structure of OTS grown from solution on Si(001) wafers (with native silicon-oxide), using GIXD Tidswell et al. [167] found only one broad scattering ring at 1.5 \AA^{-1} . The molecules appear to be packed with un distorted hexagonal local order and a mean area per molecule of 20.2 \AA^2 . The width of the diffraction peak corresponds to a translational correlation length of only about 45 \AA and the Lorentzian line shape (in reciprocal space) to an exponential decay of order in real space. The authors concluded that the in-plane order in these SAMs is more "liquid-like" (in a static sense of a disordered structure, not in the sense of being fluid) and no evidence for a truly crystalline structure was found [167].

With the in-plane structure being rather disordered, the main structural feature to be characterized is the tilt angle or the resulting thickness and the electron density. The thickness, i.e. the electron density profile along the surface normal was analyzed in [54,67] by XR and ellipsometry, including various chain lengths and also brominated compounds. A tilt angle of $\sim(20 \pm 4)^\circ$ was derived from the thickness [54,67]. However, the determination of the tilt angle from the effective thickness is somewhat indirect and not very precise, particularly, since the change of the effective thickness with tilt angle goes as $\cos(\theta_t)$, and, therefore, is not very sensitive at small angles. Nevertheless, it is consistent with a quick decay of intensity of the GIXD peak with q_z (rodscan), which results in a maximum possible tilt angle of $\sim 21^\circ$ [167].

With other techniques, also small tilt angles were found. Allara et al. [168] reported $(10 \pm 2)^\circ$ for the tilt angle and a significant density of gauche defects at the chain ends as evidenced by IR. Vallant et al. [169] found about 7° also with IR techniques and a slight increase in the tilt angle upon chain length reduction or introduction of a terminal functionality R (R = COCH₃, CN, Br) in a C₁₆ chain. In a combined NEXAFS and XPS study, Bierbaum et al. [170] found the tilt angle of OTS on oxidized silicon to be less than 10° . Furthermore, they report that *n*-alkyl-trichlorosilanes with longer as well as with shorter chain-length than OTS form less well ordered films in terms of the orientation of the chain. Similar studies of related compounds are reported in [171,172].

Despite a certain spread for θ_t , the general consensus is that the tilt angle is smaller than for alkanethiols on Au(111), which is understandable since the intermolecular spacing is less than for thiols on Au(111) (where the 5 Å are induced by the substrate corrugation), since the primary driving force for tilt is the maximization of the van der Waals contact of the chains. Obviously, for a denser packing of molecules per area, less tilt is needed.

To summarize the results from various techniques, it is generally agreed upon that OTS on oxidized silicon forms films of about 25 Å thickness, that they are mostly in the all-trans conformation exposing the terminating methyl group, and that the tilt angle is small (at most $\sim 20^\circ$). The in-plane structure is “liquid-like” (in a static sense) with a mean area of $\sim 20 \text{ \AA}^2$ per molecule and a very limited correlation length.

3.2.4. Other systems

Besides the above systems, which are the most thoroughly studied, several others have been prepared.

Selenols have been investigated as alternatives to thiols [173–175]. For docosaneselenol on Au(111) grown from solution, a fairly small coherence length of about 60 Å in an incommensurate structure with a tilt angle of about 15° was found [173].

Starting with H-terminated silicon (obtained after removal of the native oxide layer), Linford and Chidsey [38] have demonstrated the attachment of monolayers to the Si substrate by forming direct C–Si bonds. This concept has been followed also

in [176,177]. Alternative routes for linking of SAMs to H-terminated Si have been discussed in [178–180].

The formation of alkylsiloxane SAMs on Si_3N_4 has been discussed by Sung et al. [181].

Other ways for the chemical coupling to the substrate are monolayers of acidic compounds on metal oxide surfaces (see, e.g., [33,182]).

The formation and stability of SAMs on engineering metals such as steel, stainless steel, aluminum, copper, and brass has been discussed by Van Alsten [183].

An interesting area with implications for mineralogical issues is the formation of layers on mineral surfaces. As an example, stearate monolayers on calcite surfaces were studied and the molecules were found to form well-defined monolayers in an essentially standing-up configuration [184]. Remarkably, in this system the monolayer coverage is controlled reversibly by the concentration of stearate molecules in the ethanolic solution, in contrast to most other SAM systems, in which the adsorption process is largely irreversible.

3.3. Temperature-related issues: structural phase transitions, thermal stability, and desorption

The structures discussed above refer to room temperature. A thorough analysis of the structures formed by self-assembly, however, certainly has to include the effect of temperature. Generally, upon increasing the temperature of the SAM, different processes can occur, such as

1. solid–solid phase transition (e.g., commensurate–incommensurate);
2. solid–liquid phase transition (melting);
3. desorption (see also Section 4.3);
4. dissociation of the molecules.

In addition, at moderate temperatures annealing effects like healing of defects or domain size growth can be important. Besides contributing to a more fundamental understanding, the investigation of these temperature-related issues is also very important for any technological application based on SAMs, since obviously a certain thermal stability is required. As an example for very stable SAMs we will discuss the silane-based systems.

Phase transitions in reduced geometry are a very fundamental issue, which has attracted also significant theoretical interest [49,185]. SAMs are a paradigmatic case for well-defined 2D systems chemically bound to a substrate, and it turns out that thiols on Au(111) are suitable for the study of phase transitions. An interesting feature of SAMs from a fundamental standpoint is that they have internal degrees of freedom (like the orientation of the molecular backbone) and different competing interactions (van der Waals for the chain–chain interaction and a covalent interaction between the headgroup and the substrate). Compared to other (simpler) two-dimensional systems like noble gases on graphite this introduces a higher degree of complexity and raises, e.g., the question whether the chains can melt first and the headgroups only at a later stage, i.e., if there is a two-step melting process. Langmuir

films can serve as a guide, but the chemisorbed headgroup and the periodic substrate potential (in the case of Au(111)) introduce important differences. For SAMs, the number of studies of their phase transitions is not yet as high as for simpler two-dimensional systems, but some degree of understanding has been reached, as summarized briefly below.

3.3.1. Alkanethiols on Au(111)

3.3.1.1. Melting curve (full coverage). The melting of a full-coverage decanethiol SAM on Au(111), as derived from the temperature dependence of the integrated intensity of the hexagonal ($\sqrt{3} \times \sqrt{3}$) diffraction peaks, is shown in Fig. 15. The phase transition is at about 100°C, i.e., $\approx 125^\circ\text{C}$ higher than in the bulk ($T_{\text{melt}}^{\text{bulk}} = -26^\circ\text{C}$) [40,186]. Apparently, the crystalline structure is stabilized by the chemical bond to the substrate with its periodic corrugation. The disappearance of diffraction intensity above 100°C is, in fact, due to the transition of the layer to a melted (“liquid”) state, and desorption is only a small effect (it takes place at still higher temperatures and will be discussed in the context of the interaction energies in Section 4.3). This was confirmed by regaining the intensity upon cooling to room temperature. The presence of a liquid state has also been inferred from STM data for shorter chain lengths [187].

It should be noted that the determination of the exact shape of the melting curve and the nature of the transition (e.g., first vs. second order) is rather difficult, since the usually small GIXD signal from organic monolayers limits the dynamic range. Also, a small but finite rate of desorption can change the coverage, Θ , during the experiment. Since T_{melt} is strongly dependent on Θ , this can change the shape of the melting curve. A way to overcome this problem would be to work with a certain

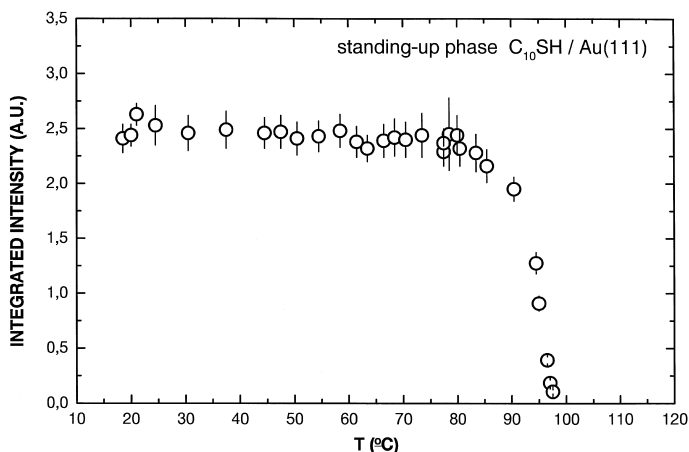


Fig. 15. Melting of full-coverage decanethiol SAM on Au(111) as derived from integrated intensity of hexagonal ($\sqrt{3} \times \sqrt{3}$) diffraction peak measured by GIXD. Phase transition at about 100°C is $\approx 125^\circ\text{C}$ higher than in bulk ($T_{\text{melt}} = -26^\circ\text{C}$). From [186].

background pressure of thiols to compensate for the desorption, but this has not been done with SAMs yet.

Recently, an interesting effect was discovered [186] for a full-coverage decanethiol SAM capped by a molecular crystalline film of 3,4,9,10-*perylene*tetracarboxylic dianhydride (PTCDA), a compound used frequently in OMBE [25–27]. The melting temperature is increased to $\approx 115^\circ\text{C}$ if the SAM is capped by a van der Waals bound PTCDA layer [186]. This sandwich structure will be discussed again in the context of organic–organic epitaxy (Section 3.4).

3.3.1.2. Coverage dependence. The melting temperatures as obtained from plots like Fig. 15 are summarized in Fig. 16 for different coverages [40]. The phase diagram of Fig. 16 comprises both “thermodynamic” measurements (as a function of temperature, T , at a given coverage, Θ) and “growth” measurements (as a function of coverage, Θ , at a given temperature, T). The growth measurements and the questions related to the appearance of different phases for $\Theta < 1$ will be discussed in Section 4. At this point we shall only note that both data sets were in agreement with each other, implying that the behavior shown including the phase boundaries reflects intrinsic equilibrium behavior [40].

We shall discuss the standing-up phase first. One of the obvious features of Fig. 16 is the pronounced coverage dependence of the melting transition. This thermody-

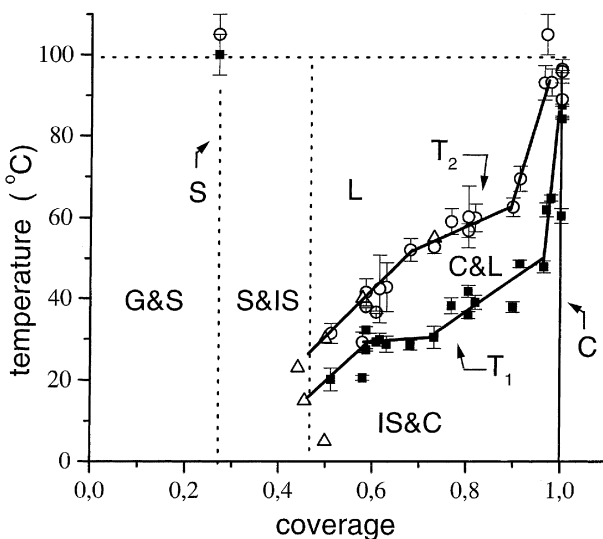


Fig. 16. Phase diagram of decanethiol on Au(111) in temperature and coverage space. Different regions and phases are denoted as G (“lattice gas”), S (stripes), IS (intermediate structures, which are explained in Section 4.2.1), C ($c(4 \times 2)$), and L (liquid). Temperatures T_1 and T_2 denote onset of melting (i.e., the beginning of significant decrease of GIXD intensity; filled squares) and completion of melting ($= T_{\text{melt}}$; open circles), respectively. For $\Theta \rightarrow 1$, transition is fairly sharp, so that T_1 is close to T_2 . Open triangles denote onset of the $c(4 \times 2)$ phase in kinetic real-time measurements during growth at given temperature, in good agreement with data points from melting. From [40].

dynamic behavior is characteristic of many (sub-)monolayer systems (e.g., N_2 on graphite [188]), where the melting point depression at reduced coverage has been shown to be related to the entropy of the high-temperature phase. The overall similarity of $T_{\text{melt}}(\Theta)$ for these chemically very different systems suggests that entropic contributions (e.g., from configurational entropy and conformational entropy due to gauche defects) also play an important role in the SAM thermodynamics. Also from a naive mechanistic approach it appears very plausible that, for sub-monolayer coverages, creating the space needed upon disordering (melting) is easier for reduced coverage. The low melting point at the onset coverage of the $c(4 \times 2)$ phase will become important again in the growth section.

The above discussion of the coverage dependence of the melting transition refers to the standing-up phase. If the coverage is so low that the lying-down phase is formed, the melting temperature can again be high. In fact, a decanethiol SAM with $\Theta = 0.27$ can actually be viewed as a “full-coverage” layer of the striped phase. Fig. 17(a) shows the melting curve for a striped phase layer with a transition temperature of about 100°C . Knowing that layers with the “ideal coverage” for a certain structure are thermodynamically particularly stable, it is not surprising that the melting temperature is as high as for the standing-up phase with $\Theta = 1$.

3.3.1.3. Chain length dependence of phase behavior. The phase behavior as a function of chain length, n , and temperature, T , is summarized in Fig. 18 (for $\Theta = 1$). If the chain length is increased above $n = 10$, the $c(4 \times 2)$ lattice is preserved, but the tilt structure is slightly different in the long-chain regime, as discussed in Section 3.1.1. Therefore, C_S and C_L both denote the $c(4 \times 2)$ structure, but distinguish the short and the long chain length tilt regime. For longer chain lengths, also the high-temperature behavior is different in that for $n \geq 14$ a solid–solid phase transition takes place and an incommensurate phase is found between the commensurate $c(4 \times 2)$ phase (C) and the melted phase (L) [50,78].

The existence of an incommensurate phase at higher T for longer chains has several implications. First of all, its appearance only for longer chains shows that it is driven by the chain–chain interaction, which dominates for large n . Second, it demonstrates that commensurability with the substrate is not required for the monolayer to remain solid. Third, it suggests that if the substrate corrugation is weaker than for the present case of $\text{Au}(111)$, incommensurability can prevail. This is consistent with the results found for alkanethiol on $\text{Ag}(111)$ compared to $\text{Au}(111)$. Finally, both the (n, T) phase diagram and the (Θ, T) phase diagram underline the richness of the phase space in these systems, the resulting structures of which are determined by a balance between several interactions.

3.3.1.4. Evolution of disorder, gauche defects, and Debye–Waller factor. As can be seen from Fig. 15, for temperatures well below T_{melt} , the GIXD intensity from a full-coverage layer changes little with temperature. This might be interpreted as the close packing in the crystalline structure (induced by the substrate) making this “soft” material “harder” compared to bulk alkanes. Nevertheless, with increasing temperature, defects like gauche conformations will be accumulated, thus reducing the

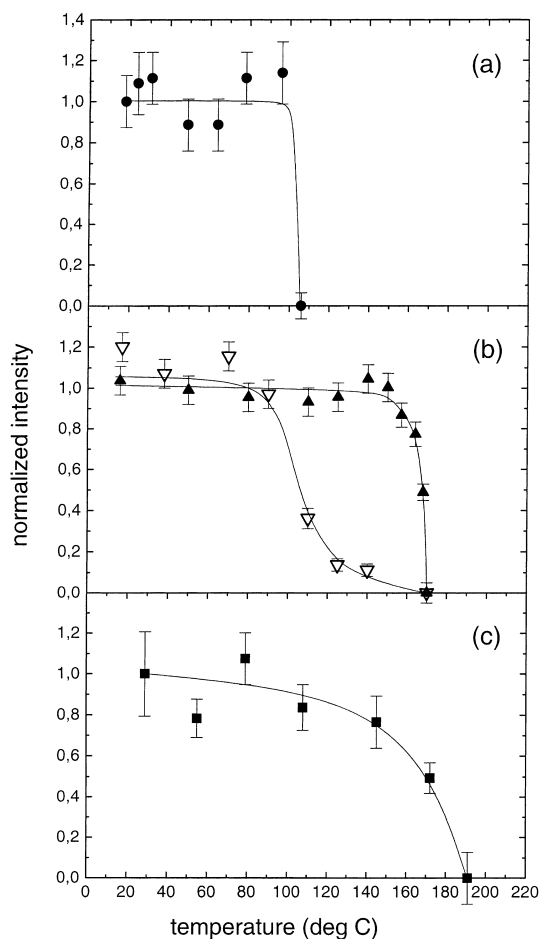


Fig. 17. Temperature dependence of integrated GIXD intensities of principle Bragg peaks for three different thiol-based systems on Au(111) in lying-down phase. (a) decanethiol [355], (b) 4-methyl-4'-mercaptobiphenyl (MMB) [110], and (c) 1,6-hexanedithiol [130]. In (b) pronounced hysteresis was observed; open symbols refer to signal upon cooling down (see text). Note that in (c) decrease of intensity is accompanied by desorption (i.e., curve cannot be reversible). Therefore, curve does not only include melting effects, and 460 K (at which all Bragg intensity is lost) should be interpreted as “lower limit” of melting temperature. In simple picture, increase in thermal stability in this series from (a) to (b) to (c) reflects increasing molecule–substrate interaction.

order in the monolayer. This is expected to be most visible at the chain termini and should play a central role in defining the temperature dependence of the structure.

LEAD as an exclusively surface-sensitive technique in fact reveals that there is a significant reduction of order in the methyl-endgroups as a function of temperature. As will be discussed below, the comparison with MMB shows that for a system with a stiffer backbone the DW attenuation determined by LEAD is significantly smaller

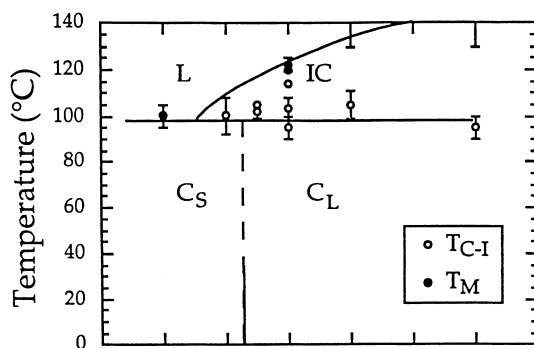


Fig. 18. Phase diagram (n, T) of alkanethiols on Au(111) as function of chain length and temperature for full coverage. C_S and C_L both denote $c(4 \times 2)$ structure, but distinguish the short and long chain length tilt regime as discussed in Section 3.1.1. For longer chain lengths ($n \geq 14$) an incommensurate phase (IC) is found between commensurate $c(4 \times 2)$ phase (C_L) and the melted phase (L). Full symbols mark melting transitions, whereas open symbols mark commensurate–incommensurate transitions. From [50].

[110], implying that the evolution of surface disorder is, of course, not decoupled from but related to the “interior” of the layer.

Using IR, the conformation of the molecules as a function of temperature can be nicely followed. First of all, Nuzzo et al. [76] showed that the type of the canted, rotated structure of the alkyl chain described for the room temperature data must also be present at the lower temperatures, consistent with the evidence from LEAD that the $c(4 \times 2)$ structure is prevailed. This is indicated by the relative intensities of the d^+ and d^- modes (i.e., the symmetric and antisymmetric C–H stretches in the methylene groups) as measured on docosanethiol ($n = 22$).

Secondly, the evolution of defects was investigated. Gauche defects were shown to be essentially quenched below 200 K. At room temperature they reach a level of about 1% and increase further at higher temperatures [35,76], with the temperature dependence exhibiting a striking similarity with results from molecular dynamics simulations [189]. Furthermore, it was shown that the defects are concentrated at the chain termini [190]. Similar IR data including also higher temperatures were presented by Bensebaa et al. [191].

The splitting of the methylene scissors mode (mentioned in the context of the structure model of the $c(4 \times 2)$ phase in Section 3.1.1) becomes clearly visible at about below 220 K for docosanethiol. For shorter chains, this appears at still lower temperatures, which is qualitatively understandable, since also the temperatures for phase transitions (melting) are lower for shorter chains.

The thermal behavior was investigated also by NMR. Insight in the ordering behavior along the chain (as a function of distance from the surface) was provided, but the use of colloidal gold particles seems to limit the comparability with planar gold substrates. Since the surface curvature of the particles causes small terraces, the absolute values of transition temperatures can be underestimated [192,193].

3.3.2. Biphenylthiols on Au(111)

Phase transitions. The alkanethiol data can be compared to MMB, which has both the same methyl endgroup and about the same overall length as decanethiol. As discussed in Section 3.1.2, MMB also exhibits a low-coverage (“lying-down”) and a high-coverage (“standing-up”) phase. The important difference to the alkanethiols is the more rigid molecular backbone. This is expected to have a strong impact on the thermal behavior. In fact, the melting temperature is higher than for decanethiol both for the case of the lying-down and for standing-up phase. The thermal behavior of MMB was investigated in [110], which we will summarize below.

The melting curve of the lying-down phase (Fig. 17(b)) shows a melting temperature, T_{melt} , of $(170 \pm 5)^\circ\text{C}$ (443 K), i.e., about 70 K higher than for decanethiol (lying-down). The higher transition temperature is plausible based on the higher interaction energies. The energy contributions can be quantified based on the analysis of TPD data discussed in Section 4.3, and they confirm the stronger molecule–substrate interaction [110]. Moreover, the 80 K higher bulk melting point of 4-methyl-biphenyl (the backbone of MMB) compared to *n*-decane (the backbone of decanethiol) underlines that also the molecule–molecule interaction is stronger in MMB.

From Fig. 17(b) one can also see that the transition is rather abrupt and exhibits a strong hysteresis (with a “width” on the temperature axis of about 60 K), which is typically taken as suggestive of the transition being first-order-like. We should emphasize, however, that due to the limited GIXD signal from a monolayer of organic material a detailed study of the exact nature of the transition has not been performed so far.

Also for the standing-up phase a higher melting temperature than for decanethiol was found, consistent with the above interpretation of stronger interactions and greater stiffness in MMB. Unfortunately, the standing-up phase was not a full-coverage layer. Therefore, the value of about 140°C or 413 K reported in [110] can only be considered as a *lower limit* for T_{melt} , since it is known from the studies of alkanethiols that the melting temperature can be a strong function of coverage. One may expect that the melting temperature will be still higher for $\Theta \rightarrow 1$.

Thermal expansion and structural changes. It was found that the thermal expansion of the lying-down phase is more than 10 times higher than that of the substrate. Therefore, the structure cannot be commensurate over the entire temperature range. For the standing-up phase, this issue was not resolved, but it was found that the tilt angle in the standing-up phase apparently does not change significantly at least up to 376 K, as evidenced by the rods can data [110].

Debye–Waller factor. Related to the rigidity of the molecules, the diffraction intensity of the lying-down phase decreases only slightly with increasing T , implying a small DW factor. In the standing-up phase, the DW factor was also small, but since in the GIXD experiments only a partial monolayer of the standing-up phase could be prepared, this could not be checked reliably at higher temperatures. In the low-temperature regime, the DW factor was investigated by LEAD [110]. The decrease of LEAD intensity, analyzed in terms of du_z^2/dT (in $\text{\AA}^2/\text{K}$), yields $0.6 \pm 0.05 \times 10^{-4}$ for the standing-up phase of MMB. This was compared to $2.2 \pm 0.1 \times 10^{-4}$ for the

standing-up phase of decanethiol and $0.32 \pm 0.03 \times 10^{-4}$ for bare Au(111). Obviously, the DW factor of MMB is significantly lower than that of decanethiol in the full-coverage phase, and MMB has to be considered much stiffer, which is understandable for this aromatic molecule.

3.3.3. Dithiols on Au(111)

SAMs of 1,6-hexanedithiol on Au(111), which were found to form two slightly different 1D incommensurate lying-down phases (termed IC1 and IC2), were investigated as a function of temperature in [130]. The structures remained incommensurate even upon annealing, with the relative content of the phase of slightly higher density (IC1) gaining at the cost of IC2. The total diffraction intensity (i.e., the degree of ordering) remained essentially unchanged up to 120°C (393 K), while significant desorption was found to take place above 150°C (423 K). After heating to 190°C (463 K) for about 2 min, the diffraction intensity dropped to the noise level. Still, compared to the lying-down phases of decanethiol and MMB, the phase transition temperature (for which, due to desorption, we can only give a lower limit) is highest for 1,6-hexanedithiol (≥ 460 K), reflecting the strong molecule–substrate interaction (see Fig. 17).

The findings for 1,6-hexanedithiol were interpreted by the following scenario. The as-deposited layers are composed of the two incommensurate phases IC1 and IC2. Upon annealing, the molecules start diffusing, resulting in larger domains with the IC2 \rightarrow IC1 transition taking place. Upon further heating, the molecules desorb from the IC1 phase, i.e., desorption takes place before melting can be found. We note that 1,6-hexanedithiol SAMs are thermally more stable than decanethiol SAMs, although their bulk boiling points are very similar. Obviously, this is just the influence of the second thiol group being strongly attached to the substrate.

3.3.4. Alkanethiols on Ag(111)

In [50], the orthorhombically distorted quasi-hexagonal (room temperature) structure was found to exhibit an irreversible change that evolved continuously into a hexagonal structure as the annealing temperature was raised above 90°C. This means each triplet of peaks defining the orthorhombically distorted monolayer coalesced into a single peak ($(\sqrt{7} \times \sqrt{7})$ R10.9° structure). Coupled with this change in lattice spacings was a related decrease in the GIXD intensity. At sufficiently high temperatures ($T > 110^\circ\text{C}$) the diffraction pattern was found to disappear, presumably due to desorption of the monolayer [50]. With regard to temperature behavior of the alkane chains, Bensebaa et al. [191] reported differences between alkanethiols on Ag(111) and on Au(111) based on IR data.

3.3.5. Alkanethiols on Cu

The phase behavior of heptanethiol on the open surface of Cu(110) was investigated in [156]. At low temperatures (< 200 K) multilayers are formed, which should, in fact, be a fairly general scenario for most systems, although not frequently investigated. Ordered monolayer structures are found around 300 K, while it is reported that for $T > 370$ K the S–C bond is cleaved and the alkyl chains desorb, in

contrast to what is found on Au(111). This system will be discussed further in the context of growth from the gas-phase (Section 4.2.2).

3.3.6. Silane-based SAMs

As explained in Section 3.2.3, for OTS grown on silicon oxide, on which we want to focus here, the in-plane order was generally found to exhibit rather short correlation lengths. Tidswell et al. [167] determined the (in-plane) thermal expansion coefficient of the monolayer to be $(5.2 \pm 0.5) \times 10^{-4}/\text{K}$, compared to $3 \times 10^{-6}/\text{K}$ of the silicon substrate. They found that any change of temperature (both increase and decrease) resulted in a further reduced correlation length of the monolayers (prepared at room temperature), probably a result of the frustration of the chains with a higher thermal expansion coefficient locked to the substrate.

Early work on the thermal stability was done by Sagiv and coworkers [194] using IR, comparing the thermal behavior of SAMs and LB films. They found that the covalently bound OTS SAMs are thermally more stable.

Calistri-Yeh et al. [195] investigated the effect of annealing on the monolayer properties by contact angle measurements and scanning force microscopy and reported detectable changes at temperatures around 125°C (398 K) to 155°C (428 K), depending on the monolayer chain length and the agent used in the contact angle experiment. Annealing effects for OTS on mica were studied in [196].

Maboudian and coworkers [197,198] investigated the behavior at higher temperatures. They reported that the monolayers are stable up to about 467°C (740 K), above which point the chains begin to decompose through C–C bond cleavage. The siloxane headgroups remain on the surface following decomposition of the monolayers until about 827°C (1100 K) [197]. Alkyl monolayers formed by reaction of 1-alkenes with hydrogen-terminated silicon surfaces were reported to be stable up to 342°C (615 K) [177].

For silane-based SAMs covered with solution-grown ZrO₂ (see Section 3.4.5), the thermal stability, particularly at the upper SAM-interface, was investigated in [55]. Upon heating, it was found that the ZrO₂ layer densifies and that the effective SAM thickness slowly decreases with T .

3.4. More complex structures: lateral structuring, multi-component structures, surface reactions, and heterostructures

In the preceding sections, we have been focussing on relatively simple and homogeneous single layers, with the help of which the general principles governing the structures can be studied more easily. Here we attempt to provide a brief overview of the use of SAMs in more complex systems, several of which are attractive from the applications perspective. In this broad area, the references provided here are rather exemplary and by no means complete.

3.4.1. Lateral structuring

The possibility to laterally pattern SAMs is one of the reasons for their attractiveness. Different routes have been developed, of which we only mention the basic

ideas. For further account of these techniques we refer to the review by Whitesides et al. (see [32] and references therein).

Traditionally very important for microstructuring surfaces is lithography. Different techniques have been employed including UV lithography, electron beam lithography, scanning probe lithography, and focused ion beam lithography [32]. An interesting alternative is the use of neutral metastable atoms for lithographic purposes [199–201].

Among the above lithographic techniques, UV lithography has the lowest lateral resolution (several 100 nm), but can pattern the largest area in a single step ($\sim 50 \text{ cm}^2$) [32]. In contrast, with scanning probe lithography a resolution in the nanometer range can be achieved, but for technological applications the disadvantage is clearly that very small areas have to be patterned step by step [32].

Recently, Mirkin and coworkers [202,203] demonstrated an interesting technique called “dip-pen” nanolithography, where an AFM tip is used to write alkanethiols with a resolution down to 50 Å on a gold film in a manner analogous to that of a dip pen. This method works in the positive printing mode and exploits capillary transport of the admolecules in a water meniscus formed between the AFM and the substrate. Liu and coworkers developed “nanografting” as another AFM-based technique for the fabrication of nanometer scale patterns within SAMs [204].

A versatile and inexpensive alternative to the above techniques has been developed in the form of *microcontact printing* (μCP) [32,205,206]. The scheme of μCP is sketched in Fig. 19. An elastomeric stamp with the desired surface relief pattern is “inked” with SAM precursor molecules (e.g., alkanethiols) and printed onto the surface. Only the regions that come into contact with the stamp are covered with the SAM. In μCP , the autophobicity of the already-formed SAM causes the SAM precursor to retract and prevents spreading beyond a certain distance and, thus,

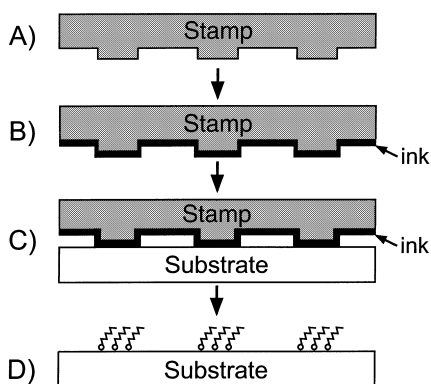


Fig. 19. Schematic of microcontact printing (μCP) technique for lateral structuring. Laterally structured elastomeric replica (stamp) (A), is “inked” with self-assembling molecules (B) and then printed to substrate (C). After release of stamp (D), laterally structured SAM is obtained on substrate. Applications can make use of either structured SAM itself or use SAM as etching mask to obtain structured substrate.

helps to obtain laterally well-defined structures [32]. For further discussion of the prospects and limitations of μCP , we refer to [32,206].

As alternative methods in the context of lateral structuring we should mention also the photoactivated preparation and patterning of SAMs with 1-alkenes and aldehydes on silicon hydride surfaces [178] as well as the use of micromachining in combination with SAMs, which has been demonstrated in [207] with a lateral resolution of the order of 100 nm.

Furthermore, naturally formed structures can be exploited, like the dendritic shape of the islands of OTS, which can be used as an etching mask [208]. Mixed SAMs, which are discussed below, also have a certain potential for structuring.

3.4.2. Multi-component and mixed SAMs

One of the ideas driving the interest in multi-component SAMs is to tailor the surface energy and the wetting properties by mixing appropriate ingredients, e.g., hydrophobic CH_3 -terminated and hydrophilic OH-terminated compounds. Furthermore, chemical patterning of surfaces has attracted some attention. Besides the interest in the adsorption and wetting properties, which are subject of the next paragraph, a very fundamental question in these systems is whether the different species will exhibit phase separation.

Several groups have investigated the problem, using different systems (different endgroups and chain lengths) [33,113,136,209–211]. Whitesides and coworkers studied various systems of mixed SAMs and found indications that the phases separate to some extent, but no complete phase separation [210,211]. Bertilsson and Liedberg [113] conclude random molecular mixing rather than phase separation from their IR data, which indicate no traces of intermolecular interactions (hydrogen bonding) between neighboring OH groups mixed with CH_3 -terminated molecules. In [136] the effect of heat treatment was investigated, but only a very low or non-existing mobility of the molecules within the layer was concluded, and heat-induced phase separation was excluded (on the time scales under consideration, i.e., several hours).

Phase separation on the nanometer scale (islands a few nanometers large) was reported from STM data, but no large-scale domains were found [209]. Deviations from random mixing were also found in a study of OH- and CH_3 -terminated alkanethiols for various chain lengths if the chain length of the methyl-terminated species was significantly greater [212]. Phase separation for alkanethiols of strongly different chain length grown at specific solution concentration ratios was observed by AFM [213]. Since some degree of phase separation takes place (as confirmed also by time-dependent measurements which showed coarsening of the domains to some extent), one might speculate that the true equilibrium structure in some systems actually consists of phase separated domains. This notion is supported by simulations of Siepmann and McDonald [214], although the authors later pointed out certain shortcomings of their work [32]. However, in a real film after finite time scales, with the apparently low mobility of the molecules in a once-formed SAM, phase separation seems to be strongly hindered, at least to the extent that it is not observed on a *macroscopic* scale.

An extreme case of mixed SAMs is the dilution of a “guest component” in a “host SAM”. The idea to “support and hold up” a guest molecule in a sea of “nonconducting” alkanethiol molecules in order to study its electrical properties was used, e.g., in [215,216] (see also Section 5.3).

3.4.3. Adsorption on SAMs

A very attractive feature of SAMs is the possibility of using them to tailor, by virtue of different endgroups, the surface energies and, thus, the adsorption properties. Here we shall distinguish the cases of “simple adsorbates” like alkanes or H₂O as used as, e.g., wetting agents, and “complex adsorbates” like proteins.

“Simple” adsorbates on SAMs and wetting. The perhaps most prominent examples for studies of simple adsorbates are related to wetting [33,34,63,217–221]. H₂O, which probes the polar characteristics of a surface, has a high contact angle on CH₃-terminated SAMs ($\theta_a \approx 110^\circ$), i.e., it tends to dewet. On the other hand, H₂O tends to wet OH-terminated SAMs, i.e., θ_a is small ($0 \dots 10^\circ$).

If hexadecane is used as a wetting agent, the contact angle on CH₃-terminated SAMs is $\sim 45^\circ$ (with differences for alkanes of other chain length). OH-terminated SAM-surfaces are wet by hexadecane ($\theta_a = 0^\circ$). The differences between alkanethiol surfaces with CH₃- and with CF₃-termination, the latter of which leads to an overall decrease of the surface tension, were discussed in [222].

In the context of surface engineering it is very useful that the contact angle can be tuned by a suitable choice of the endgroup or a mixture of different endgroups. In fact, as shown by several groups, the contact angle of, e.g., H₂O can be continuously tuned by the relative concentration of CH₃ and OH endgroups [33,63,217–219].

Since the interactions with the adsorbates are essentially determined by the outermost few Angstroms, SAMs and their adsorption and wetting behavior can also serve as models for polymer surfaces. The energetics of several adsorbates based on TPD data for various surface-terminations was discussed in [63].

For some adsorbates, also the structural phases have been determined. For instance, for the important case of H₂O, different phases adsorbed on SAMs are reported in [219,223,224]. Overlayers of Xe, Kr, H₂O, CH₃OH, and *n*-C₆H₁₄ physisorbed on CH₃-terminated SAMs were investigated by LEAD [225]. Among the adsorbates studied, only Xe and Kr showed order detectable by LEAD.

Adsorption of bio-related molecules on SAMs. Besides the adsorption properties for simple wetting agents, the (potentially selective) adsorption of large, bio-related molecules is of great interest [226–232]. The molecular conformation in *oligo(ethylene glycol)* (OEG) terminated SAMs and its influence on protein adsorption was studied in [233,234]. It was found that the predominantly crystalline helical and the amorphous forms of OEG on gold substrates are resistant to adsorption of proteins, while a specific densely packed “all-trans” form present on silver surfaces adsorbs proteins. The relevance of an interfacial water layer for the observed effects was discussed [233,234]. Petrash et al. [235] studied the variation in tenacity of

protein adsorption on SAMs with monolayer order by XR. Other work on bio-related molecules, in some cases immobilized directly on the (inorganic) substrate, i.e., with the biomolecule itself forming the SAM, can be found, e.g., in [236–238]. Although here we cannot go into the details of this fascinating area, clearly the use of concepts from self-assembled monolayers to tackle problems of biological relevance provides great opportunities also from the applications perspective (see also Section 5.3).

3.4.4. Chemical reactions of SAMs with adsorbates

The ability to customize the endgroup makes SAMs very attractive for the study of surface reactions, some of which are difficult to investigate otherwise. SAMs with hydroxyl (OH) or carboxylic acid (COOH) termination were investigated by several groups.

Poirier et al. [117] found that the adsorption of H₂O on 6-mercapto-1-hexanol (SH-(CH₂)₆-OH) transforms the mosaic of oblique ($3 \times \sqrt{13}$, $\alpha = 74^\circ$) domains into an arrangement with linear features and finally into disordered regions. It was concluded that H₂O actually disrupts the packing of the SAM, implying that the H₂O admolecules exert a long-range influence extending down to the S–Au interface. This is also important in the context of wetting, since it would mean that upon adsorption of water one cannot assume that the (macroscopic) behavior is only driven by the (SAM–H₂O) interface energy, while the SAM remains entirely intact. In fact, it was shown that in humid environments 6-mercapto-1-hexanol SAMs are covered already with one or several layers of water and that these water layers alter the crystalline packing arrangement of the SAM [117].

An example of a molecule used specifically for surface reactions is *trifluoroacetic anhydride* (TFAA). It is known that on polymer surfaces, the yield of TFAA derivatizations of OH groups can reach nearly 100%. This effect was studied for OH terminated SAMs in [113,239,240]. In all cases, the reaction was observed, but different results on the yield were reported. In [113], the distribution of OH groups in a mixed SAM of 16-mercapto-1-hexadecanol and alkanethiols was studied by reacting it with TFAA in *tetrahydrofuran* (THF) solution. The yield was estimated to 80–90%, and steric effects were assumed to limit the yield. For vapor-phase derivatization performed in [239] it was speculated that there were not sufficient degrees of freedom for the CF₃ groups to pack at the same density as the underlying monolayer. Recently, Pan et al. [240] reported a nearly complete surface reaction and concluded that the steric hinderance of the CF₃ groups was not significant.

Himmel et al. [114] studied the surface derivatization of OH and COOH terminated SAMs by phenyl isocyanate (C₆H₅NCO, PIC). In both cases the reactivity to gas-phase PIC was very low for the sample at room temperature. However, reaction yields of more than 80% could be achieved by depositing multilayers on a sample cooled down to 120 K and subsequently heating it up to 290 K.

The reaction of ambient air species like ozone with simple methyl-terminated SAMs such as decanethiol SAMs has been investigated in [241] and references therein.

3.4.5. SAMs as building blocks for heterostructures

Oxides on SAMs. SAM-covered surfaces have been used as a substrate for the growth of (usually nanocrystalline or amorphous) metal oxides like ZrO_2 from aqueous solution (see Fig. 20, for example). In most cases, silane-based SAMs have been employed. This concept, in which the SAM helps to “anchor” the adsorbates to the substrate, is fairly versatile and has been applied to various coating materials [55,242–245]. The formation of zirconia on dithiol SAMs has been discussed in [246]. Recently, Aizenberg et al. [247] have shown how to control the crystal nucleation of calcite by patterned self-assembled monolayers.

Clusters and nanoparticles on SAMs. SAMs can also be employed for the attachment of clusters to surfaces. Various routes for the case of semiconductor nanocrystals were discussed by Alivisatos et al. (see [248] and references therein).

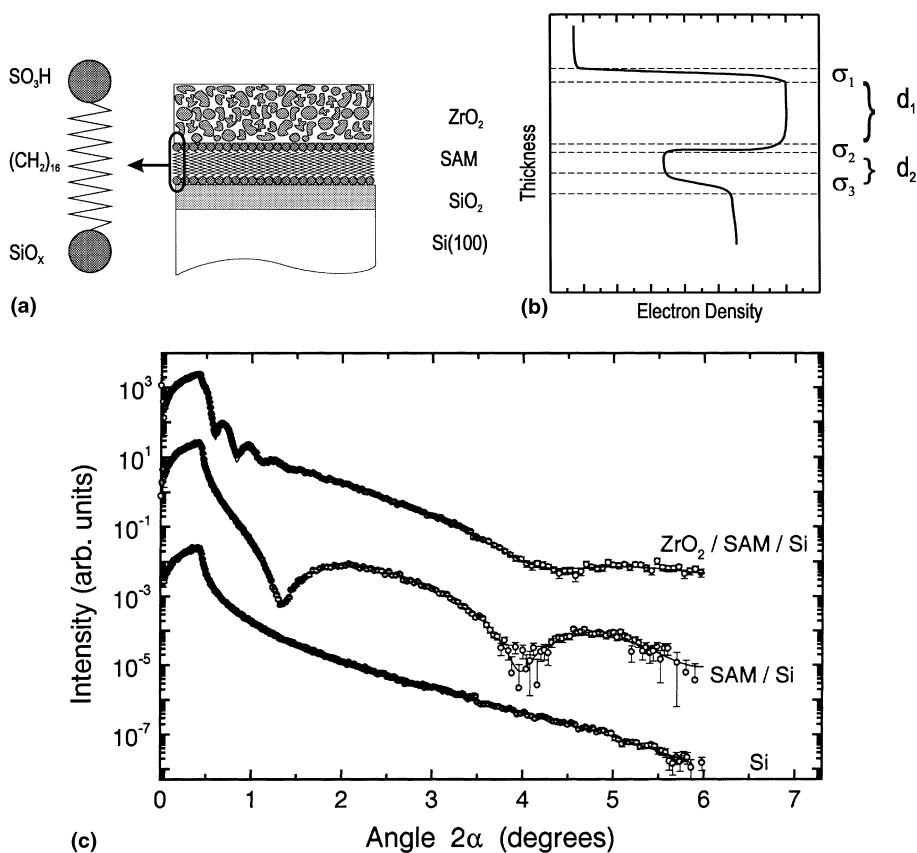


Fig. 20. Example for SAM-based heterostructure. (a) Schematic of solution-grown ZrO_2 layer on SAM. (b) Schematic of corresponding electron density profile, which determines X-ray reflectivity. (c) X-ray reflectivity scans of bare Si substrate, SAM/Si, and ZrO_2 /SAM/Si heterostructure (with wavelength of 1.54 Å). From [55].

The electrodeposition of metals on SAMs was discussed, e.g., by Kern et al. and by Kolb et al. (see [249,250] and references therein).

Another interesting application of SAMs is their use as spacers between an adsorbate and the substrate, as demonstrated in the case of exciton quenching in C_{60} near metal surfaces [251,252].

Organic–organic heterostructures with SAMs. Recently, decanethiol SAMs on Au(111) have been employed as a “substrate” for the growth of PTCDA [186,253–255], a molecular crystal material used as a model system in OMBE [25–27]. For PTCDA on a $c(4 \times 2)$ phase SAM the X-ray scattering data showed that the organic–organic interface is very sharp. A well-defined crystallographic (in-plane and out-of-plane) orientation of the PTCDA adlayer on the methyl-terminated SAM was found. Moreover, the results suggested that PTCDA grows essentially unstrained which would be a model case of “soft-on-soft epitaxy” [186,253,254]. Using STM, also for the case of PTCDA on the lying-down phase of decanethiol an ordered structure with a well-defined epitaxial relation was found [255].

Other examples of SAMs as substrates or templates include their use as patterns for adsorption of liquid crystals [256], SAMs as substrates for phospholipids [257], LB films on SAMs [258], or polymer films [259].

Alternating adsorption of oppositely charged polyions for the assembly of multilayer structures was shown in [260,261]. Various routes for multilayer formation are also discussed in [33,164,262].

The use of SAMs as a chemical anchor at the endgroup of which to start polymerization has been demonstrated in [263]. The idea is to form a “brush-like” polymer film, which is chemically bound to the substrate, very stable, and, therefore, attractive for applications, e.g., in coating technology (see also [264] and references therein).

4. Growth

Since self-assembly is the defining feature of SAMs, the understanding of this self-assembly process, i.e., the growth, is of fundamental importance. The following questions may serve to illustrate the main issues.

- What are the driving forces of self-assembly and what determines the kinetics?
- What is the role of the various phases occurring as a function of coverage?
- Is the chemical bond to the substrate formed instantaneously or are there precursor states and what is their impact on the kinetics?
- What are the respective roles of the chemisorbing group and the molecular backbone in the ordering process?
- What is the impact of the internal degrees of freedom of these molecules with possible internal low-energy excitations?
- Are there collective processes involved in the self-assembly?
- What are the external control parameters?

As explained in Sections 1 and 2, many SAMs can be prepared both from solution and from the gas phase. The traditional route is solution deposition. Growth from the gas phase generally requires a more expensive experimental setup (i.e., usually a

vacuum chamber), but offers also some advantages, such as a better control of the cleanliness of the environment, the substrate and the substances and their respective temperatures as well as the applicability of essentially all the established methods known in surface science including in situ structural methods with molecular resolution (GIXD, LEAD, LEED, STM, AFM, etc.), TPD to determine the energetics, various electron spectroscopies, etc. In contrast, the number of in situ methods for solution growth is limited.

While the resulting structures should be the same for both preparation routes, the growth process, the means to control it, and possible non-equilibrium effects exhibit differences. Among the control parameters to be investigated are the solution concentration, c , which determines the impingement rate in the liquid, and its corresponding control parameter in the gas phase, the partial pressure, P , and the temperature, T . The impact of these and other parameters will be discussed below, including the role of the solvent in solution deposition and possible ways to bridge and compare solution and gas phase deposition. A comprehensive discussion of the growth behavior and differences between solution and gas phase deposition follows in Section 4.4.

4.1. Growth from solution

Growth from solution is the traditional route for the preparation of SAMs. Specific studies of the growth, however, have mostly been limited to a few model systems, mostly alkanethiols on Au(1 1 1) and simple silane-based SAMs, which will also be in the focus here. Those systems, for which a comparative study of solution and gas phase deposition was done (e.g., dithiols, biphenyl thiols, and dialkyl disulfides), are discussed in Section 4.2.

4.1.1. Thiols on gold

4.1.1.1. Overview. The archetypal system of alkanethiols on Au(1 1 1), typically using ethanol or hexane solution with concentrations in the micromolar to millimolar range, was investigated by several groups, but the results remained controversial [39,59,66,187,217,265–278]. Particularly in solution-growth, the cleanliness of the substrate is not easy to control, which can have a strong impact on the growth behavior [279]. In most cases evaporated films and not single crystals were employed. Films tend to exhibit preferentially (1 1 1)-oriented terraces, but the size of these and the density of defects can vary substantially, which also influences the growth (see, e.g., [280]). In addition, the cleanliness of the solution itself as well as the control of the exact concentration can be an issue. An effect frequently observed for solution growth concerns a certain delay of the onset of the growth due to contaminants on the surface [59,66,217,274]. While the contaminants are ultimately displaced by the growing SAM, this can obviously have some impact on the kinetics and limits to some extent the comparability of results from different laboratories. Despite these problems, we try to provide a comprehensive picture below. However, due to the lack of consistency in the literature, some issues remain unresolved.

The uptake curve is expected to follow, in a first approximation, the Langmuir growth curve, which is characterized by the growth rate being proportional to the number of available sites

$$\frac{d\Theta}{dt} = R(1 - \Theta), \quad (4.1)$$

giving rise to the simple growth law

$$\Theta = 1 - e^{-Rt}. \quad (4.2)$$

If the growth nucleates only after a certain time, t_c , this can be taken into account phenomenologically by a time offset

$$\Theta = 1 - e^{-R(t-t_c)}. \quad (4.3)$$

An example of an uptake curve of the chemisorbed coverage (as determined by SHG [59]) is shown in Fig. 21. Uptake curves qualitatively similar to this were reported by many groups.

Nevertheless, while the fit according to Eq. (4.3) apparently provides a reasonable description of the data shown (dotted line in Fig. 21), also systematic deviations have been reported. These as well as the dependence on various control parameters will be discussed below.

4.1.1.2. Existence of multiple time scales and phases. It was frequently found that the first adsorption step results in $\sim 80 \dots 90\%$ coverage, typically after a time scale of the order of minutes for usual solution concentrations. After that, the growth proceeded

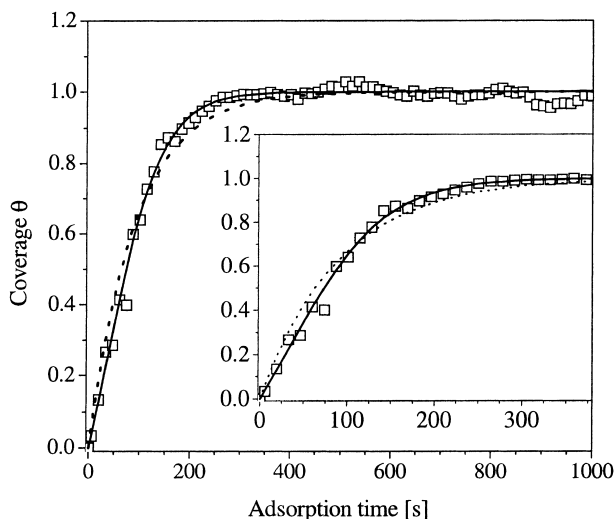


Fig. 21. Uptake curve of dodecanethiol from hexane solution on evaporated Au film as detected by SHG. Dotted line is fit according to simple Langmuir growth (Eq. (4.3)). Slightly better fit (solid line) includes small modification of model (Eq. (4.7); see text). From [59].

with a much slower rate. These different time scales were reported by several groups [59,66,217,273].

(i) *Long-term effects.* In the later stages of the growth a long-term reorganization effect of the alkyl chains was found by NEXAFS for docosanethiol ($\text{CH}_3-(\text{CH}_2)_{21}-\text{SH}$) deposited from ethanolic solution [278]. The issue of long-term effects in the ordering process was recently investigated in detail by SFG [277]. In that study, three steps of the self-assembly process were reported, each with its own time scale and characteristic signature in the vibrational spectra (Fig. 22). In this scenario, the fastest step is related to the chemisorption of the headgroup. The second step (3–4 times slower than the first) was seen to comprise the straightening of the hydrocarbon chains. The third and final step (again 35–70 times slower than the second)

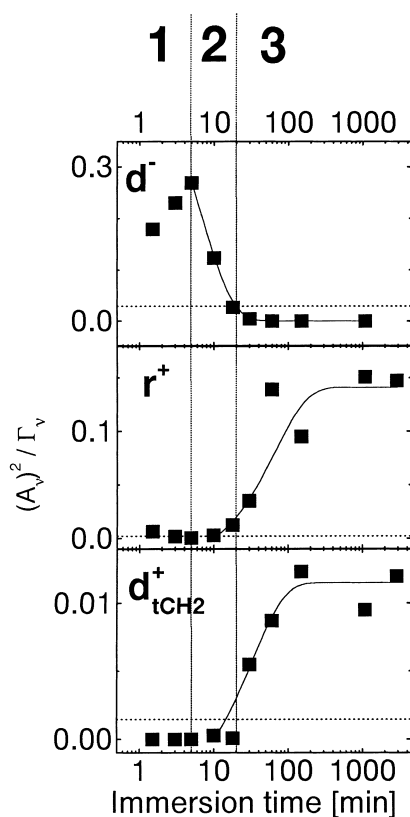


Fig. 22. Different time scales (including long-time effects) in solution-growth of docosanethiol ($\text{SH}-(\text{CH}_2)_{21}-\text{CH}_3$) on Au, derived from vibrational mode intensity (detected by SFG) as function of immersion time. First step (regime 1) is chemisorption of S headgroup, i.e., signal similar to that of Fig. 21). Regime 2 corresponds to straightening of chains, represented by decrease of the d^- mode (antisymmetric; CH_2). CH_2 group adjacent to endgroup already exhibits slower ordering (represented by d_t^+ mode; symmetric). End of chain shows slowest ordering (regime 3), as evidenced by evolution of r^+ mode of endgroups (symmetric; CH_3). For details see [277].

was related to the reorientation of the terminal groups. The sequence of the changes in the vibrational spectra was taken as suggestive of an ordering and annealing of the film from the interface to the film surface.

Recently, long-term effects in the island growth and coalescence of hexadecanethiol ($n = 16$) were followed by AFM [281]. It was found that on the scale of several hours to days the islands exhibit a coalescence process leading to the formation of fewer and larger islands. During their diffusion, the molecules tend to stay on the same substrate terrace, avoiding crossing of terrace steps. The island ripening is associated with a densification of the layer and the removal of defects. Furthermore, an increase of the mechanical strength of the layer was reported, as manifested in the increase in threshold pressure needed for tip penetration through it [281].

We should note that for (shorter) alkanethiols deposited from the gas phase (to be discussed below) these long-term effects were not seen in the GIXD data, although GIXD would be sensitive to them.

(ii) *Evolution of phases.* The lying-down phase, although more difficult to observe during solution growth, was found by STM and AFM in the initial stage of the growth [39,187,274–276]. For the in situ and real-time observations it turned out to be helpful to use very dilute solutions (submicromolar) [274,275], since otherwise the time window before formation of the standing-up phase was too small. The appearance of an additional phase suggests that there should also be a separate time constant for the kinetics. A model taking into account this additional adsorption step was presented in [274], where the lying-down phase was considered physisorbed. Since this separate time constant (before the onset of the standing-up phase), the existence of which seems natural based on the fact that it corresponds a separate phase, has not been seen in several other studies, one may speculate that the molecules are, in fact, only physisorbed (and, therefore, would not be seen in the above SHG experiments [59]) or that at the usual (higher) concentrations the lying-down phase disappears so fast that it has only a minor (and hardly detectable) impact on the later kinetics of the standing-up phase.

4.1.1.3. Deviations from the Langmuir growth law and alternative models. The Langmuir growth law as introduced in Eq. (4.1) is strictly valid only if the adsorbate molecules do not interact with each other (such that the rate of growth is only determined by the number of available sites and not by possible island distributions). In a more realistic picture one would expect that the energy gain for adsorption at a domain boundary is larger than for an isolated molecule, which would introduce modifications of Eq. (4.1). Also, if the supply of adsorbate molecules is limited by diffusion effects from the bulk of the liquid, deviations will be found.

We briefly summarize possible alternatives to the Langmuir model below [59,66]. In each case, they describe only the main uptake step (with one time constant, as explained in the introductory lines), where R' denotes the characteristic growth rate parameter, which depends on c as well as the microscopic processes involved.

1. For adsorption entirely controlled by diffusion one finds

$$\Theta = R't^{1/2}, \quad (4.4)$$

where R' is proportional to $D^{1/2}$, and D is the diffusion constant. This approach can, if anything, only describe a certain stage of the growth (like the initial stage), since it does not include saturation after one monolayer.

2. Also, a diffusion-limited first-order Langmuir adsorption model was proposed, which yields

$$\Theta = 1 - e^{-R't^{1/2}}. \quad (4.5)$$

3. Furthermore, a second-order non-diffusion-limited model was suggested, according to which one should find

$$\Theta = 1 - \frac{1}{(1 + R't)}. \quad (4.6)$$

4. Different sticking coefficients for areas already covered and for those still free of thiols can be taken into account in a modified Kisliuk model [59,282]. Assuming that the desorption rate from a precursor state is much higher than the chemisorption rate one gets [59,282]

$$\frac{d\Theta}{dt} = R'(1 - \Theta)(1 + k_E\Theta), \quad (4.7)$$

where the term $k_E\Theta$ describes the deviation from the Langmuir growth law due to changes of the sticking coefficient by already adsorbed thiols. This results in

$$\Theta = \frac{1 - e^{-R'(1+k_E)t}}{1 + k_E e^{-R'(1+k_E)t}}. \quad (4.8)$$

We note that ruling out certain models in favor of others is difficult, since more than one produce a curve similar to Fig. 21. Also, one has to bear in mind the sensitivity of different methods for different features of the growing SAM.

Nevertheless, in [59] the best fit (full line in Fig. 21) was obtained using Eq. (4.8). This deviation from pure Langmuir growth, although small, is plausible, since the molecules do interact with each other, so the presence of islands should have an impact on the growth kinetics (shape of the curve), which is indeed found.

The evolution of the SAM through islands was shown in many AFM and STM studies (see, e.g., [39,213,274,283]), consistent with the notion of deviations from pure Langmuir growth. We should note that the island size in the final solution-grown SAM as determined by GIXD was typically smaller than for gas phase deposition (see below). Only for very low concentrations in the micromolar range domain sizes are obtained comparable to those found under suitable conditions from the gas phase [265,266].

4.1.1.4. Dependence on control parameters. (i) Dependence on chain length for alkanethiols. Investigations as a function of chain length for alkanethiols show that the

rate of the initial rapid adsorption process decreases with increasing chain length [59,66]. This behavior, which is found for different types of solvents (polar and non-polar) [59], could be related to the fact that the mobility of molecules is typically reduced for longer chains. Since different groups discuss their data using different models and kinetic steps [59,66,217], a comparison of later stages of the growth is difficult.

(ii) *Dependence on concentration.* Most groups find the expected increase of the initial growth rate with c [59,217,272,273]. Karpovich and Blanchard, who also observed a monotonous increase of the rate with concentration, reported that the rate of octadecanethiol ($\text{CH}_3-(\text{CH}_2)_{17}-\text{SH}$) becomes independent of c for high c [271]. A more complicated behavior was reported in [66]. A superlinear dependence as the P^2 effect for gas phase deposition (see Section 4.2.1) has not been observed for growth from solution.

(iii) *Dependence on the nature of the solvent.* An important parameter to be investigated is, of course, the solvent itself. The easiest way is to vary the chain length in simple alkanes. Dannenberger et al. [59] studied the impact of changing the solvent chain length on the growth of docosanethiol ($\text{CH}_3-(\text{CH}_2)_{21}-\text{SH}$). They found that the (initial) rate of chemisorption was significantly slower for longer-chain solvents. Specifically, the rate was roughly scaling with the inverse chain length for the three chain lengths under investigation (6, 12, and 16). The slower adsorption for solvents with longer chains is plausible considering that the interaction of the solvent molecules with the surface (from which they have to be displaced by the thiols) is larger for longer chains and that also the mobility of the molecules in solution is reduced for longer chains.

Of course, also other solvents were used, such as ethanol, cycloalkanes, etc., [59,66,217,270,271]. However, if the chemical nature of a solvent is changed, this has an impact on a number of parameters, such as steric constraints, polarity, viscosity/mobility, solubility for a given SAM molecule, etc. Since this makes it difficult to identify which parameter is responsible for possible changes, we will not pursue this issue here.

The principal effects of the presence of a solvent and the differences to gas phase deposition will be discussed in Section 4.4.3.

(iv) *Dependence on temperature.* For the temperature dependence, only few data exist [32,265,266]. In contrast to the situation for gas phase deposition (which is characterized by a strong decrease of the rate with temperature; see Section 4.2.1), the temperature dependence appears to be fairly weak [265,266].

(v) *Comparison with other substrates.* For other substrates, the possible reactivity of the solvent towards the substrate can also have an impact on the self-assembly process. This was discussed for the case of Cu in [284].

4.1.2. Growth of silane-based and related SAMs

In contrast to alkanethiols on Au(111), for OTS on oxidized silicon, which is probably the most popular silane-based SAM, no structures with long-range order have been reported. This makes it also difficult to characterize possible

intermediate stages of the growth by diffraction. The possible cross-linking (polysiloxane formation in partial monolayers; see discussion in Section 3.2.3 and [165]) can have a strong impact on the structure and the growth. Related to these fundamental differences to the thiol/Au-based systems, also the robustness of the preparation conditions is different, which can cause difficulties in the comparability of work by various groups. The precise control of the water content, the cleanliness of the preparation environment, the exact temperature, and a possible rinsing procedure can have a crucial impact. We discuss these issues further below. In this context, we note that recently Barness et al. [285] have reported the superior stability of trialkoxysilanes with respect to various synthetic operations.

A basic question for the growth of OTS on oxidized silicon is whether it proceeds in a “uniform mode” where a homogeneous layer grows in thickness (with the tilt angle decreasing) or in the “island mode” where the thickness of the (close-packed) islands already corresponds to that of the complete monolayer with straight, fully extended molecules which are oriented normal to the surface. Of course, one can also imagine intermediate scenarios.

Early work by Sagiv et al. [194] employing IR found that the molecules in partial monolayers appear to have an alignment only slightly worse than that of the full monolayer, supporting evidence that incomplete monolayers form in partially ordered islands rather than as a sparse, homogeneous layer, in contrast to early work done with XR and ellipsometry [54,67], which found the thickness of partial layers to be reduced and the density to be the same as for complete layers, suggesting that the uniform mode applies.

Bierbaum et al. [286] investigated the growth of OTS on oxidized silicon by AFM and found the growth to proceed via islands (which can have a fractal appearance). These findings, which contradict the uniform growth model, were supported by other AFM studies [208,287]. Longer-chain molecules also showed growth via islands under certain conditions, but the islands appeared different from those observed for OTS, whereas short-chain molecules did not show island growth behavior [286].

NEXAFS data [170] indicate that already for incomplete monolayers there seems to be a preferred orientation of the molecular chains, with the average tilt angle gradually decreasing for increasing coverage.

Already from these few examples (mostly measured *ex situ*, i.e., after taking incomplete monolayers out of solution) and many others (see, e.g., the discussion in [288,289]), it appears that the results in the literature are conflicting. Therefore, we try to address the issues that explain some of the difficulties and apparent inconsistencies of the data.

(i) *Differences in the analytical methods.* An important point is the difference in the analytical methods, i.e. their sensitivity to different features. XR is sensitive to the thickness and the density. It averages over the (projected) coherence length of the beam, i.e., typically on the scale of microns [288]. In contrast, AFM is sensitive to the local structure. While the AFM can detect the height difference between the layer and the substrate or standing-up and lying-down molecules, it has to be taken

into account that differences can occur between chemisorbed molecules and molecules which are not yet strongly attached to the substrate. Spectroscopic techniques (like IR) typically average over macroscopic lengths and are often particularly sensitive to the tilt angle of the molecular backbone. They detect molecules in disordered as well as in ordered areas (which can lead to an effectively decreased overall tilt angle), whether they are strongly attached to the substrate or not. With these differences in mind, all data taken together point towards an intermediate case, e.g., that the partially formed films consist of islands with essentially upright molecules and in between (possibly not yet strongly bound) molecules with larger tilt angles. However, when comparing results from different groups, also the sensitivity to the preparation conditions and the environment has to be taken into account.

(ii) *Ex situ vs. in situ*. One key to the understanding are possible differences due to the rinsing procedure, which is why it is important to investigate the growth in situ, i.e., in solution without taking the substrate out for the measurement. Ex situ the partially formed film might “dry out” and the molecules might “fall over”. In fact, by comparing XR data taken in situ and ex situ, Richter et al. [289] found that quenching the growth before full film formation causes the thickness and the density to decrease. Rinsing appeared to cause an irreversible process to occur, as re-immersion in solvent did not restore the film to its pre-rinsed thickness. It was proposed that the solvent molecules help to keep the adsorbed molecules vertical and that rinsing causes some of the molecules to be removed from the film, creating free volume, which enables some of the molecules to tilt over, thereby lowering the thickness [289].

By following the growth of OTS on oxidized silicon wafers in situ and in real time by XR (averaging over a coherence length of about 1 μm), it was found that the thickness stays essentially constant throughout the growth, whereas the density continuously increases [288]. This would be consistent with island-type growth. However, it was mentioned that the interface layer required in the fits may indicate the presence of some horizontal or highly tilted molecules.

Another in situ study [169] by IR reported that the hydrocarbon chains of the film molecules show initially a random, isotropic configuration and gradually align and stand up on the surface with increasing coverage, which would not be expected for pure island-type growth.

Taking into account the technique-related differences outlined above, the results are not necessarily mutually excluding each other, but could rather suggest that the actual growth mode is between the limiting cases of island growth and uniform growth, e.g., islands of upright-standing molecules are surrounded by molecules lying down or at least exhibiting a higher tilt angle.

The kinetics were also studied in situ, and found to follow in a first approximation simple Langmuir kinetics [169,289], with the exception of the very early stage [289].

(iii) *Temperature dependence of the growth*. Another important step was to investigate the temperature dependence of the growth behavior, which revealed critical changes close to room temperature. This observation makes some of the lab-to-lab

variations in the growth understandable, since obviously small differences in the growth conditions can have a dramatic impact.

Rondelez et al. [290] studied *n*-alkyltrichlorosilane monolayers on oxidized silicon wafers as a function of the temperature of the silanization reaction. They found that the critical surface tension showed a systematic change at a well-defined temperature, which for OTS is 28°C. Furthermore, they found this threshold temperature to exhibit a systematic increase with chain length (about 3.5°C per additional methylene group).

This observation of a critical growth temperature was confirmed by additional analytical methods (ellipsometry, IR) [291]. The authors found changes of surface energy and wetting behavior in the same temperature region as those of coverage and chain organization. It was concluded that when prepared at low *T*, the films exhibit a heterogeneous structure with closely spaced islands of densely packed, nearly *all-trans* alkyl chains arranged almost vertical to the surface. In contrast, when prepared at above the critical temperature, the films exhibit monotonically diminishing coverage with increasing preparation temperature and the alkyl chains increasingly assume higher contents of conformational disorder. A mechanism was suggested, which involves, prior to siloxy group cross-linking, the intervention of intermediate structural phases of mobile alkylsiloxy species adsorbed on a water layer adjacent to the solid substrate surface [291].

These studies pointed out analogies to the triple point temperature at which gas, liquid-expanded, and liquid-condensed phases coexist for C₁₈ chain Langmuir monolayers at the air/bulk water interface. The notion of a transient Langmuir-like film at the substrate–solution interface was supported by a recent AFM study [292]. These authors also provided a time scale for cross-linking of the molecules and bonding to the substrate, which was crudely estimated as tens of minutes and up to an hour at room temperature.

(iv) *Water content in solution and cleanliness.* Since the presence of a water layer at the interface plays an important role for the growth of the SAM, it is not surprising that the water content in solution needs to be carefully controlled. For insufficient water concentrations, incomplete layers are formed, whereas excess water facilitates polymerization in solution. It was reported that increasing water content or also increasing age of the solution favors island-type growth more strongly [293]. Since the growth of these silane-based SAMs is so sensitive to the level of moisture, which on the other hand is difficult to control precisely, this is one source of problems in the comparability of results from different groups, as discussed in [33]. For a discussion of other aspects related to the bonding and substrate effects, see also [294–298]. Furthermore, some authors have pointed out the importance of cleanroom conditions [286,287].

(v) *Related systems: monolayers on mica.* Besides silicon wafers with their native oxide, mica has been frequently used [196,299–304]. Particularly with the AFM technique several investigations were performed. In an early *ex situ* study of OTS on mica Schwartz et al. [299] analyzed the fractal shape of the islands. They found that with increasing coverage, the fractal dimension of the growing domains evolves from 1.6 to 1.8. The results were compared to Monte-Carlo simulations.

Recently, Resch et al. performed comparative in situ and ex situ studies by AFM [301]. From in situ studies, they found that in the beginning of film growth comparatively large, fractally shaped islands adsorb onto the surface. They further conclude that polysiloxane oligomers, formed in the presence of traces of water in solution, adsorb onto active centers of the surface faster than monomeric silanol molecules. They find their conclusion supported by the fact that the observed height of the islands (~ 25 Å) indicates perpendicularly oriented molecules on the surface from the beginning of the process. Furthermore, they find that the islands are slowly growing in a subsequent, much slower process and that the gaps between the individual islands are filled by adsorption of monomers from the solution.

By studying the growth of OPA on mica in situ, Schwartz et al. [302–304] found island growth. Three regimes were identified: (1) an initial growth regime where nucleation of islands is significant, (2) an aggregation regime where nucleation essentially stops and existing islands grow, and (3) a coalescence regime where individual islands merge, resulting in fewer islands [303,304]. We note that, in contrast to the case of alkanethiols on Au(1 1 1), the different regimes observed should not be identified with different structural phases. They rather correspond to different degrees of coverage (of the same phase, which can be considered a “standing-up phase”). Based on a statistical analysis of the island formation and growth, Schwartz et al. [303] could show that the growth scenario can be described by the point island model and a critical nucleus of two molecules. The data were found to be consistent with the typical scaling laws expected from this growth model. At short times, t , they found

$$\text{island number density} \propto t^{1/3}. \quad (4.9)$$

For the growth individual islands, one has

$$\text{island area} \propto t^{2/3}. \quad (4.10)$$

For details of the analysis see [303,304].

4.2. Growth from gas phase

4.2.1. Alkanethiols on Au(1 1 1)

The study of the growth of *n*-alkanethiols on Au(1 1 1) from the gas phase offers probably the best chances for a detailed understanding of the self-assembly process, since these molecules are relatively simple (i.e., completely saturated) and UHV allows a precise control of the cleanliness of the substrate and the use of a wide range of techniques with molecular resolution. This was applied, e.g., in [40,71,72] with GIXD, LEAD, HAR, XPS, and XSW, in [42] with LEAD, in [41] with GIXD, in [39,43] with STM, and in [44] with STM, TDS, and AES.

(i) *Uptake curve.* An overview of the growth process over four orders of magnitude of thiol exposures at room temperature, obtained from a multitechnique study [40] of the growth of decanethiol on Au(1 1 1) single crystals, is shown in Fig. 23. The XPS data of the evolution of the sulfur K(1s) photoelectron yield, Y , provide a

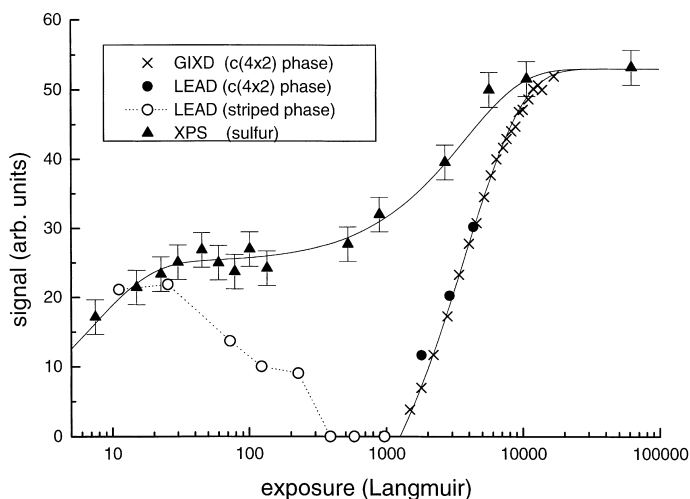


Fig. 23. Vapor phase deposition of decanethiol on Au(111) as followed by XPS, LEAD, and GIXD at 25°C. XPS (sulfur 1s) data reflect essentially mass coverage with small correction in standing-up phase due to attenuation caused by hydrocarbon chain. LEAD and GIXD data show which particular phase is formed at given coverage. Note strongly different exposure scales for initial (striped) phase and final $c(4 \times 2)$ phase. From [40].

measure of the mass coverage. This follows to a good approximation a two-stage process²

$$Y = A_1(1 - e^{-t/\tau_1}) + A_2(1 - e^{-t/\tau_2}), \quad (4.11)$$

with $\tau_1 = 7.2$ L for the initial stage and $\tau_2 = 3750$ L for the later stage. Parallel measurements of the gold $M_V(3d_{5/2})$ photoelectron yield exhibited a similar evolution [40], but in which the photoelectron yield decreased at each of the two stages of the growth due to absorption in the thiols. Together, these data demonstrate that the observed adsorption kinetics is driven by the evolution of coverage and is not an artefact of changes in the molecular orientation or conformation at a fixed coverage. Recently, the multi-step adsorption with strongly differing time constants was independently confirmed by Kondoh et al. [44] for hexanethiol.

(ii) *Evolution of phases.* The structural phases associated with the different stages of the uptake process were revealed (and correlated with those described in Section 3.1) by STM [39,43,44], LEAD, and GIXD [40].

The LEAD spectra after various exposures of decanethiol (Fig. 24) show that the structure accompanied with the first rapid adsorption process is that of the striped phase [99,187]. Upon further deposition, the LEAD spectra change and ultimately transform into the one of the full-coverage structure with the $c(4 \times 2)$ phase. This

² More precisely, the second term would have to include some offset time, t_2 , determined by the completion of the initial (τ_1) process. However, this can be neglected, since $\tau_1 \ll \tau_2$.

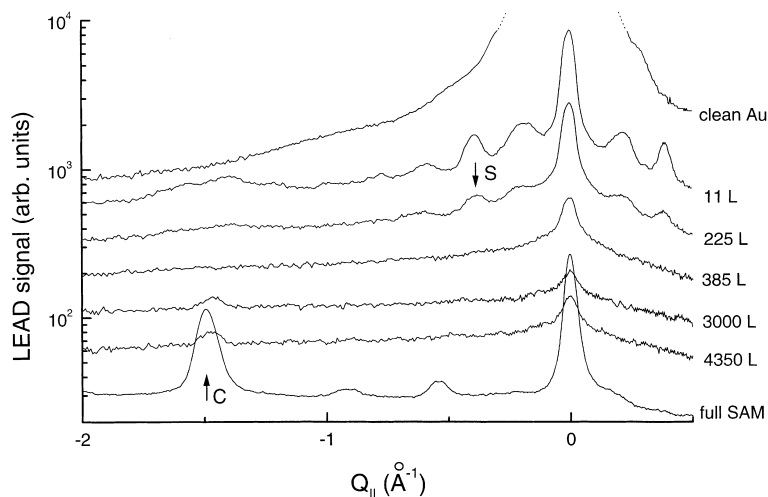


Fig. 24. LEAD spectra at various coverages of decanethiol on Au(111). Bragg peaks marked by S (striped) and C ($c(4 \times 2)$) were used in Fig. 23. Note that no diffraction was observed in LEAD data for exposures between ~ 300 and ~ 1000 L. From [40].

evolution of phases is consistent with STM data reported for decanethiol [43], hexanethiol [44], and mercaptohexanol [39]. The initial formation of a lying-down configuration (presumably preceded by a lattice gas for very low coverages) and, finally, the transformation to a standing-up configuration are, in fact, a rather general scenario for several systems. This is shown also for the case of mercaptohexanol (Fig. 25), which is discussed further below.

Fig. 23 shows the integrated diffraction peaks (from GIXD and LEAD), which provide a direct measure of the growth kinetics of a given structural phase. It can be seen that the ~ 500 times slower time constant (τ_2) is associated with the formation of the denser (“standing-up”) phase ($c(4 \times 2)$). This phase nucleates and grows with a Langmuir-like evolution to completion (normalized coverage $\Theta = 1$), as evidenced by XPS, GIXD, and LEAD data.

It might be expected that the $c(4 \times 2)$ phase would form for any coverage exceeding the ideal striped coverage (for decanethiol, this is 0.27 ML, where 1 ML of the $c(4 \times 2)$ phase corresponds to 4.6×10^{14} molecules/cm²). Instead, the LEAD data show that the striped phase breaks down as the exposure is increased above ~ 300 L, but that the $c(4 \times 2)$ phase nucleates only for exposures above 1000 L at a coverage of about 0.47 ML [40].³

³ One monolayer of striped phase molecules corresponds to 0.7 Langmuir (L) (1 L = 10^{-6} Torr s) and one monolayer of $c(4 \times 2)$ to 2.6 L, both assuming a unity sticking coefficient. Generally, it should be noted that the absolute calibration of fluxes of molecules is difficult [40]. Also, the sensitivity of an ionization gauge is higher for alkanethiols than for N₂, which requires correction of the ionization gauge readings (see Eq. (4.14)).

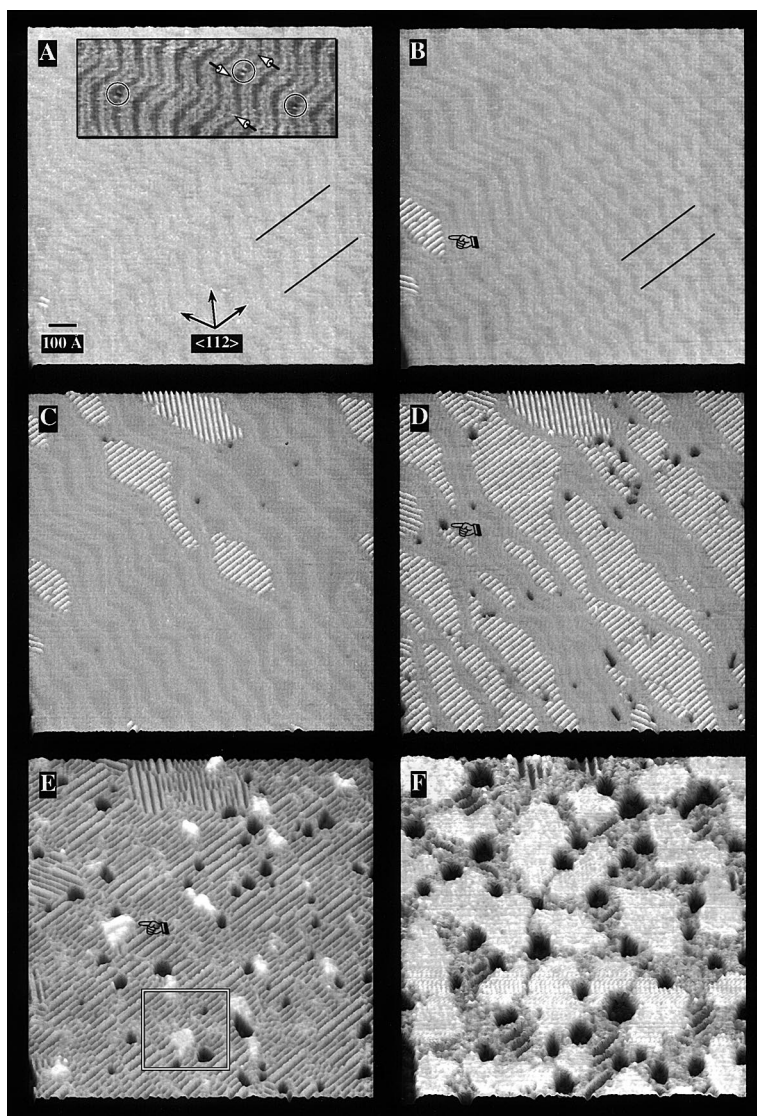


Fig. 25. Constant-current STM topographs for increasing exposures of mercaptohexanol vapor on Au(111). (A) clean $((22 \times \sqrt{3})$ “herringbone” reconstructed) Au(111) surface; inset shows three stable islands nucleated between herringbone double rows after first stage of exposition. (B) Striped phase island (pointing finger). (C) Continued striped phase growth displacing herringbone elbows. (D) Continued striped phase growth with Au vacancy islands (pointing finger) becoming visible. (E) Nucleation of standing-up phase within striped phase after about 1000 L. (F) Growth of standing-up phase at expense of striped phase until saturation. From [43].

This means that adsorption beyond the striped phase's maximum coverage (0.27 ML) apparently disrupts the molecular order, but is insufficient to induce the nucleation of the denser $c(4 \times 2)$ phase, suggesting that additional phases may exist at intermediate coverages between the striped and the $c(4 \times 2)$ phase. However, in [40], no well-defined diffraction features were found for the intermediate-coverage regime, indicating the loss of long-range order. Moreover, the HAR signal exhibits a minimum in the intermediate region (lower than in the $c(4 \times 2)$ phase and the striped phase) [42], implying a lesser degree of smoothness of the surface potential experienced by the helium atoms, which can, e.g., be caused by molecular chains in different conformations or heights above the surface. This region was labelled “intermediate structures” (IS) in Fig. 16.

The question of the structure evolution at intermediate coverage ($0.27 \text{ ML} \leq \Theta \leq 0.47 \text{ ML}$) turns out to be rather complex. While the lack of long-range order mentioned above [40,42] was confirmed in [44] for hexanethiol by STM, other studies reported evidence for ordered arrangements of the molecules in the intermediate region. We summarize these in Fig. 26, but we emphasize that they do not necessarily all manifest stable equilibrium structures, but metastable (transition) states. After formation and subsequent decay of the striped phase, for which actually two slightly different unit cells were found (see Section 3.1.1), a structure characterized by a $c(19 \times \sqrt{3})$ unit cell (coverage 0.316 ML) and presumably partial overlap of the chains was reported [43]. The major evidence for this structure comes from STM data and not from diffraction, which may be due to the fact that the structure does not cover the entire surface with long-range order as, e.g., the stripes do. Most

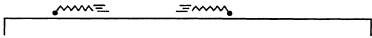
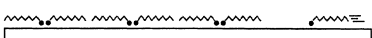

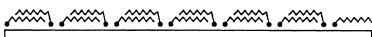

	structure	area per molecule (\AA^2)	normalized coverage Θ
A	 “lattice gas”		
B	 $c(23 \times \sqrt{3})$ (also found: $p(11 \times \sqrt{3})$)	82.8 79.2	0.26 0.27
C	 $c(19 \times \sqrt{3})$	68.4	0.32
D	 $h(5\sqrt{3} \times \sqrt{3})R30^\circ$	54.0	0.40
E	 $(2\sqrt{3} \times 3)$ (also denoted “ $c(4 \times 2)$ ”)	21.6	1.00

Fig. 26. Schematic representation of evolution of structures of decanethiol on Au(111) during growth. We emphasize that they do not necessarily all manifest stable equilibrium structures. (A) “Lattice gas” at very low coverage. (B) Striped phase (for which two slightly different structures were reported). (C) Intermediate structure with $c(19 \times \sqrt{3})$ unit cell. (D) Intermediate structure with $h(5\sqrt{3} \times \sqrt{3}) R30^\circ$ unit cell. (E) $c(4 \times 2)$ phase, which can be denoted either by $c(4 \times 2)$ superlattice of hexagonal $(\sqrt{3} \times \sqrt{3}) R30^\circ$ base or by rectangular $(2\sqrt{3} \times 3)$ unit cell. See also [40,43] and text for discussion.

importantly, it was found to be only metastable [43], i.e., a “transient configuration” rather than a thermodynamically stable phase.

Slightly higher in coverage is the $(5\sqrt{3} \times \sqrt{3})$ R30° structure (coverage 0.4 ML), which has been observed by different methods (STM, LEED, and LEAD) for different preparation conditions including gas phase growth and partial desorption from a $c(4 \times 2)$ layer [43,47,101,102,305].

In addition, close to the transition lines in coverage space, mixed arrangements of these structures have been observed [43].

While the starting structure and the end structure of the growth (i.e., striped and $c(4 \times 2)$ phase) are well-established, it is difficult to present a scenario for the intermediate region, since the experimental evidence appears to be conflicting. The crucial question is to which extent the intermediate structures are really equilibrium states, i.e., stable against annealing and on long time scales (see below). Remarkably, Barrena et al. [281] recently found indications, that even a striped phase layer transforms into the $c(4 \times 2)$ on long time scales (days). We should also point out that differences are possible between growth experiments performed in a continuous and an interrupted mode (i.e., temporarily interrupting the exposure in order to measure the structure at intermediate stages).

Since the IS region in coverage space is defined by the disruption of one phase (the striped phase) and the nucleation of another phase (the $c(4 \times 2)$) and both these defining borders (disruption and nucleation) depend very sensitively on the growth conditions (rate, temperature, possible interruption and relaxation times, number of defects on the substrate surface, etc.), it is not surprising that different groups obtained somewhat different results. In this context, one also has to see the “kinetic traps” (intermediate-coverage structures which are very stable against further deposition) discussed further below.

One way to gain further insight is to try to relate the growth rates to the evolution of the respective structural phases. It might be expected that if the growth proceeds via more than two phases, in general there also should be more than two time constants involved. In fact, the uptake curve of Fig. 23 at room temperature under equilibrium conditions can be described by two time constants, but that may be coincidence to some extent and is not a proof of *only* two processes taking place. Nevertheless, in [40] for decanethiol as well as in [44] for hexanethiol the uptake curves could each be described by only one time constant for the post-stripes growth, i.e., both the intermediate region and the region of $c(4 \times 2)$ growth.

In [42], using LEAD, it was tried to determine the characteristic time scale(s) in the intermediate regime by following the decay time of the stripes. This is supposed to be associated with the growth of the layer in the post-stripes structure. It was found that the “acceptance coefficient”⁴ of molecules growing on the stripes phase (and, thereby, forming the intermediate phase), in fact, was different from that of

⁴ Unlike the term “sticking coefficient”, “acceptance coefficient” as used in [42] refers to the probability of a molecule to be chemisorbed into the growing SAM. The two terms may be thought of as the same for the initial growth of the striped phase on bare gold.

molecules growing on the intermediate phase (and, thereby, forming the $c(4 \times 2)$) [42], but a quantitative analysis is complicated by the fact that the helium scattering cross-section for a newly incorporated molecule is not known, because the perturbation that it introduces may extend to its neighbors to some degree. While the lack of knowledge of the cross-sections makes an absolute comparison of these rates difficult, their different response to temperature changes could be qualitatively rationalized [42].

(iii) “*Kinetic traps*” and related effects. The above described evolution of phases seems to be a natural consequence of the increasing coverage upon deposition until the highest-coverage phase, the $c(4 \times 2)$, is reached. However, the observations of different groups indicate that for gas phase deposition of alkanethiols under certain conditions only intermediate-coverage structures were obtained [42,47,306], although one might expect the $c(4 \times 2)$ phase to be most favorable in terms of energy per surface area, since the highest number of chemical bonds is made possible.

In [42], these effects were termed “kinetic traps”. They were reported to appear more likely for slow growth rates (i.e. high T and low P) and also in the presence of longer waiting periods at intermediate stages when the technique of interrupted growth was used.

No systematic dependence of the effect of kinetic traps on external control parameters was reported (which is difficult due to their very nature), so we can only speculate about the reasons. The type and distribution of defects in the existing layer (which, in turn, will be related also to the substrate quality) should play an important role. Generally, for the disruption of an existing (low-coverage) phase by an increase of coverage, the molecules have to overcome a certain threshold, presumably corresponding to the van der Waals interaction of the molecular backbone with the substrate when they stand up.

Even if the final state is energetically more favorable for the *entire system*, this threshold might be significant, i.e., the intermediate-coverage phase could correspond to a deep local minimum on the energy surface. We note that the effect was not reported for solution growth, maybe because the relative energy differences between various configurations are different at the film–solution interface (see Section 4.3).

As can be seen below for other thiols (such as dithiols; see below), one can view the absence of a standing-up phase in gas phase deposition (or, more precisely, the apparent difficulties to obtain it even by extended dosing) also as due to a very effective kinetic trap. For certain systems, the threshold might be so high, that it is effectively never overcome. In that sense, the apparent stability of an actually metastable configuration (which does not minimize the energy per area but only the energy per already adsorbed molecule) is a rather general phenomenon.

(iv) *Other equilibrium vs. non-equilibrium issues*. As mentioned above, it is important to investigate whether the growth behavior is determined by equilibrium or not. As a criterion for equilibrium, here the stability against annealing and subsequent cooling shall be used.

The phase diagram shown in Fig. 16 was explored in Ref. [40] both as a function of temperature at a given coverage (i.e., “thermodynamically”) and as a function of coverage at a given temperature (i.e., in real-time “kinetic” measurements),

specifically for the regime of the $c(4 \times 2)$ phase. Excellent agreement between the phase boundaries (melting temperatures and onset coverages) as derived through the “kinetic” and “thermodynamic” measurements was found, implying that Fig. 16 reflects the intrinsic equilibrium behavior of the system [40].

An example for non-equilibrium effects is the coexistence of the striped and the $c(4 \times 2)$ phase. This was found after growth at low temperature, as evidenced by diffraction features from both phases in one LEAD spectrum [42]. After heating the layer to only 300 K, the intensity of the diffraction peak representative of the $c(4 \times 2)$ phase *decreased*, which, at 300 K, cannot be explained by desorption effects. The layer had only been annealed closer to its equilibrium state (with molecules in the intermediate phase not contributing to the $c(4 \times 2)$ diffraction intensity), indicating that the onset of the $c(4 \times 2)$ had been premature. It is interesting to note that the accompanied *decrease* of the specular helium intensity (i.e., the HAR signal) indicates that in this case annealing to a lower energy state leaves the surface with *higher* overall corrugation (i.e., less flatness, or more “bumps”), typical of the intermediate region [42]. The mechanism for the premature onset of the $c(4 \times 2)$ phase may be related to the fact that the density of molecules *locally* but *not globally* exceeded the threshold value for the nucleation of the $c(4 \times 2)$ phase. This is a typical non-equilibrium growth effect, where, due to limited mobility on the surface, the flux of incoming molecules cannot be appropriately accommodated.

The existence of different stability regions in the phase diagram has important consequences for the growth process, during which these regions are crossed. This does not only affect the evolution of phases, but also the evolution of the 2D coherence length (i.e., the domain size, L_D), as determined from the width of the corresponding diffraction peak. In [40] it was found that there are two distinct types of behavior that occur as a function of temperature (Fig. 27). For growth at higher

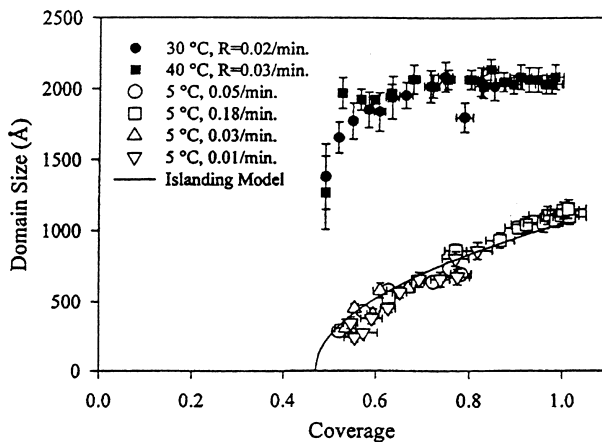


Fig. 27. Domain size evolution of decanethiol on Au(111) during gas phase growth for different temperatures and rates. Two different regimes are found (below and above 15°C; see text). From [40].

temperatures ($T > 15^\circ\text{C}$), the domain size saturates at a substrate-limited value of $\sim 2000 \text{ \AA}$ almost as soon as the $c(4 \times 2)$ phase is observed. This behavior is indicative of a high degree of molecular mobility during growth, and it is characteristic of equilibrium growth conditions. In contrast, at low temperatures ($T < 15^\circ\text{C}$), the domain size increases monotonically and slowly during growth and saturates at a significantly lower value, which is instead indicative of a non-equilibrium growth process. Surprisingly, the evolution of the domain size below 15°C was found independent of the growth rate (under the conditions employed), which was taken as suggestive of surface diffusion or molecular reorganization not being the rate-limiting processes in this regime [40].

The observed domain size evolution below 15°C is well described by a model in which a *fixed* number of islands grows monotonically in size (solid line in Fig. 27), which, in the isotropic case in 2D, yields [40]

$$L_D \sim \Theta^{1/2}. \quad (4.12)$$

These observations, coupled with the equilibrium (Θ, T) phase diagram (in which the lowest occurring melting temperature is about 15°C), suggest that the two growth regimes are due to the presence or absence of a liquid phase during growth. At higher temperatures, the liquid phase might provide a medium for molecular exchange between islands allowing the islands to grow (e.g., through Ostwald ripening), while at lower temperature no liquid phase is present, molecular exchange between islands is hindered, and the islands are stable once formed.

(v) *Temperature and flux dependence of the growth rate.* In order to understand better the processes involved in the growth, the dependence on the impingement rate (or partial pressure), P , and substrate temperature, T , was investigated [40–42]. For the lying-down phase, the initial sticking coefficient is of the order of unity. Therefore, the growth rate of the lying-down phase is determined by the impingement rate and practically not by the temperature under the conditions employed [40–42].

In contrast, the temperature and pressure dependence of the $c(4 \times 2)$ growth is more complicated. It was found in [40–42], that a simple functional form corresponding to Eq. (4.3) was sufficient to describe the $c(4 \times 2)$ uptake under all conditions employed,

$$\Theta_{c(4 \times 2)} = 1 - e^{-R(t-t_c)}, \quad (4.13)$$

where t_c is again a parameter describing the onset of the $c(4 \times 2)$ phase. Possible small deviations from the shape of the Langmuir growth law due to lateral interactions of the molecules (4.7) were not reported and can be neglected here, since we focus on changes of the rate as a function of temperature and pressure. $R = R(T, P)$ is the inverse of the growth time parameter τ_2 (4.11) and refers to the growth rate of the $c(4 \times 2)$ phase, as measured by an integrated diffraction peak representative of this phase (see Fig. 23). This determination of R is independent of the specific structure model discussed in Section 3.1. We should note that a calibration of the partial pressure of thiols is difficult. Besides general problems with measuring absolute pressures, the sensitivity of ionization gauges for hydrocarbon chains is

different from that for nitrogen, which is typically used for calibration [64,307]. The difference in sensitivity for alkanes (with n carbons) relative to nitrogen was found to be [64]

$$S_{\text{alkanes}}/S_{\text{N}_2} = 1.1n + 0.4, \quad (4.14)$$

i.e., for decane the pressure reading is about one order of magnitude higher than the actual pressure. However, these difficulties of determining the *absolute* pressure and impingement rate do not affect the general findings derived from *relative* changes of $R(T, P)$ as reported in [41,42].

Fig. 28 summarizes the temperature and the pressure dependence of the growth rate, indicating two distinct processes. At high T and low P the growth rate increases linearly with P as expected. In contrast to this simple behavior, at low T and high P , the growth rate increases *quadratically* with P (see in particular the 5°C data on the left-hand side of Fig. 28). This superlinear increase immediately suggests a cooperative adsorption process. Specifically, an exponent of 2 implies a bimolecular process (the probability of finding two molecules for adsorption increases quadratically with P).

The two distinct processes resulting in the $R \sim P$ and $R \sim P^2$ regime are also reflected in the temperature dependence of the rate (see right-hand side of Fig. 28). Each regime, linear and quadratic, exhibits a distinct exponential decrease of the rate

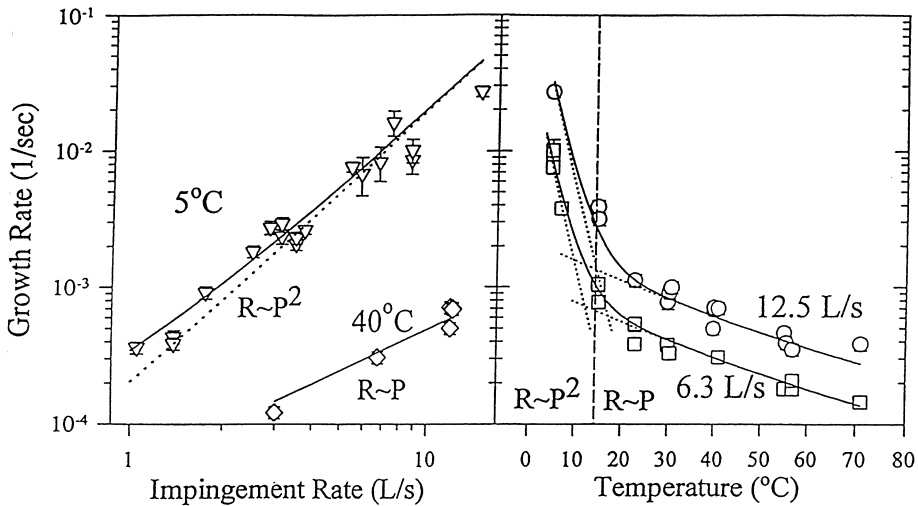


Fig. 28. Dependence of $c(4 \times 2)$ growth rate, R , of decanethiol on Au(111) deposited from gas phase at substrate temperature, T , and thiol partial pressure (i.e., impingement rate), P . At 40°C pressure dependence is linear ($R \sim P$), but at 5°C growth rate increases *quadratically* with P for high pressures (left panel). Temperature dependence of two-component growth rate at two fixed values of P is shown in right panel. Solid lines are fit to Eq. (4.15), i.e., sum of two different processes, each of which is shown as dashed line. Transition point indicating dominance of one of two processes is clearly visible in both lines of right panel, and shifts with changes in P . From [41].

with increasing temperature, which is usually taken as evidence that the adsorption proceeds via a physisorbed precursor state to chemisorption [308].

The temperature dependence of the rate, particularly the existence of a transition region and the domination of the faster process in each regime, suggests that the two processes operate in parallel, as opposed to one complex growth mode with two different rate-limiting steps. The growth data shown in Fig. 28 can be described empirically by

$$R(T, P) = A_1 P e^{E_1/k_B T} + A_2 P^2 e^{E_2/k_B T}, \quad (4.15)$$

with

$$E_1 = 0.30 \pm 0.05 \text{ eV}, \quad E_2 = 2.1 \pm 0.2 \text{ eV}$$

as obtained from fitting the growth rates at various temperatures and pressures [41]. (4.15) describes the data well within a broad range of pressures (i.e., impingement rates (0.2–20 L/s)) and substrate temperatures (5–70°C) as shown independently in [41,42]. It is only for very high P or very low T that the growth rate cannot continue to grow as P^2 , as discussed below.

Combining the Langmuir-like growth (4.13) with the empirical relation for the rate (with its linear and quadratic component, Eq. (4.15)), an appropriate *ansatz* for precursor-mediated growth (which is evidenced by the decrease of the rate with temperature) is [309]

$$\frac{d\Theta_{c(4 \times 2)}}{dt} = (k_1 \Theta_{\text{phys}} + k_2 \Theta_{\text{phys}}^2)(1 - \Theta_{c(4 \times 2)}), \quad (4.16)$$

where k_1 and k_2 are the transition rates for, respectively, the monomolecular and the bimolecular chemisorption process. The physisorbed precursor-coverage, Θ_{phys} , is determined by a balance of adsorption from the gas phase with (partial) thiol pressure, P , and a certain accommodation coefficient, α_P , re-desorption with a rate of k_d , and the rate of chemisorption to the $c(4 \times 2)$ phase

$$\frac{d\Theta_{\text{phys}}}{dt} = \alpha_P P (1 - \Theta_{\text{phys}}) - k_d \Theta_{\text{phys}} - \frac{d\Theta_{c(4 \times 2)}}{dt}. \quad (4.17)$$

Note that the first term on the right-hand side includes the factor $(1 - \Theta_{\text{phys}})$ which takes into account that there is only a finite number of sites in the first physisorbed layer. By doing so, the description is limited to transitions into the chemisorbed layer only from the first physisorbed layer. In order for the $c(4 \times 2)$ growth (4.16) to follow first-order Langmuir kinetics (with the rate, R , in Eq. (4.1) being time-independent), the precursor population must remain constant (i.e., the time derivative on the left-hand side of (4.17) must be equal to zero). With this specification ($d\Theta_{\text{phys}}/dt = 0$), solving Eq. (4.17) for Θ_{phys} and inserting into (4.16) at $\Theta_{c(4 \times 2)} = 0$ yields after some algebra

$$\left(\frac{d\Theta_{c(4 \times 2)}}{dt} \right)^2 - \left(\frac{d\Theta_{c(4 \times 2)}}{dt} \right) \left[\frac{k_1 k'_d}{k_2} + 2\alpha_P P + \frac{k'_d{}^2}{k_2} \right] + (\alpha_P P)^2 + \frac{k_1 \alpha_P P k'_d}{k_2} = 0, \quad (4.18)$$

with the abbreviation $k'_d = \alpha_P P + k_d$.

Equation (4.18), which can be easily solved for $(d\Theta_{c(4 \times 2)}/dt)$ (at $\Theta_{c(4 \times 2)} = 0$), describes the growth of the $c(4 \times 2)$ phase as a function of pressure and temperature. The temperature enters through the transition rates, k_d , k_1 , and k_2 .

During its residence time limited by the time scale for desorption ($\sim 1/k_d$) a molecule in the physisorbed precursor state can chemisorb either via the linear (k_1) or the quadratic (k_2) process. All three regimes (P^1 , P^2 , and P^0) are contained in (4.18).

Assuming $k_1 \gg k_2$, the linear process is easily recovered as a limiting case for low P

$$\left(\frac{d\Theta_{c(4 \times 2)}}{dt}\right)_{\Theta_{c(4 \times 2)}=0} \rightarrow \alpha_P P \left[\frac{k_1}{k_1 + k'_d}\right]. \quad (4.19)$$

The quadratic (bimolecular) process will become significant for high, but not too high physisorption coverages, which are caused by either high P (incident flux) or a long residence time ($\sim 1/k_d$) at low temperature.

Once the physisorbed precursor approaches saturation ($\Theta_{\text{phys}} \rightarrow 1$ for $P \rightarrow \infty$), no further increase of the effective growth rate of the $c(4 \times 2)$ phase is possible, and the rate is limited by the sum of the linear and quadratic transition rate

$$\left(\frac{d\Theta_{c(4 \times 2)}}{dt}\right)_{\Theta_{c(4 \times 2)}=0} \rightarrow [k_1 + k_2]. \quad (4.20)$$

as seen from (4.16). Obviously, once the rate-limiting step is the chemisorption process itself, a further increase of the supply from the gas phase to the physisorbed precursor has no effect and $R(P)$ has to saturate.

In fact, the beginning of saturation at lower T (corresponding to higher P) was evidenced by a less than linear increase of R after changing the impingement rate from 4.7 to 17.4 L/s at a substrate temperature of -5°C [42]. The entire growth scenario with the linear, the quadratic, and the saturation regime is shown schematically in Fig. 29, where the transition regions from $R \sim P^1$ to $R \sim P^2$ and from $R \sim P^2$ to $R \sim P^0$ (i.e., saturation) are indicated as shaded areas.

4.2.2. Unsaturated hydrocarbon thiols and other systems

4.2.2.1. *n-Alkenethiols on Au.* Given the strong similarity with alkanethiols, which is reflected in the same unit cell symmetry (see Section 3.1.2), one expects also the growth behavior not to be very different. While a systematic study has not been performed, the data existing so far in terms of formation of the standing-up phase support the notion that the growth behavior is indeed similar to the case of alkanethiols [103,104].

4.2.2.2. *Oligophenylthiols on Au.* For thiols with phenyl rings in the backbone, the impact of the molecule's stiffness on the growth can be investigated. This was done for the case of MMB for growth from solution, from the gas phase, and for "alkane-assisted" growth (see Section 4.4.2) [110]. For growth from solution, no other phase than the hexagonal phase was observed. The domain size was reported to be poor ($\sim 65 \text{ \AA}$), and in several growth attempts, no features of ordered structures were

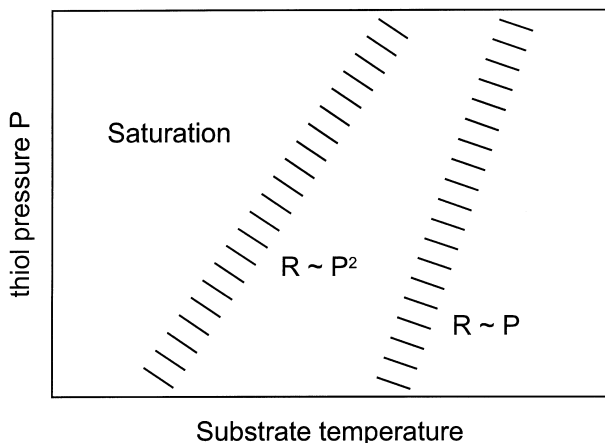


Fig. 29. Schematic of different growth regimes in pressure (i.e., impingement rate), P , and temperature, T , space. For high T and low P , the growth rate, R , increases linearly with P , whereas for lower T and higher P , R increases *quadratically* with P . Still lower T and higher P lead to growth rates that are almost independent of pressure, i.e., R begins to saturate. Note that boundaries between these three regimes (P^1 , P^2 , and saturation) are not sharp but rather transition regions. The $P^1 \rightarrow P^2$ transition can be seen in Fig. 28. Typical parameters for saturation regime are temperatures below 270 K and impingement rates above 10 L/s [42].

found at all, as confirmed by GIXD, LEAD, and STM. Relating to this, in [109] no evidence of an ordered structure was found for 4-mercaptobiphenyl, which is very similar.

For gas phase deposition, typically the lying-down phase was found, apparently forming rather fast. The domain size was reported to vary considerably as a function of substrate temperature, from about 180 Å at 279 K to values only limited by the substrate (i.e., above 1000 Å) at 387 K. For the layers grown at lower temperatures, the domain size could be easily increased by annealing. The standing-up phase turned out to be very difficult to form. Also in attempts at low temperature and high flux, which are expected to maximize the overall coverage, and subsequent annealing, a full-coverage layer was not achieved.

It appears that MMB also fits into the general picture of the fast formation of the lying-down phase, which can then act as an effective “kinetic trap” against the evolution of the standing-up phase. Since octadecanethiol has a similar interaction energy with Au(1 1 1) as MMB, but does not present problems forming the standing-up phase, it appears to be the role of the molecular backbone with its higher rigidity, i.e., less conformational degrees of freedom, and presumably the higher interaction energy which makes it harder for MMB to stand up.

Apparently, also the domain size evolution reflects these features in that they lead to a lower mobility on the surface at a given temperature. Compared to decanethiol/Au(1 1 1), which can form high-quality SAMs at room temperature, for MMB obviously the mobility on the surface is reduced. For higher temperatures, at least for the lying-down phase, similar domain sizes can be found. Since for MMB only the

backbone is different to decanethiol, these results underline the importance of also this molecular feature for the growth.

4.2.2.3. OH-terminated thiols on Au. The growth of mercaptohexanol ($\text{SH}-(\text{CH}_2)_6-\text{OH}$) was studied in detail using STM [39]. Although the full-coverage phase does not correspond to the usual $(\sqrt{3} \times \sqrt{3})$ structure (see Section 3.1.2), the scenario of a lying-down phase followed by a standing-up phase was found also for this system. This is shown for different stages of the growth in Fig. 25. Similar to alkanethiols (Section 4.2.1), the nucleation of the standing-up phase of mercaptohexanol requires relatively high exposures (of the order of 1000 L according to [39]), implying that the effective sticking coefficient for the growth of the standing-up phase is well below one.

4.2.2.4. Dithiols on Au. For dithiols, the potentially chemisorbing second thiol group can have a strong impact both on the growth and the resulting structures. As outlined in Section 3.1.2, the structures were investigated in detail for alkanedithiols, particularly for 1,6-hexanedithiol on Au(111) [130], for which very stable lying-down phases were found. In fact, as reported in [130] for 1,6-hexanedithiol on Au(111), the standing-up configuration has not been obtained with long range order, neither by vacuum deposition under various conditions (different substrate temperatures and extended exposures) nor by solution deposition (we should emphasize that this may be different for other chain lengths, for which the less chemisorption energy per unit area in the lying-down phase is less).

Similar to the lying-down phase of alkanethiols, the growth kinetics of 1,6-hexanedithiols are governed by a sticking coefficient close to unity [130]. Since even extensive vapor deposition did not result in higher-density phases, it has to be assumed that the lying-down phase at least forms a very effective “kinetic trap” and that the second thiol group sticks to the substrate so strongly that it is very difficult to lift it up, although the standing-up configuration might be energetically more favorable (in terms of energy per area). If compared with (4.11) for alkanethiols, this kinetic trap can be viewed as having the same effect as $\tau_2 \rightarrow \infty$.

The presence of a second potentially chemisorbing group also influences the mobility of the molecules on the surface. In contrast to alkanethiols, deposition around ambient temperatures resulted in only small domain sizes (~ 100 Å). Leung et al. [130] found that in order to obtain well-ordered structures with large coherence lengths, deposition at elevated temperatures is needed (typically around 80°C). In that case domain sizes only limited by the substrate (~ 2000 Å) could be obtained. The growth data for alkanedithiols, both the stability of the lying-down structure against further exposure as well as the very limited mobility of the molecules on the Au(111) surface at room temperature, underline the important role of the second chemisorbing thiol group.

4.2.2.5. Dialkyl disulfides and dialkyl sulfides on Au. For long-chain dialkyl disulfides, the structure of which was reported to be indistinguishable from that of the corresponding alkanethiols, no detailed growth studies were performed in the gas phase. Nevertheless, it was pointed out that the chemisorption of dimethyl disulfide is much

faster than for methanethiol. It was suggested that this is due to the fact that chemisorption of the disulfides does not require breaking of the S–H bond and formation of H₂ (see [47,135] and discussion therein), but we note that also the presumably longer lifetime of a physisorbed precursor of disulfides may play a role.

The comparison of dialkyl disulfides and alkanethiols appears to be different for solution growth of longer chain lengths. Jung et al. [134] reported that SAMs of disulfides form 40% more slowly than thiols, referenced to the number of thiol groups. This may be understandable in view of the fact that the rate-limiting step appeared to be the displacement of solvent molecules. Chemisorption of disulfides requires the simultaneous availability of two sites, which is less probable than the one site required for a thiol molecule. Bain et al. [132] reported that if mixtures of disulfides and thiols are grown from solution, adsorption of the thiol was strongly preferred.

For dialkyl sulfides, usually no chemisorption features are detected [135,310], which is consistent with the finding of only poorly ordered layers (see Section 3.1.2). Nevertheless, a recent study reported that S–C bond cleavage and chemisorption of the S group should be possible under special conditions [311].

4.2.2.6. Thiols on Cu. For alkanethiols on Cu ((1 1 1), (1 1 0), and (1 0 0)), Wöll and coworkers [156,312] reported the remarkable result that a chemisorbed lying-down phase could not be found. In the lying-down configuration, only a physisorbed state was found. Whether this is due to the different energetics compared to Au(1 1 1), the smaller lattice constant, which imposes some constraints, or other reasons remains to be investigated.

The growth of heptanethiol on the open surface of Cu(1 1 0) has been studied in detail [156]. Below 200 K, multilayer formation is reported. At somewhat higher temperatures (>200 K), a physisorbed monolayer is found, which serves as a precursor for chemisorption at still higher *T*. In contrast to the rather disordered physisorbed overlayers, several superstructures for the various coverages have been observed for the chemisorbed layer. For *T* > 370 K, the authors report S–C bond cleavage and the desorption of the alkyl chains, with the S atoms remaining on the surface in the form of ordered adlayers (in contrast to the case on Au(1 1 1)).

4.3. Physisorption and chemisorption: energetics and kinetics

The growth kinetics as well as the resulting structures depend on several energy parameters and their respective balance. These multiple energy scales are also one of the defining characteristics of self-assembly compared to the growth of “simple” (atomic) adsorbates. Various parameters related to interaction energies or energy differences were investigated, some of which have already been discussed at other places of this review. Before discussing these in detail, we first try to provide an overview of various energy terms below. 100 kJ/mol corresponds to 23.9 kcal/mol and to 1.0366 eV (per molecule).

Molecule–substrate interaction: adsorption. The adsorption energy is the strongest of all interactions and presumably the primary driving force for the self-assembly

process. Chemisorption and physisorption need to be distinguished. Due to the additive contributions of the van der Waals forces of the entire chain, the physisorption (e.g., ~ 104 kJ/mol (1.08 eV) for decanethiol on Au(111)) can become comparable to the chemical bond formed by the headgroup to the substrate (e.g., ~ 126 kJ/mol (1.30 eV) for decanethiol on Au(111)). We should note that in principle also the headgroup bond *angle* (e.g., the Au–S–C angle) enters the energy balance for the resulting structure, since it will generally not act like a freely rotatable joint, but exhibit preferential orientations.

Molecule–substrate interaction: corrugation. While the adsorption energy refers to the difference between the free molecule and the adsorbed state, the substrate corrugation refers to the difference between different adsorption sites. It is important for the mobility of the molecules during the growth (domain size evolution) and also has an impact on the detailed energy balance in the resulting molecular structure. In principle, one would have to distinguish the corrugation experienced by the entire molecule including the chain in the lying-down phase and that experienced by only the chemisorbing headgroup in a standing-up configuration. Since the Au(111) surface is closed packed and its electron distribution very smooth, one would expect a small corrugation, which is supported by the fact that thiols exhibit a detectable mobility during the growth at room temperature.

Chain–chain interaction. For higher coverages the chain–chain interaction will become more and more important and, ultimately, play a crucial role in the packing. Based on the heat of vaporization (i.e., the molecule–molecule interaction), e.g., for decanethiol in the bulk one would expect about 66 kJ/mol (0.68 eV) (including thiol–thiol interaction).

Conformational energies. The energy cost of a gauche defect in an isolated hydrocarbon chain is ~ 0.022 eV [313], which can be thermally activated at room temperature. This gives the molecule a certain flexibility, which might support the structure formation process, although in the final standing-up structure at full coverage the molecular backbone of the alkanethiols needs to be straight to be accommodated in the $c(4 \times 2)$ structure. The same applies to the striped phase.

Endgroup–endgroup interaction. Generally, one should distinguish this term from the chain–chain interaction, since the endgroup can be changed with the chain unchanged. For methyl-terminated molecules the endgroup–endgroup interaction is not be very strong, but for other terminations, it can play a significant role.

Chemisorption barrier on bare substrate. This term refers to the energy barrier between the physisorbed and the chemisorbed state. It has a great impact on the kinetics of chemisorption. The barrier height was found to be around 29 kJ/mol (0.3 eV) for alkanethiols on the bare Au(111) surface.

Chemisorption barrier on existing (intermediate coverage) layer. These barriers were determined from the $c(4 \times 2)$ growth kinetics in Section 4.2 ($E_1 = 29 \pm 5$ kJ/mol (0.30 ± 0.05 eV) for linear growth and $E_2 = 203 \pm 19$ kJ/mol (2.1 ± 0.2 eV) for quadratic growth). However, relating these to fundamental processes is not a trivial task, since they refer to growth on an already existing layer and not the bare surface. In that sense, one might consider them as *effective* barriers, which result from the balance of several different contributions.

Admolecule energetics. Once a certain coverage is reached, the additional impinging molecules will experience the interaction with the molecules of the existing layer. Initially, these molecules will form a partial second layer on top of those molecules already adsorbed, before they are potentially included in the growing layer. The strength of the admolecule interaction is expected to be between the bulk interaction and the physisorption interaction with the surface. For decanethiol, this would be between 66 kJ/mol (0.68 eV) and about 104 kJ/mol (1.08 eV). Furthermore, the energy of admolecules is also important for wetting studies with other species than the SAM-forming molecules.

4.3.1. Measurements of adsorption and desorption

The determination of the physisorption and chemisorption energetics is a key point for the understanding of the growth, particularly in the initial stage of adsorption. The adsorption and desorption of a variety of sulfur-containing hydrocarbons onto Au(1 1 1) have been investigated in [135,64] using HAR and TPD techniques. The desorption enthalpies, E_{des} , were estimated from the temperature of maximum desorption, T_{des} , in a temperature ramp experiment with heating rate, β , using the Redhead equation [314,315]

$$E_{\text{des}} = R_{\text{g}} T_{\text{des}} [\ln(v T_{\text{des}} / \beta) - 3.64], \quad (4.21)$$

where R_{g} is the gas constant and v is a typical oscillation frequency on the surface, assumed to be $\sim 1 \times 10^{13} \text{ s}^{-1}$. While this assumption as well as the use of the Redhead equation itself (particularly for larger molecules with many internal degrees of freedom) might introduce some uncertainty for the absolute value of E_{des} , the relative differences between various compounds can be directly discussed, since the TPD data were obtained under the same conditions, so that a given difference in energy comes from a corresponding difference in desorption temperature. Therefore, the discussion and the conclusions below are not affected by this uncertainty.

In most cases, two TPD peaks were observed, one originating from a physisorbed state of the respective molecule, the other from a chemisorbed state. The results for the energetics obtained from TPD data like in Fig. 30 are summarized in Table 1 and will now be discussed.

4.3.2. Chemisorption energetics

As can be seen from Table 1, the chemisorption enthalpies are independent of chain length $126 \pm 2 \text{ kJ/mol}$ (1.30 eV).⁵ Only for those compounds where steric hindrance effects are expected to have an impact on the bond formation, deviations

⁵ In this context, the chemisorption energy shall be the energy *only* of the chemical bond mediated by the sulfur. The *total* interaction energy of a chemisorbed alkanethiol lying down on the surface includes both this energy of the chemical bond and the van der Waals forces of the molecular backbone.

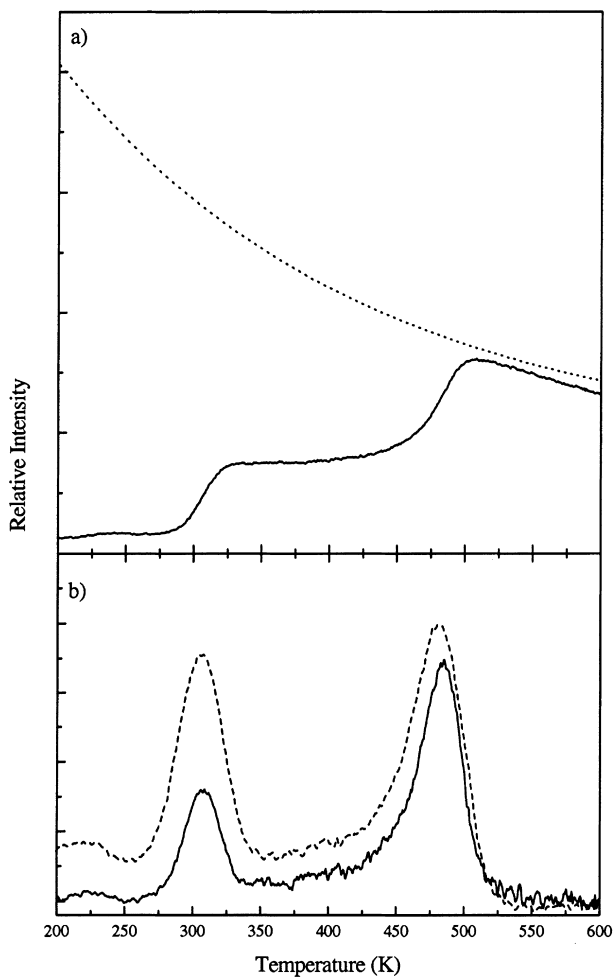


Fig. 30. TPD spectra of hexanethiol on Au(111) as derived from HAR data. Upon thermal desorption of molecules, raw HAR signal increases in step-wise fashion (a). Dotted line reflects Debye–Waller attenuation (clean Au surface). Temperature derivative of HAR signal (b) (with and without correction for Debye–Waller attenuation), is comparable to traditional TPD data. Low-temperature peak (which changes with chain length) corresponds to physisorbed state, high-temperature peak (which does not change with chain length) to chemisorbed state. TPD temperatures shown correspond to a desorption enthalpy of 79 kJ/mol for physisorbed state and 126 kJ/mol for chemisorbed state. From [40] (where it was incorrectly labelled “octanethiol/Au(111)” instead of “hexanethiol/Au(111)”).

were found (marked^{hin}). Both *tert*-butanethiol and 2-propanethiol show physisorption enthalpies consistent with predictions based on the additive contribution to binding per methylene unit, but a lower than normal chemisorption enthalpy of 107 kJ/mol. Adding one methylene group between the thiol and the *tert*-butyl group forms neopentanethiol, which already behaves “regularly” with a chemisorption

Table 1

Desorption enthalpies (in kJ/mol) of various hydrocarbons with and without thiol group from physisorbed and chemisorbed state on Au(1 1 1) after [64,135]^a

Molecule	Physisorption	Chemisorption
Methane	14.5	
Ethane	24.1	
Butane	40.5	
Hexane	55.9	
Heptane	62.7	
Octane	69.7	
Nonane	75.2	
Decane	80.1	
Dodecane	93.6	
Ethylene	27.0	
<i>trans</i> -2-Butene	41.7	
<i>cis</i> -2-Butene	44.5	
2-Methylpropene	45.4	
1-Hexene	56.6	
1-Octene	70.1	
1-Nonene	76.2	
1-Decene	81.1	
1-Undecene	87.8	
Cyclohexane	50.6	
Cyclooctane	63.1	
Benzene	57.9	
Toluene	66.1	
Propylene	35.0	
Allene	34.2	
1,3-Butadiene	46.2	
Ethanethiol	57	127
Butanethiol	68	127
Hexanethiol	79	124
Octanethiol	87	125
Nonanethiol	103	127
Decanethiol		126
Dodecanethiol		127
Tetradecanethiol		128
Hexadecanethiol	150	
Octadecanethiol	150 ± 10	
Docosanethiol	169 ± 10	
Diethyl sulfide	68	
Dibutyl sulfide	86	
Diethyl disulfide		124
<i>tert</i> -Butanethiol	64	107 ^{hin}
2-Propanethiol	64	107 ^{hin}
Neopentanethiol	68	128
1,6-Hexanedithiol		129
Thiophene	60	

^a Error is about 2 kJ/mol. For a comparison with data from other authors see text. For some compounds steric effects give rise to hindered bond formation and, therefore, reduced chemisorption enthalpies (marked^{hin}).

enthalpy of 128 kJ/mol. The extra methylene group removes the steric hindrance of the *tert*-butyl group [135].

The dialkyl sulfides did not exhibit a chemisorption feature, suggesting that they remain intact on the surface and experience no C–S bond cleavage [135], consistent with the results of [310], but in contrast to [316] which reported C–S bond cleavage in several organosulfides under electrochemical conditions.

For some compounds, not only the chemisorption peak corresponding to 126 ± 2 kJ/mol or 1.30 eV (for the sterically not hindered thiols), was found, but also an unexpected additional higher-energy peak (around 150 ± 2 kJ/mol or 1.55 eV) termed “chem2” [135]. This feature was observed only for chains with more than eight carbons. Its origin could not be entirely resolved, but since its occurrence was related to high flux dosing conditions and since its intensity compared to the “regular” TPD feature corresponding to 126 ± 2 kJ/mol (“chem1”) could be decreased by waiting or annealing periods, it was speculated that it might be related to defects in the structure introduced by non-equilibrium growth conditions [135].

4.3.3. Physisorption energetics

The TPD peaks related to physisorption (Table 1) were analyzed in detail in [135,64], and a bond-additive model was developed which predicts the physisorption enthalpy of a large number of compounds. As a fairly robust rule for various molecules it was found that the physisorption enthalpies scale with the bulk heat of vaporization (with a slope of 1.15, but a non-zero y -intercept), suggesting that the interaction with the surface is also due to van der Waals forces [135]. For alkanes as well as for alkanethiols a simple linear dependence on the chain length with essentially the same slope holds. The data are summarized in Fig. 31, including also the chemisorption contribution. The best fits for the desorption enthalpies from the physisorbed state are [135]

$$E_{\text{des}}^{\text{alkanethiol}} = [6.08(\pm 0.74)n + 43.5(\pm 5)] \text{ kJ/mol}, \quad (4.22)$$

$$E_{\text{des}}^{\text{alkane}} = [6.16(\pm 0.16)n + 19.4(\pm 1.4)] \text{ kJ/mol}, \quad (4.23)$$

where n is the number of carbon atoms. The contributions from the polarizability of various parts of the molecules could be separated based on a comparison of a large number of compounds [135,64]. It was found that a CH_2 group contributes 6.2 ± 0.1 kJ/mol in a linear chain. Earlier estimations by Dubois et al. [47,63] had resulted in 7.9 kJ/mol. The value for a CH_2 group in cyclic compounds is 8.1 kJ/mol. A CH_3 group contributes 15.5 kJ/mol. The additional contribution of a double-bond (in alkenes) is 6.1 kJ/mol. An SH group contributes 33.5 kJ/mol and a single S atom 24.1 kJ/mol [135,64]. This can be compared to studies of alcohols, ethers, and alkanes on Cu(001) and Pt(111) [317] where 5–6.5 kJ/mol were found for a CH_2 group and 42 kJ/mol for an oxygen lone pair on Pt(111) and 35 kJ/mol on Cu(001). Similar values (6.3 kJ/mol per methylene unit on Cu(001)) were also reported by Teplyakov et al. [318]. For a comparison with TPD data for larger aromatic compounds see [319]. A theoretical discussion of the physisorption of

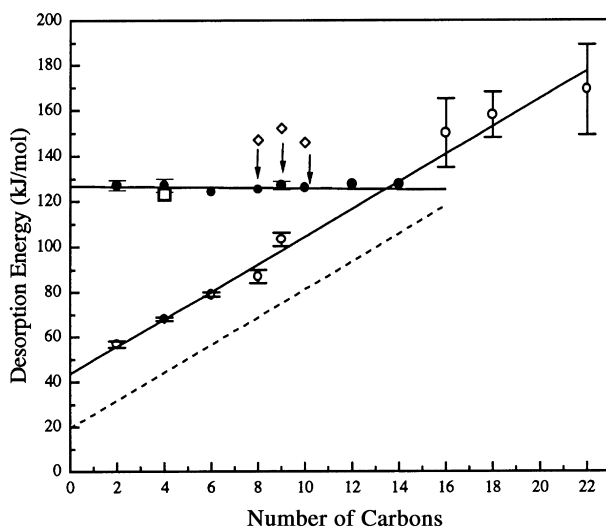


Fig. 31. Physisorption (open symbols) and chemisorption (full symbols) enthalpies on Au(111) for various alkanethiols as function of number of carbon atoms, n . For comparison, physisorption data for alkanes are indicated as dashed line. Open diamonds indicate “chem2” state discussed in text. Open square stands for chemisorption enthalpy of diethyl disulfide. From [135].

hydrocarbons on metals including the effect of the deformability of the surface can be found in [320].

For decanethiol on Au(111) discussed thoroughly above, 104 kJ/mol or $1.08(\pm 0.05)$ eV were obtained for physisorption and 126 kJ/mol or $1.30(\pm 0.05)$ eV for chemisorption, i.e., the two interactions are already comparable. Due to the linear increase with chain length, the physisorption contribution for alkanethiols on Au(111) is stronger than the chemisorption starting at $n \sim 14$.

For some compounds such as diethyl disulfide and 1,6-hexanedithiol no data for the physisorbed state were obtained, since apparently the conversion to chemisorption was too rapid [64]. The kinetic aspects of the adsorption process will now be discussed.

4.3.4. Adsorption kinetics

The energetics discussed above have a direct impact on the kinetics of adsorption, which was analyzed in [135,64]. Again, we emphasize that the data discussed here refer to the initial stage of the adsorption, not to the later stage such as the formation of the $c(4 \times 2)$ structure.

Intuitively, one expects that a high physisorption interaction supports a high initial sticking coefficient. In fact, at low temperature, the initial sticking coefficient is near unity for the alkanethiols used in SAMs. As expected, a decrease of the sticking coefficient is observed as the surface temperature is increased. This effect does not become pronounced until the surface temperature is approximately 50 K below T_{des} of each species.

To compare the behavior of different molecules, the sticking coefficients were plotted against the reduced temperature $T^* = T/T_{\text{des}}$ (Fig. 32) [64]. Since in this representation the data overlap for all *n*-alkanes and 1-alkenes, apparently the mechanism of initial adsorption (in the physisorbed state) is the same for all these species (the alkanethiols from 2 to 10 carbons (not shown) follow a similar behavior [64]).

In [64], it was concluded that the origin of the decrease in sticking coefficient is due to incomplete accommodation of the molecule by the Au(111) surface at higher temperatures. Even though the adsorbate molecules are only arriving with an average of 3.6 kJ/mol of translational energy ($E = (3/2)k_B T$ at 300 K), this quantity is sufficient to allow the molecule to avoid physisorption at surface temperatures near T_{des} . At low surface temperature, both phonon creation and intramolecular energy transfer from translational to rotational (and less likely, vibrational modes) can allow the molecule to become trapped in the physisorption well of the surface. However, at higher surface temperatures, the surface is unable to readily accept energy from the molecule resulting in incomplete accommodation [64].

The strong physisorption also has an impact on the chemisorption, since it is supposed to keep the alkanethiol molecule on the surface for a relatively long period of time and thereby increase its chances to chemisorb, i.e., overcome the barrier to chemisorption, E_{pc} . This chemisorption from a physisorbed precursor state can be a highly effective pathway for large molecules that are still capable of physisorption at high surface temperatures where the available thermal energy is sufficient to over-

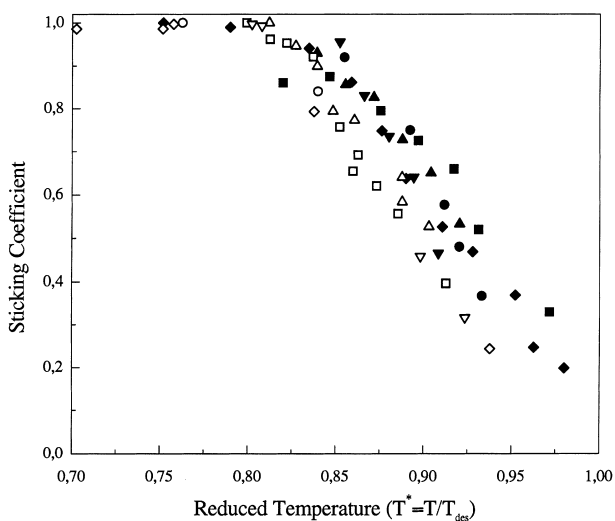


Fig. 32. Initial sticking coefficient on Au(111) as function of temperature (normalized to respective desorption temperature). Filled symbols refer to alkanes: heptane (squares), octane (circles), nonane (diamonds), decane (up-triangles), and dodecane (down-triangles). Open symbols refer to alkenes: hexene (squares), octene (circles), nonene (up-triangles), decene (down-triangles), and undecene (diamonds). Within certain scatter of data, behavior is universal. From [64].

come E_{pc} . Since the chemisorption rate is related to the population of adsorbates and the residence time, the rate of chemisorption from the physisorbed precursor (which competes with desorption) will generally *decrease* with increasing surface temperature.

Although in the direct chemisorption process (the probability of which *increases* with surface temperature) the molecule might have more free energy to overcome the barrier, for alkanethiols on Au(111), e.g., the precursor-mediated route is actually the dominant process to chemisorption, since the physisorbed molecule is held in relative proximity to the surface for a period much longer than the few picoseconds of a typical single elastic or mildly inelastic surface encounter [135,64].

The conversion rates from the physisorbed precursor to chemisorption were determined in [135]. The rate was found to decrease from, e.g., 4×10^{-4} s for butanethiol to 3.3×10^{-5} s for hexanethiol, both at 208 K. Using an Arrhenius plot for the temperature dependence of this rate, the effective height of the barrier, E_{pc} , between physisorption and chemisorption could be estimated to 29 kJ/mol (0.3 eV), independent of chain length for the molecules under investigation (ethanethiol, butanethiol, hexanethiol, and decanethiol) and with an error bar of about ± 5 kJ/mol. Within the limits imposed by the error bar, the data suggest that, while the physisorbed well depth increases with chain length, the location of the curve crossing with the chemisorbed state remains the same, and therefore the activation barrier to chemisorption remains constant with increasing chain length [135]. Based on collision experiments with Xe, E_{pc} was recently determined to (0.41 ± 0.06) eV for ethanethiol, which is consistent with the above value within error bar [321]. A schematic of the interaction potential is shown in Fig. 33.

4.3.5. Admolecule (“2nd layer”) energetics

As outlined in the introductory words of this subsection, the energetics of admolecules (as a “2nd layer” on an existing layer) is very important for the growth, particularly for the later stages when not only the interaction with the bare substrate is relevant. The adlayer energetics determine the stay time in a possible physisorbed second layer, which ultimately has an impact on the chances of a given molecule to chemisorb.

In [42], it was attempted to measure the admolecule energetics of decanethiol on decanethiol-SAMs at different coverages during the growth of the SAM, but a reliable experimental determination is not easy. Among other things, this is due to the fact that at intermediate coverages the additional admolecules can, of course, also be accommodated in the SAM structure, which would make a classical TPD experiment difficult.

By following the time evolution of the partial desorption (with typical time scales below 2 s) after dosing a small amount of the molecules (on layers of intermediate coverage), and also TPD (for admolecules on a full-coverage layer), both detected by HAR, it was found that, as a rough rule, the interaction energy of the decanethiol admolecule decreased with increasing coverage of the SAM. This might be expected

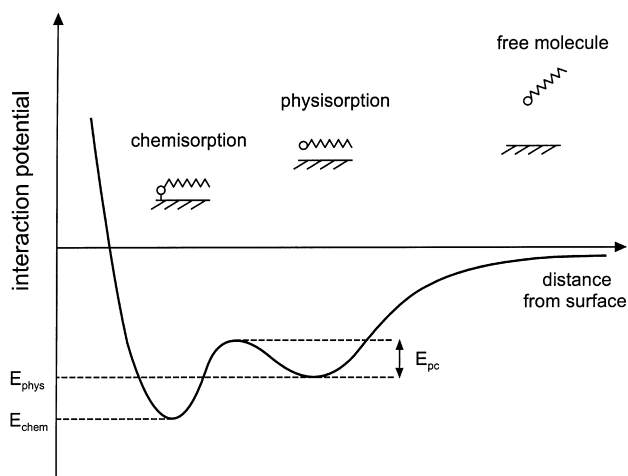


Fig. 33. Schematic of interaction potential between decanethiol and bare Au(111) surface as function of distance, as derived from measurements at low coverage. Physisorption and chemisorption interaction are derived from TPD data. Note that chemisorption value refers only to chemical bond mediated via sulfur atom, although (additive) van der Waals forces are still acting on molecular backbone as long as it is lying flat on surface (so that *total* energy can actually be higher). Activation barrier for conversion from physisorbed precursor to chemisorbed state is obtained from rate of this process as function of temperature. Shape of potential and distances corresponding to minima are not exactly known.

due to the decreasing contribution of the van der Waals interaction with the substrate. More precisely, it decreases from about 1.1 eV physisorption energy on the bare Au(111) surface [135] to 0.74–0.80 eV on the stripes phase and to about 0.70 eV on the full coverage $c(4 \times 2)$ [42]. However, it has to be emphasized that these values should be considered only as estimates. Also, the experiments of the time evolution after dosing on the stripes showed that there was not only one time scale involved, indicating the presence of sites of different energy, which makes an interpretation even more difficult. Interestingly, under suitable conditions the adlayer was even observed to be well-ordered [42].

The data for the adlayer energetics (with adlayer species being the same as those forming the SAM) might be compared to studies of “microscopic wetting” by Dubois et al. [63], where water, methanol, and *n*-hexane on SAMs with various types of surface terminations (acid, methyl, amide, ester, alcohol) were investigated. It turned out that established analytical methods failed to treat the type of complex TPD data found [63], and it was concluded that E_{des} and ν are coverage-dependent. Therefore, the analysis was limited only to an estimation according to the Redhead equation (Eq. (4.21)). For *n*-hexane on a methyl-terminated surface, $E_{des} \sim 8.1$ kcal/mol (34 kJ/mol; 0.35 eV) was found. Furthermore, it was found that the data on the energetics obtained from TPD do not exhibit a simple correlation with contact angle data. The authors concluded that the two techniques measure different aspects of the relevant interfacial thermodynamics [63]. Generally, we note that besides the nature of the endgroup of the SAM also the long-range van der Waals interaction with the

substrate can play a role, which can lead to differences in the wetting angle as a function of chain length for a given endgroup [220]. For other adsorbates and a discussion of wetting studies see Section 3.4.3.

4.3.6. Adsorption from solution

For solution deposition, it is very difficult to determine the energetics. We might assume that the absolute chemisorption energy and also the physisorption energy will be the same as in UHV, but in growth from solution the energy *difference* between the adsorbed molecule and the non-adsorbed molecule (i.e., in vacuum or dissolved in solution, respectively) will be less. In that sense, the chemisorption or physisorption on the surface is related to a smaller energy gain in solution. Other differences between solution and gas phase deposition are discussed in Section 4.4.3.

4.4. Discussion of growth behavior

In the above sections, it has become obvious that there are several issues related to the growth which constitute significant deviations from trivial behavior. Using the supposedly “simple” alkanethiols as a paradigmatic case, below we summarize these deviations, which are ultimately related to the various internal degrees of freedom and multiple energy scales of the molecules. In addition, we discuss further means to influence the growth with (external) control variables. We also compare the results from solution and gas phase deposition.

4.4.1. Deviations from “simple” growth behavior

An important deviation and also the reason for other non-trivial effects is the occurrence of low-coverage phases like the striped phase and the IS as observed for decanethiol on Au(111) before the growth of the $c(4 \times 2)$ (Fig. 16). Since the molecules can arrange themselves in different configurations, a scenario with multiple phases is rather typical than exceptional for SAM-forming molecules. Related to this are the multiple time scales (at least two very different for gas phase deposition of decanethiol on Au(111)) (Fig. 23), since in general one might expect as many time constants as phases on the coverage axis at a given temperature. An additional time scale can be the long-term reorganization effect observed for long-chain thiols deposited from solution (Fig. 22), although this was not found for shorter-chain thiols deposited from vapor.

The observation of kinetic traps ultimately seems also related to the multiple phases, since for growing a higher-coverage phase out of a stable low-coverage phase a certain threshold has to be overcome. Kinetic traps and other observations related to the effect of a lower-coverage phase minimizing the *energy per molecule* (e.g., in a lying-down configuration) and thereby hindering the growth of a higher-coverage phase minimizing *energy per unit area* are not only observed for decanethiol. In fact, they are a rather general phenomenon (at least for gas phase deposition), as seen from the fact that the standing-up configuration is difficult to obtain also for e.g., dithiols and biphenylthiols. Obviously, not only the energetics, i.e., the (equilibrium) thermodynamics, determine the phases but also the kinetics of the growth.

While the effect of kinetic traps can be, in some sense, related to the impingement rate being “too low”, at higher impingement rate/lower temperature also deviations from simple behavior were found. One of these is the P^2 effect (Fig. 28) which is the signature of a collective (bimolecular) adsorption channel. Other deviations from simple growth behavior at low temperature and high rate are the coexistence of phases due to inhomogeneous nucleation of higher-coverage phases under non-equilibrium conditions and the different regimes of domain size evolution (Fig. 27). The second chemisorption state (Section 4.3), the origin of which was not resolved, also seems to be a non-trivial observation.

4.4.2. Means to influence the growth

The primary control parameters are certainly the substrate temperature, T , and the solution concentration, c , or the partial pressure, P , respectively. As shown above, the growth rate can be varied in a wide range, and various degrees of order and crystalline coherence (domain size) can be obtained changing only T and c or P (and the deposition time, t). This can be exploited, e.g., for obtaining a pre-determined (intentionally small) island size with non-full coverage at low T , which is complemented later with other molecules, forming a laterally structured film.

Of course, various molecular features such as the stiffness and length of the backbone or the endgroup also have an impact on the growth and the structures, but these are rather intrinsic parameters inherent to a specific SAM system, and here we want to focus on *external* control parameters.

Besides changing the above parameters, two ways to control the growth have been explored. In addition to offering chances to “engineer” the growth, they provide further insight in the intrinsic growth mechanisms.

Nanografting. This methodology, which employs an AFM tip, was explored for solution deposition in [322]. After imaging an existing layer with the AFM and positioning the tip above a selected site, the tip load is slowly increased to slightly above the displacement threshold for thiol adsorbates. During the scan, the AFM tip displaces the matrix thiols underneath the tip and exposes the Au(111) surface to the thiol solution. This creates a transient microenvironment in which the freshly exposed Au(111) surface is spatially constrained by the surrounding thiols and the AFM tip. Within this area, thiols will self-assemble onto the newly exposed Au(111) surface, which is finally imaged at a reduced imaging force.

It was found that this spatially constrained self-assembly process occurs at least a factor of 10 faster than the conventional (unconstrained) self-assembly. Moreover, a scar-free morphology and long-range order of the newly formed SAM were reported [322].

The mechanism proposed for the accelerated self-assembly during this “nanografting” [322] assumed that sufficient spatial confinement can sterically hinder or prevent thiol molecules from adopting a lying-down phase and instead favor a standing-up configuration. While this is probably difficult to prove directly, it is certainly a plausible explanation and consistent with the observations in the un-

constrained (“regular”) growth where the existence and stability of low-coverage phases is apparently the reason for the much slower growth of a subsequent (standing-up) phase.

Surfactant-modified growth. Whereas for inorganic films the use of surfactants for the modification of the growth is rather well established in certain systems (such as submonolayer Sb deposition in Ag homoepitaxy or the use of As in Si/Ge/Si(001) heterostructures) [323,324], for SAMs it is rather uncommon. For the purpose of language clarification, we should note that occasionally the term “surfactants” (surface active agents) is used already for the molecules forming the SAM. However, in the present context we use the term surfactants only for those molecules (e.g., alkanes), which are pre- or co-deposited to modify the adsorption energetics, the stay time before chemisorption, and the mobility and, thus, the growth behavior of the actual SAM molecules. Since also typical solvent molecules can be employed, this concept, which has been tested on only a few SAM systems [110,325], also forms a link between gas phase and solution deposition.

Preliminary data for the use of octadecane as surfactant for decanethiol on Au(111) indicate that the onset of the growth of the $c(4 \times 2)$ phase is delayed [325]. However, after the growth has nucleated, it is not correspondingly retarded, but catches up at later growth times. This scenario suggests that the thiols, which are initially prevented from immediate chemisorption in the $c(4 \times 2)$ phase, stay in a physisorbed layer and are not lost for the $c(4 \times 2)$ growth. We should note that the effect on the growth kinetics appears to be more pronounced for longer alkane chains (octadecane was compared to dodecane, i.e., $n = 18$ vs. $n = 12$) and for temperatures below room temperature [325]. The concept of surfactant-modified growth was also applied to MMB [110].

4.4.3. Solution vs. gas phase deposition

While the resulting equilibrium structures should be and are, in fact, equivalent (in a crystallographic sense) for solution and gas phase deposition, the growth exhibits some differences (see also Table 2).

From the point of view of the absolute chemisorption interaction and also the physisorption interaction, we might assume that they will be the same in solution as in UHV, although for solution deposition it is very difficult to determine the energetics. The main difference in terms of the energetics will be that for growth from solution the energy *difference* between the adsorbed molecule and the non-adsorbed molecule (due to the attraction by the solvent) will be less compared to the corresponding energy difference for UHV deposition. In other words, the chemisorption or physisorption on the surface is related to a smaller energy gain in solution.

This attraction by the solvent might still be relevant even when the headgroup has chemisorbed, since it can make the threshold for the backbone to stand up smaller. In that sense, it might be easier to form the standing-up phase.

Conversely, the lying-down phase turned out to be more difficult to observe for solution growth, although it was eventually found. This may be due to the fact that the standing-up phase can nucleate more easily (i.e., at a lower threshold in coverage)

Table 2

Simplified comparison of solution and gas phase deposition of SAMs, based on results from alkanethiols on Au(111)^a

	Solution deposition	Gas phase deposition in UHV
Apparatus Environment	Simple and inexpensive Contaminations difficult to exclude	Sophisticated and expensive Clean
In situ analysis	Only those techniques working “through” solution	All UHV-based techniques applicable
Adsorption process	Involves physical “displacement” of solvent molecules	No “displacement” of solvent molecules needed
Impact of presence/absence of solvent		
For lying-down phase	Formation might be hampered	Formation easier
For standing-up phase	Formation might be facilitated	Energy barrier can be higher for transition from lying-down
Mass transport to the surface during growth	Diffusion	“Free” motion

^aNote that this can only be applied to systems in which solvent does not play chemically active role in adsorption process. Also, comparison for lying-down and standing-up phase is only applicable if both phases appear as function of coverage.

and, secondly, that the presence of the solvent molecules makes it more difficult to form the lying-down phase. This is understandable already in a simple mechanistic picture. At the very start of the growth, the surface is covered entirely by solvent molecules. For the displacement of these solvent molecules (which are in van der Waals contact with the surface) a certain energy threshold has to be overcome. Since in the lying-down configuration a large portion of the molecule (the hydrocarbon chain) will also only be bound by van der Waals forces, the energy gain upon formation of the striped phase in solution is not so high and results only from one chemical bond on a fairly large area ($\sim 80 \text{ \AA}^2$ for decanethiol). Again, this does not exclude the presence of a lying-down phase, but it makes plausible, why it is more difficult to observe. In contrast, for the standing-up phase a much smaller area (21.6 \AA^2 in the $c(4 \times 2)$ phase of alkanethiol on Au(111)) per chemical bond has to be provided and the upright-standing hydrocarbon tail is even “supported” by the attraction by surrounding solvent molecules. On the other hand, for gas phase deposition, the molecules do not need to displace other species, and it is natural to expect them to lie down at low coverage first (as they do). These differences also have an impact on the various steps and time scales, through which the system passes during growth. Whereas for both preparation routes multiple time scales have been observed [40,277], the mechanisms behind these are different.

The adsorption process can also be different with regard to the precursor states and their lifetime, which determine the chances to chemisorb. Moreover, for gas phase deposition, in many cases a structural coherence (domain size) only limited by the substrate was obtained, which was frequently not the case for solution deposition. Apparently, the mobility of the molecules on the surface can be very different in these different environments.

Other issues are that obviously the choice of the solvent will also determine the kinetics to some extent, which is generally different from that of gas phase deposition. In principle, there can also be the effect of growth limited by diffusion from the bulk reservoir of the solution, although even for very low concentrations this was found not to be the rate-limiting step in the experiments [59].

It should be noted that for certain SAM systems, the solution may even play a chemically active role in the adsorption process, like in the case of silane-based SAMs.

In conclusion, while the structures are the same for solution and for gas phase deposition, the pathways during growth are apparently not equivalent and the adsorption process, the growth mechanisms and the quantitative results like growth rates are generally different. One way to bridge the observations of gas phase and solution deposition is the use of preadsorption of solvent molecules in gas phase growth, as it was demonstrated in the “alkane-assisted” growth experiments discussed above.

5. Discussion

5.1. Relationship of molecular features, structures, and growth

In the preceding sections, we have discussed the structure and growth of various SAMs. Although we have certainly not covered all systems, we may attempt to draw some general conclusions regarding the relationship of the specific molecular features, the growth behavior, and the resulting structures. The best characterized system is alkanethiol/Au(111), and it can be used to try to understand the role of different features by comparison of different chain lengths, small modifications of the molecules, and chemical nature or symmetry of the substrate. The molecular features determine the interactions and the steric constraints and, thereby, the possible structures depending on coverage and temperature.

5.1.1. Impact of molecular features on the structure

The comparison of different molecular systems gives a chance to understand the role of various molecular features on the full-coverage structure. The variation of the chain length in the alkanethiol/Au(111) system reveals slight, but distinct changes in the tilt structure as a result of the delicate balance of the molecule–molecule and the molecule–substrate interaction. For phenyl-based systems, stronger interaction of the molecular backbone with the substrate and also the greater stiffness (and less low-energy excitations) have an impact on the growth and

the structure, which is plausible. These features also cause the melting temperature to be higher than for alkanethiols of similar length. If the endgroups are changed, the possibly stronger endgroup–endgroup interaction can have an impact on the structure.

While for the above cases the impact of the modifications of the molecules on the structure (compared to the alkanethiol reference system) seems at least plausible, we should emphasize that not all modifications lead to results easily predictable based on simple size or energy arguments. The unexpected incommensurate full-coverage structures of fluorinated thiols on Au(1 1 1) and alkanethiols on Ag(1 1 1) are typical examples, showing that due to the competition of various interactions a system apparently similar to alkanethiols on Au(1 1 1) can be rather different. In this context, however, one should remember that long-chain alkanethiols on Au(1 1 1) undergo an incommensurability transition at high temperatures, making other incommensurate structures less special.

Of course, other systems such as silane-based SAMs, which deviate more strongly from the alkanethiol Au(1 1 1) case in terms of headgroup bonding structure, steric constraints, or the energy terms discussed in Section 4.3, can exhibit very different structures and growth behavior.

5.1.2. Evolution of phases

In the generic case of alkanethiol on Au(1 1 1), the appearance of a low-coverage and a high-coverage phase is, on a general level, plausible. This scenario of the existence of a lying-down and a standing-up phase for different coverages is apparently fairly general. It applies also to several other systems, but it has to be emphasized that this is only true in principle.

For instance, in the case of 4-methyl-4'-mercaptobiphenyl (MMB, $\text{CH}_3-(\text{C}_6\text{H}_4)_2-\text{SH}$) on Au(1 1 1), the interaction of the molecular backbone with the substrate is stronger than for alkanethiol, which makes it more difficult to detach the backbone and let the molecules stand up upon increasing the coverage. The transition (lying-down to standing-up) leads to an energetically more favorable state for the entire layer in terms of energy per unit area, since more molecules can chemisorb on a given area, although it is usually less favorable for the individual molecule in terms of energy per molecule. Therefore, the system has to overcome a threshold (from lying-down to standing-up), which can shift the boundary on the exposure axis between different phases significantly compared to the alkanethiol case.

The question of the transition from a low-coverage phase to a higher-coverage phase and the possible existence of intermediate phases is a crucial point during the growth, showing that not only the absolute energies of the respective phases, but also the threshold between these are important. If the threshold is too high, the system does not grow past some intermediate state, i.e., it is caught in what might be called “kinetic trap”.

Although the scenario with the existence of a lying-down phase and a standing-up phase can be considered intrinsic in many thiol-based systems and should apply to both solution and gas phase deposition, the presence of a solvent causes some differences. As a coarse rule, it seems to be more difficult (but possible) to observe the

lying-down phase for solution deposition, whereas the formation of the standing-up phase is facilitated, possibly because the solvent decreases the transition threshold or the molecules do not form the lying-down phase to start with.

The relationship of the growth behavior with the phase diagram manifests itself not only in the evolution of different phases with coverage, but also in the domain size evolution, as seen from the two different growth regimes found for decanethiol, which correlates with the minimum of the melting temperature as a function of coverage (Section 4.2.1). Obviously, this has a great impact on the mobility of the molecules during growth. Furthermore, mobility and, consequently, the domain size evolution are determined by the low-energy excitations of the molecules and the potential corrugation experienced on the substrate surface.

5.1.3. Processes and interactions involved in self-assembly

The primary driving force of the self-assembly process is the formation of a chemical bond between the headgroup of the molecules and the substrate resulting in an energy gain at the cost of entropy. Nevertheless, the van der Waals interaction of the molecular backbone including the endgroup and also its shape (i.e., the question of steric constraints, etc.) play a crucial role for the SAM formation. The detailed investigation of the growth has revealed that self-assembly is, in fact, determined by the interplay of many different processes and interactions, as discussed in the preceding section. This concerns the important role of precursor-mediated adsorption, possible collective processes like the bimolecular adsorption process found for decanethiol, the multiple interactions involved, and the internal degrees of freedom of these molecules with possible low-energy excitations, which govern the growth and the various structural phases depending on coverage and temperature. The multiple phases and time scales during growth ultimately reflect the many degrees of freedom and the competing interactions in these systems. These issues underline that self-assembly of molecular monolayers is a process with a degree of complexity different from, e.g., the growth of monoatomic thin film systems.

5.2. Theoretical models and simulations

Since the delicate balance of several interactions of different origin (see Section 4.3) determines the behavior of SAMs, a full theoretical treatment is difficult. Various models and approximations have been used, focussing on different aspects such as the headgroup bonding structure or the thermal behavior of the chains. We will only briefly summarize a few results here, since simulations of SAMs (with emphasis on thiols on gold) have been reviewed recently by Siepmann and McDonald in [32].

Following the pioneering work of Klein's group [326,189], a number of simulations has employed force fields to explore the structure and dynamics of alkanethiols on Au(1 1 1). Most of these yield the $(\sqrt{3} \times \sqrt{3})$ R30° structure and a reasonable tilt angle, typically $\sim 28^\circ$ [32]. The simulations also explored the thermal behavior [189,327,328], and the disordering (melting) transition was reproduced. Of course,

differences in the models result in variations of the transition temperatures and different scenarios for the change of the tilt structure with temperature. Remarkably, the predicted temperature evolution of gauche defects is very similar to what is gleaned from experimental IR data [35,189]. The rotator phases reported from simulations [189,327] were not observed experimentally [32]. For details of the comparison of different force fields and the technical issues of simulations see [32].

The general phase behavior in the framework of simple models approximating the interactions by two effective force-sites (one for the headgroup and one for the chain) was discussed in [329].

While successful in several respects regarding the phase behavior of the chains, the above force fields failed to yield the $c(4 \times 2)$ superlattice. (To be fair we note that the early simulations were performed before the $c(4 \times 2)$ superlattice was found experimentally in 1993.) Stimulated by the experimental findings, the $c(4 \times 2)$ structure was found as the stable low-temperature structure in a study using force fields based on quantum mechanics and including explicit sulfur–sulfur bonds [93].

Later Bhatia and Garrison [330] did an extensive molecular dynamics study of the phase space leaving the sulfur headgroups mobile on the Au(111) substrate and making no assumptions regarding the existence of dimers. As a result, they propose four unique structures consistent with the $c(4 \times 2)$ superlattice and a complex interplay of possible tilt configurations.

Simulating the details of the ground state of alkanethiols on Au(111), i.e., the $(\sqrt{3} \times \sqrt{3}) R30^\circ$ structure including its $c(4 \times 2)$ superlattice, the tilt structure of the chains, and the headgroup binding configuration, by means of realistic electronic structure calculations, is very difficult. Several papers have been dealing with SCH_3 adsorbed on Au and Ag [331–334]. While it is clear that SCH_3 cannot reflect the degrees of freedom connected with long alkane chains, which also contribute significantly to the molecule–molecule interactions, it may serve as a guide for the bonding and the corrugation of the surface potential experienced by the thiol group. In a recent paper by Häkkinen et al. [333] using density-functional calculations for 24 SCH_3 molecules on Au_{34} nanocrystals, the electronic structure and different adsorption sites were investigated. It was found that the adsorption structure reported in [71,72] (see Section 3.1.1) leads indeed to a local, but not to a global energy minimum. Very recently, it was shown by Vargas et al. that the bonding configuration of methylthiols on Au(111) surfaces is actually coverage-dependent and that a dimerization can occur at high coverage [356]. It remains to be investigated whether the $c/(4 \times 2)$ superlattice can also be reproduced in electronic structure calculations with longer-chain alkanethiols.

Also more complex structures and other issues related to SAMs have been investigated in simulations. For adsorbates on SAMs, namely H_2O on SAMs with (polar) OH-termination and with (non-polar) CH_3 -termination, Hautman and Klein [221] found a remarkable correspondence of the results of the simulations with experimental wetting angles. Morgner [335] performed simulations of the growth of methanethiol from the gas phase. Siepmann and McDonald [214] explored the phase behavior of mixed monolayers. For other issues such as, e.g., the dynamics of SAMs, mechanical relaxation, SAMs on colloidal particles, etc., see [32].

5.3. Applications of SAMs

In several sections, it has been indicated that SAMs can also be utilized in various technical applications. It is beyond the scope of this review to give precise directions for the design of devices. We rather give a few examples to outline possible strategies for the utilization of SAMs. We emphasize that the references are far from complete. Some applications can also be found in [32].

It is obvious that the modular design of self-assembling molecules allows for a broad range of applications, from coatings, where the SAM might play an essentially passive role, to SAMs as active elements in sensors. In each case the understanding of the growth and the structures of the SAMs is a prerequisite for a successful use in technical applications.

5.3.1. Protective coatings

Protective coatings are “passive” applications of SAMs. One example is their use for corrosion protection [155,336–339]. SAMs can also be employed for mechanical protection of surfaces. Stratmann [157,158] modified iron and steel surfaces with SAMs to make them more “resistant” and to also attach polymers (see also below). SAMs coatings on engineering metals has also been discussed in [183].

5.3.2. Wetting control

As mentioned in Section 1, the control of wetting properties was historically among the first applications of organic monolayers. By changing the endgroup (hydrophilic vs. hydrophobic), control of the wetting properties can be obtained. In particular, mixed SAMs are attractive for this, since they allow for a continuous change of the contact angle as a function of concentration (see Section 3.4.1).

5.3.3. Friction and lubrication control

Similar to tailoring the wetting properties by various endgroups, also the “mechanical” properties relevant to friction and lubrication problems can be modified with the help of SAMs and a suitable endgroup (see, e.g., [340,341]). Moreover, SAMs can serve as model systems for the study of the relationship between friction and molecular structure [342,343].

5.3.4. Adhesion

The chemical versatility of SAMs can also be exploited for adhesion applications as discussed in [344,345] and references therein.

5.3.5. SAMs as building blocks in heterostructures and chemical anchors

A very broad area is the use of SAMs for the attachment of further layers of material, which otherwise may not be preparable in the required form or are not sufficiently stable (see also Section 3.4.5). Depending on the application, the SAM can serve as a “soft substrate” or a template to initiate growth of the adlayer in the desired mode (e.g., adlayers with a certain molecular orientation or with a minimum amount of strain).

Another strategy is to use a specific coupling of the adsorbate via the SAM to chemically anchor and, thus, stabilize an adlayer film, like nanocrystalline ceramics (e.g., ZrO_2).

The idea to chemically anchor the adlayer is also exploited when SAMs are used as a basis from which to start polymerization. This can lead to polymer films with one end being chemisorbed on the substrate [263,264], which is very different from most results obtained by spin coating on the bare substrate. The latter typically leads to physisorbed films, which can be unstable against annealing (dewetting).

5.3.6. SAMs as model systems for surface chemistry

By virtue of a suitable headgroup and chain, one can prepare and stabilize a surface with a desired functionality. This is exploited, e.g., in wetting studies of SAMs, which also serve as model systems for the surface of polymer films. Moreover, chemical reactions at surfaces can be followed under very controlled conditions. In the case of crystalline order of the SAM, which determines the orientation of the endgroup, the reaction can be followed even as a function of the relative orientation of the reactants (i.e., the anisotropy of the reaction cross-section can be determined). In addition, SAMs are attractive for electrochemical applications [346].

5.3.7. Bio-related applications

Immobilization of bio-molecules can allow a better-defined investigation of these by techniques such as STM, AFM, and GIXD than in solution. Moreover, the potential of *selective* adsorption (Section 3.4.3) can be used for filtering and analytical purposes in biotechnology. Several studies have shown possible directions of bio-compatible applications [226–231,347]. Generally, since SAMs form the link between organic and inorganic matter, they are ideal for interfacing biological materials.

5.3.8. Lateral structuring

The use of SAMs for lateral structuring is attractive for applications, and in the case of microcontact printing (μCP) also very inexpensive (see Section 3.4.3). It is also an interesting perspective for interfacing bio-related applications to (laterally structured) microelectronics.

5.3.9. Non-linear optical applications

The modular design of the molecules offers the possibility to anchor a functional group with strong non-linear optical properties to a surface via a SAM. For an introduction to non-linear optical effects in organic monolayers see [19] and references therein.

5.3.10. Electronic properties

We can distinguish two categories of using SAMs in the context of electronic properties. The first is related to the use of SAMs to learn something about the

molecules themselves. This concerns mostly fundamental studies of electron transfer through molecules, which are brought in a well-defined orientation by a SAM and then investigated using an STM tip or a conducting AFM tip. This can be done either by forming a homogeneous SAM of the molecules under consideration or by embedding and supporting the molecule of interest in a sea of host molecules of a SAM. Examples of such studies, mostly done on thiols on Au, are discussed in [123,124,215,216,348–350]. For a discussion of the electronic structure of alkylsiloxane SAMs on silicon and a comparison with theoretical calculations see [351].

The second category is related to the use of SAMs for modifying the electronic interface properties in a heterostructure. For instance, if molecules with a permanent dipole are forming a SAM at the interface between a metal electrode and an electroluminescent material, the electron transfer properties are modified. The control of the charge injection of such a device structure by using SAMs was demonstrated in [352].

For a detailed discussion of the electronic properties of organic molecules on surfaces and the topic of molecular electronics, we refer to [353–355].

6. Conclusion

It seems justified to conclude that the general behavior of relatively simple model systems in terms of the molecular packing, the appearance of various phases during growth, and also, which molecular features give rise to certain changes of the structure and growth behavior, can be understood within certain limits.

Nevertheless, several fundamental issues remain open. Since the balance of the various interactions is delicate, theoretical predictions from first principles are difficult. This concerns, e.g., the exact binding to the substrate including the specific site, variations between different substrates (e.g., Au(111) vs. Ag(111)), and the issue of incommensurate structures. Also for the growth dynamics, it is very difficult to make reliable theoretical predictions. Furthermore, the area of phase transitions and their nature, although first studies have been performed, offers still a number of interesting questions for SAMs as 2D model systems.

On the other hand, based on the experimental experience with simple SAM system, the concept of SAMs is ready to be exploited for applications of monolayers with pre-designed properties. This ranges from the use of SAMs as building blocks for heterostructures to wetting control and to the specific adsorption of biomolecules.

With this broad range of fundamental issues and, at the same time, very diverse applications, the importance of SAMs stems less from the usefulness of one specific system, but rather from the flexibility of the general concept of SAMs. We are certain that this concept will prove to be vital and fruitful for many technical applications as well as in view of its role as low-dimensional molecular model system.

Acknowledgements

The author is indebted to many collaborators, with whom it has been a pleasure to interact. These include present and former members of the Princeton and the Stuttgart group, namely G. Bracco, A. Eberhardt, P. Eisenberger, P. Fenter, M. Gerstenberg, D. Katz, J. Krich, D. Lavrich, T. Y. B. Leung, J. Libuda, P. Schwartz, S. Wetterer, and L. Zhou as well as A. Dürr, B. Edinger, K.-P. Just, B. Krause, V. Kruppa, and K. Ritley. The author would like to thank in particular G. Scoles for numerous discussions and support. Fruitful interactions with P. Engels, A. Levi, B. Nickel, T. Niesen, and J. Pflaum are also gratefully acknowledged. The author would like to acknowledge enlightening discussions with numerous colleagues in the field, who cannot all be mentioned. Many of these greatly assisted the compilation of this review by responding to requests for figures and preprints, or by sharing their ideas. The staff of the Max-Planck library has been of great help by patiently searching for several references as has been I. Schofron with some figures. The author wishes to thank the ESRF (Grenoble), HASYLAB (Hamburg), and the NSLS (Brookhaven) for making synchrotron-based work on SAMs possible. The generous support of H. Dosch is gratefully acknowledged. Finally, this work would not have been possible without the help of the Deutsche Forschungsgemeinschaft and the Max-Planck-Gesellschaft.

References

- [1] B. Franklin, *Philos. Trans. R. Soc. London* 64 (1774) 445.
- [2] A. Pockels, *Nature* 43 (1891) 437.
- [3] A. Pockels, *Nature* 46 (1892) 418.
- [4] A. Pockels, *Nature* 48 (1893) 152.
- [5] A. Pockels, *Nature* 50 (1894) 223.
- [6] L. Rayleigh, *Philos. Mag.* 48 (1899) 321.
- [7] W.B. Hardy, *Proc. R. Soc. London A* 86 (1912) 610.
- [8] H. Devaux, *Smithson. Inst. Ann. Rep.* 261 (1913).
- [9] I. Langmuir, *J. Am. Chem. Soc.* 39 (1917) 1848.
- [10] I. Langmuir, *Trans. Faraday Soc.* 15 (1920) 62.
- [11] K. Blodgett, *J. Am. Chem. Soc.* 57 (1935) 1007.
- [12] K. Blodgett, *Phys. Rev.* 51 (1937) 964.
- [13] E. Schmidt, W. Schurig, W. Sellschopp, *Tech. Mech. Thermodyn.* 1 (1930) 53.
- [14] W.M. Nagle, T.B. Drew, *Trans. Am. Inst. Chem. Eng.* 30 (1933) 217.
- [15] H. Emmons, *Trans. Am. Inst. Chem. Eng.* 35 (1939) 109.
- [16] W.C. Bigelow, D.L. Pickett, W.A. Zisman, *J. Colloid Interface Sci.* 1 (1946) 513.
- [17] L.C.F. Blackman, M.J.S. Dewar, *J. Chem. Soc.* 162 (1957), Part I–IV.
- [18] G.L. Gaines Jr., *Insoluble Monolayers at Liquid–Gas Interfaces*, Interscience, New York, 1966.
- [19] A. Ulman, *An Introduction to Ultrathin Organic Films: From Langmuir–Blodgett to Self-Assembly*, Academic Press, Boston, 1991.
- [20] P.G. de Gennes, *Rev. Mod. Phys.* 57 (1985) 827.
- [21] S. Dietrich, in: C. Domb, J.L. Lebowitz (Eds.), *Phase Transitions and Critical Phenomena*, vol. 12, Academic Press, New York, 1988.
- [22] C.D. Bain, G.M. Whitesides, *Angew. Chem. Int. Ed. Engl.* 28 (1989) 506.

- [23] D.W. Schubert, *Polym. Bull.* 38 (1997) 177.
- [24] V.M. Kaganer, H. Möhwald, P. Dutta, *Rev. Mod. Phys.* 71 (1999) 779.
- [25] S.R. Forrest, *Chem. Rev.* 97 (1997) 1793.
- [26] E. Umbach, M. Sokolowski, R. Fink, *Appl. Phys. A* 63 (1996) 565.
- [27] P. Fenter, F. Schreiber, L. Zhou, P. Eisenberger, S.R. Forrest, *Phys. Rev. B* 56 (1997) 3046.
- [28] O.M. Magnussen, B.M. Ocko, M. Deutsch, M.J. Regan, P.S. Pershan, L.E. Berman, D. Abernathy, J.F. Legrand, G. Grübel, *Nature* 384 (1996) 250.
- [29] R.G. Nuzzo, D.L. Allara, *J. Am. Chem. Soc.* 105 (1983) 4481.
- [30] J. Sagiv, *J. Am. Chem. Soc.* 102 (1980) 92.
- [31] J.D. Swalen, D.L. Allara, J.D. Andrade, E.A. Chandross, S. Garoff, J. Israelachvili, T.J. McCarthy, R. Murray, R.F. Pease, J.F. Rabolt, K.J. Wynne, H. Yu, *Langmuir* 3 (1987) 932.
- [32] A. Ulman (Ed.), *Self-assembled monolayers of thiols*, *Thin Films*, vol. 24, Academic Press, San Diego, 1998.
- [33] A. Ulman, *Chem. Rev.* 96 (1996) 1533.
- [34] G.M. Whitesides, P.E. Laibinis, *Langmuir* 6 (1990) 87.
- [35] L.H. Dubois, R.G. Nuzzo, *Ann. Rev. Phys. Chem.* 43 (1992) 437.
- [36] G.E. Poirier, *Chem. Rev.* 97 (1997) 1117.
- [37] A.R. Sandy, S.G.J. Mochrie, D.M. Zehner, K.G. Huang, D. Gibbs, *Phys. Rev. B* 43 (1991) 4667.
- [38] M.R. Linford, C.E.D. Chidsey, *J. Am. Chem. Soc.* 115 (1993) 12631.
- [39] G.E. Poirier, E.D. Pylant, *Science* 272 (1996) 1145.
- [40] F. Schreiber, A. Eberhardt, T.Y.B. Leung, P. Schwartz, S.M. Wetterer, D.J. Lavrich, L. Berman, P. Fenter, P. Eisenberger, G. Scoles, *Phys. Rev. B* 57 (1998) 12476.
- [41] A. Eberhardt, P. Fenter, P. Eisenberger, *Surf. Sci. Lett.* 397 (1998) L285.
- [42] P. Schwartz, F. Schreiber, P. Eisenberger, G. Scoles, *Surf. Sci.* 423 (1999) 208.
- [43] G.E. Poirier, *Langmuir* 15 (1999) 1167.
- [44] H. Kondoh, C. Kondama, H. Sumida, H. Nozoye, *J. Chem. Phys.* 111 (1999) 1175.
- [45] R.C. Thomas, L. Sun, R.M. Crooks, A.J. Ricco, *Langmuir* 7 (1991) 620.
- [46] H. Lüth, *Surfaces and Interfaces of Solids*, Springer, Berlin, 1993.
- [47] L.H. Dubois, B.R. Zegarski, R.G. Nuzzo, *J. Phys. Chem.* 98 (1993) 678.
- [48] R. Feidenhans'l, *Surf. Sci. Rep.* 10 (1989) 105.
- [49] H. Dosch, *Critical Phenomena at Surfaces and Interfaces*, *Springer Tracts in Modern Physics*, vol. 126, Springer, Heidelberg, 1992.
- [50] P. Fenter, *Self-assembled monolayers of thiols*, in: A. Ulman (Ed.), *Thin Films*, vol. 24, Academic Press, San Diego, 1998.
- [51] G. Scoles (Ed.), *Atomic and Molecular Beam Methods*, vols. 1 and 2, Oxford University Press, Oxford, 1992.
- [52] C.E.D. Chidsey, G.-Y. Liu, P. Rowntree, G. Scoles, *J. Chem. Phys.* 91 (1989) 4421.
- [53] M. Tolan, *X-ray Scattering from Soft-Matter Thin Films*, *Springer Tracts in Modern Physics*, vol. 148, Springer, Heidelberg, 1999.
- [54] I.M. Tidswell, B.M. Ocko, P.S. Pershan, S.R. Wasserman, G.M. Whitesides, J.D. Axe, *Phys. Rev. B* 41 (1990) 1111.
- [55] K.A. Ritley, K.-P. Just, F. Schreiber, H. Dosch, T.P. Niesen, F. Aldinger, *J. Mater. Res.* (in press).
- [56] R.G. Nuzzo, L.H. Dubois, D.L. Allara, *J. Am. Chem. Soc.* 112 (1990) 558.
- [57] A.N. Parikh, D.L. Allara, *J. Chem. Phys.* 96 (1992) 927.
- [58] F. Eisert, O. Dannenberger, M. Buck, *Phys. Rev. B* 58 (1998) 10860.
- [59] O. Dannenberger, M. Buck, M. Grunze, *J. Phys. Chem. B* 103 (1999) 2202.
- [60] M.S. Yeganeh, S.M. Dougal, R.S. Polizzotti, P. Rabinowitz, *Phys. Rev. Lett.* 74 (1995) 1811.
- [61] G.J. Kluth, C. Carraro, R. Maboudian, *Phys. Rev. B* 59 (1999) R10449.
- [62] J. Stöhr, *NEXAFS Spectroscopy*, Springer, New York, 1992.
- [63] L.H. Dubois, B.R. Zegarski, R.G. Nuzzo, *J. Am. Chem. Soc.* 112 (1990) 570.
- [64] S.M. Wetterer, D.J. Lavrich, T. Cummings, S.L. Bernasek, G. Scoles, *J. Phys. Chem. B* 102 (1998) 9266.
- [65] E.F. Aust, M. Sawodny, S. Ito, W. Knoll, *Scanning* 16 (1994) 353.
- [66] K.A. Peterlinz, R. Georgiadis, *Langmuir* 12 (1996) 4731.

- [67] S.R. Wasserman, G.M. Whitesides, I.M. Tidswell, B.M. Ocko, P.S. Pershan, J.D. Axe, *J. Am. Chem. Soc.* 111 (1989) 5852.
- [68] B. Heinz, H. Morgner, *Surf. Sci.* 372 (1997) 100.
- [69] T. Risse, T. Hill, M. Beckendorf, U.J. Katter, H. Schlien, H. Hamann, H.J. Freund, *Langmuir* 12 (1996) 5512.
- [70] J. Zegenhagen, *Surf. Sci. Rep.* 18 (1993) 199.
- [71] P. Fenter, F. Schreiber, L. Berman, G. Scoles, P. Eisenberger, M. Bedzyk, *Surf. Sci.* 412/413 (1998) 213.
- [72] P. Fenter, F. Schreiber, L. Berman, G. Scoles, P. Eisenberger, M. Bedzyk, *Surf. Sci.* 425 (1999) 138.
- [73] L. Strong, G.M. Whitesides, *Langmuir* 4 (1988) 546.
- [74] C.E.D. Chidsey, D.N. Loiacono, *Langmuir* 6 (1990) 682.
- [75] A.I. Kitaigorodskii, *Organic Chemistry Crystallography*, Consultants Bureau, New York, 1961.
- [76] R.G. Nuzzo, E.M. Korenic, L.H. Dubois, *J. Chem. Phys.* 93 (1990) 767.
- [77] N. Camillone, C.E.D. Chidsey, G.-Y. Liu, G. Scoles, *J. Chem. Phys.* 98 (1993) 4234.
- [78] P. Fenter, P. Eisenberger, K.S. Liang, *Phys. Rev. Lett.* 70 (1993) 2447 (note that the melting temperature ($\sim 70^\circ\text{C}$) determined for dodecanethiol was probably for a coverage slightly below 1).
- [79] G.E. Poirier, M.J. Tarlov, *Langmuir* 10 (1994) 2853.
- [80] E. Delamarche, B. Michel, C. Gerber, D. Anselmetti, H.-J. Güntherodt, H. Wolf, H. Ringsdorf, *Langmuir* 10 (1994) 2869.
- [81] J.P. Bucher, L. Santesson, K. Kern, *Appl. Phys. A* 59 (1994) 135.
- [82] M.A. Bryant, J.E. Pemberton, *J. Am. Chem. Soc.* 113 (1991) 8284.
- [83] D. Anselmetti, A. Baratoff, H.-J. Güntherodt, E. Delamarche, B. Michel, C. Gerber, H. Kang, H. Wolf, H. Ringsdorf, *Europhys. Lett.* 27 (1994) 365.
- [84] E. Delamarche, B. Michel, H.A. Biebuyck, C. Gerber, *Adv. Mater.* 8 (1996) 719.
- [85] J. Als-Nielsen, H. Möhwald, in: S. Ebashi, M. Koch, E. Rubenstein (Eds.), *Handbook of Synchrotron Radiation*, vol. 4, Elsevier, New York, 1991.
- [86] P. Fenter, A. Eberhardt, K.S. Liang, P. Eisenberger, *J. Chem. Phys.* 106 (1997) 1600.
- [87] M.D. Porter, T.B. Bright, D.L. Allara, C.E.D. Chidsey, *J. Am. Chem. Soc.* 109 (1987) 3559.
- [88] C.A. Alves, E.L. Smith, M.D. Porter, *J. Am. Chem. Soc.* 114 (1992) 1222.
- [89] J. Kang, P.A. Rowntree, *Langmuir* 12 (1996) 2813.
- [90] P. Fenter, A. Eberhardt, P. Eisenberger, *Science* 266 (1994) 1216.
- [91] N. Nishida, M. Hara, H. Sasabe, W. Knoll, *Jpn. J. Appl. Phys.* 35 (1996) L799.
- [92] J. Voets, J.W. Gerritsen, R.F.P. Grimbergen, H. van Kempen, *Surf. Sci.* 399 (1998) 316.
- [93] J.J. Gerdy, W.A. Goodard, *J. Am. Chem. Soc.* 118 (1996) 3233.
- [94] P.E. Laibinis, R.L. Graham, H.A. Biebuyck, G.M. Whitesides, *Science* 254 (1991) 981 (X-ray radiation of 1486.6 eV (Al K_α) was used).
- [95] N. Camillone, C.E.D. Chidsey, P. Eisenberger, P. Fenter, J. Li, K.S. Liang, G.-Y. Liu, G. Scoles, *J. Chem. Phys.* 99 (1993) 744.
- [96] C. Schoenberger, J.A.M. Sondag-Huethorst, J. Jorritsma, J.G.J. Fokkink, *Langmuir* 10 (1994) 611.
- [97] E. Delamarche, B. Michel, H. Kang, C. Gerber, *Langmuir* 10 (1994) 4103.
- [98] G.E. Poirier, *Langmuir* 13 (1997) 2019.
- [99] N. Camillone, P. Eisenberger, T.Y.B. Leung, P. Schwartz, G. Scoles, G.E. Poirier, M.J. Tarlov, *J. Chem. Phys.* 101 (1994) 11031.
- [100] R. Staub, M. Toerker, T. Fritz, T. Schmitz-Hübsch, F. Sellam, K. Leo, *Langmuir* 14 (1998) 6693.
- [101] N. Camillone, T.Y.B. Leung, P. Schwartz, P. Eisenberger, G. Scoles, *Langmuir* 12 (1996) 2737.
- [102] R. Gerlach, G. Polanski, H.-G. Rubahn, *Appl. Phys. A* 65 (1997) 375.
- [103] T.Y.B. Leung, Ph.D. Thesis, Princeton University, Princeton, 1998.
- [104] T.Y.B. Leung, F. Schreiber, G. Scoles, unpublished.
- [105] S.E. Creager, C.M. Steiger, *Langmuir* 11 (1995) 1852.
- [106] J.F. Kang, R. Jordan, A. Ulman, *Langmuir* 14 (1998) 3983.
- [107] A. Dhirani, R.W. Zehner, R.P. Hsung, P. Guyot-Sionnest, L.R. Sita, *J. Am. Chem. Soc.* 118 (1996) 3319.

- [108] E. Sabatani, J. Cohen-Boulakia, M. Bruening, I. Rubinstein, *Langmuir* 9 (1993) 2974.
- [109] Y.-T. Tao, C.-C. Wu, J.-Y. Eu, W.-L. Lin, K.-C. Wu, C.-H. Chen, *Langmuir* 13 (1997) 4018.
- [110] T.Y.B. Leung, P.V. Schwartz, G. Scoles, F. Schreiber, A. Ulman, *Surf. Sci.* 458 (2000) 34.
- [111] J.F. Kang, A. Ulman, R. Jordan, D.G. Kurth, *Langmuir* 15 (1999) 5555.
- [112] L.-J. Wan, Y. Hara, H. Noda, M. Osawa, *J. Phys. Chem.* 102 (1998) 5943.
- [113] L. Bertilsson, B. Liedberg, *Langmuir* 9 (1993) 141.
- [114] H.-J. Himmel, K. Weiss, B. Jäger, O. Dannenberger, M. Grunze, C. Wöll, *Langmuir* 13 (1997) 4943.
- [115] O. Dannenberger, K. Weiss, H.-J. Himmel, B. Jäger, M. Buck, C. Wöll, *Thin Solid Films* 307 (1997) 183.
- [116] M. Sprik, E. Delamarque, B. Michel, U. Röthlisberger, M.L. Klein, H. Wolf, H. Ringsdorf, *Langmuir* 10 (1994) 4116.
- [117] G.E. Poirier, E.D. Pylant, J.M. White, *J. Chem. Phys.* 104 (1996) 7325.
- [118] J. Li, K.S. Liang, G. Scoles, A. Ulman, *Langmuir* 11 (1995) 4418.
- [119] C.A. Alves, M.D. Porter, *Langmuir* 9 (1993) 3507.
- [120] G.-Y. Liu, P. Fenter, C.E.D. Chidsey, D.F. Ogletree, P. Eisenberger, M. Salmeron, *J. Chem. Phys.* 101 (1994) 4301.
- [121] L. Houssiau, M. Graupe, R. Colorado, H.I. Kim, T.R. Lee, S.S. Perry, J.W. Rabalais, *J. Chem. Phys.* 109 (1998) 9134.
- [122] M. Jaschke, H. Schönherr, H. Wolf, H.-J. Butt, E. Bamberg, M.K. Besocke, H. Ringsdorf, *J. Phys. Chem.* 100 (1996) 2290.
- [123] R.P. Andres, T. Bein, M. Dorogi, S. Feng, J.I. Henderson, C.P. Kubiak, W. Mahoney, R.G. Osifchin, R. Reifenger, *Science* 272 (1996) 1323.
- [124] M.A. Reed, C. Zhou, C.J. Muller, T.P. Burgin, J.M. Tour, *Science* 278 (1997) 252.
- [125] J.M. Tour, L. Jones II, D.L. Pearson, J.J.S. Lamba, T.P. Burgin, G.M. Whitesides, D.L. Allara, A.N. Parikh, S.V. Atre, *J. Am. Chem. Soc.* 117 (1995) 9529.
- [126] M. Brust, P.M. Blass, A.J. Bard, *Langmuir* 13 (1997) 5602.
- [127] H. Rieley, G.K. Kendall, F.W. Zemicael, T.L. Smith, S. Yang, *Langmuir* 14 (1998) 5147.
- [128] K. Kobayashi, J. Umemura, T. Horiuchi, H. Yamada, K. Matsushige, *Jpn. J. Appl. Phys.* 37 (1998) L297.
- [129] M. Cavallini, M. Bracali, G. Aloisi, R. Guidelli, *Langmuir* 15 (1999) 3003.
- [130] T.Y.B. Leung, M.C. Gerstenberg, D.J. Lavrich, F. Schreiber, G. Scoles, G. Poirier, *Langmuir* 16 (2000) 549.
- [131] A. Wesch, O. Dannenberger, C. Wöll, J.J. Wolff, M. Buck, *Langmuir* 12 (1996) 5330.
- [132] C.D. Bain, H.A. Biebuyck, G.M. Whitesides, *Langmuir* 5 (1989) 723.
- [133] G. Nelles, H. Schönherr, M. Jaschke, H. Wolf, M. Schaub, J. Küther, W. Tremel, E. Bamberg, H. Ringsdorf, H.-J. Butt, *Langmuir* 14 (1998) 808.
- [134] C. Jung, O. Dannenberger, Y. Xu, M. Buck, M. Grunze, *Langmuir* 14 (1998) 1103.
- [135] D.J. Lavrich, S.M. Wetterer, S.L. Bernasek, G. Scoles, *J. Phys. Chem. B* 102 (1998) 3456.
- [136] H. Schönherr, H. Ringsdorf, M. Jaschke, H.-J. Butt, E. Bamberg, H. Allison, S.D. Evans, *Langmuir* 12 (1996) 3898.
- [137] T. Ishida, S. Yamamoto, W. Mizutani, M. Motomatsu, H. Tokumoto, H. Hokari, H. Azebara, M. Fujihira, *Langmuir* 12 (1996) 3898.
- [138] K. Heister, D.L. Allara, K. Bahnck, S. Frey, M. Zharnikov, M. Grunze, *Langmuir* 15 (1999) 5440.
- [139] J. Noh, M. Hara, *Langmuir* 16 (2000) 2045.
- [140] J. Li, K.S. Liang, N. Camillone, T.Y.B. Leung, G. Scoles, *J. Chem. Phys.* 102 (1995) 5012.
- [141] G.E. Poirier, *J. Vac. Sci. Technol. B* 14 (1996) 1453.
- [142] N. Camillone, C.E.D. Chidsey, G.-Y. Liu, G. Scoles, *J. Chem. Phys.* 98 (1993) 3503.
- [143] P. Fenter, P. Eisenberger, J. Li, N. Camillone, S. Bernasek, G. Scoles, T.A. Ramanarayanan, K.S. Liang, *Langmuir* 7 (1991) 2013 (note that the structure reported in this reference was corrected somewhat in [50]).
- [144] M. Himmelhaus, I. Gauss, M. Buck, F. Eisert, C. Wöll, M. Grunze, *J. Electron Spectros. Relat. Phenom.* 92 (1998) 139.

- [145] T.T. Ehler, N. Malmberg, L.J. Noe, *J. Phys. Chem. B* 101 (1997) 1268.
- [146] P.E. Laibinis, G.M. Whitesides, D.L. Allara, Y.-T. Tao, A.N. Parikh, R.G. Nuzzo, *J. Am. Chem. Soc.* 113 (1991) 7152.
- [147] M.M. Walczak, C.S. Chung, M. Stole, C.A. Widrig, M.D. Porter, *J. Am. Chem. Soc.* 113 (1991) 2370.
- [148] H. Rieley, G.K. Kendall, *Langmuir* 15 (1999) 8867.
- [149] M.G. Samant, C.A. Broen, J.G. Gordon II, *Surf. Sci.* 365 (1996) 729.
- [150] J.-P. Bucher, L. Santesson, K. Kern, *Langmuir* 10 (1994) 979.
- [151] A. Dhirani, M.A. Hines, A.J. Fisher, O. Ismail, P. Guyot-Sionnest, *Langmuir* 11 (1995) 2609.
- [152] H. Rieley, G.K. Kendall, R.G. Jones, D.P. Woodruff, *Langmuir* 15 (1999) 8856.
- [153] A. Imanishi, K. Isawa, F. Matsui, T. Tsuduki, T. Yokoyama, H. Kondoh, Y. Kitajima, T. Ohta, *Surf. Sci.* 407 (1998) 282.
- [154] H. Rieley, G.K. Kendall, A. Chan, R.G. Jones, J. Lüdecke, D.P. Woodruff, B.C.C. Cowie, *Surf. Sci.* 392 (1997) 143.
- [155] J. Scherer, M.R. Vogt, O.M. Magnussen, R.J. Behm, *Langmuir* 13 (1997) 7045.
- [156] G. Loepf, S. Vollmer, G. Witte, C. Wöll, *Langmuir* 15 (1999) 3767.
- [157] M. Stratmann, *Adv. Mater.* 2 (1990) 191.
- [158] M. Stratmann, *Stahl u. Eisen* 113 (1993) 101.
- [159] Z. Mekhalif, J. Riga, J.-J. Pireaux, J. Delhalle, *Langmuir* 13 (1997) 2285.
- [160] C.W. Sheen, J.-X. Shi, J. Mårtensson, A.N. Parikh, D.L. Allara, *J. Am. Chem. Soc.* 114 (1992) 1514.
- [161] Y. Gu, Z. Lin, R.A. Butera, V.S. Smentkowski, D.H. Waldeck, *Langmuir* 11 (1995) 1849.
- [162] H. Yamamoto, R.A. Butera, Y. Gu, D.H. Waldeck, *Langmuir* 11 (1995) 1849.
- [163] D. Zerulla, D. Mayer, K.H. Hallmeier, T. Chassé, *Chem. Phys. Lett.* 311 (1999) 8.
- [164] R. Moaz, J. Sagiv, D. Degenhardt, H. Möhwald, P. Quint, *Supramol. Sci.* 2 (1995) 9.
- [165] M.J. Stevens, *Langmuir* 15 (1999) 2773.
- [166] P. Fontaine, M. Goldmann, F. Rondelez, *Langmuir* 15 (1999) 1348.
- [167] I.M. Tidswell, T.A. Rabedreau, P.S. Pershan, S.D. Kosowsky, J.P. Folkers, G.M. Whitesides, *J. Chem. Phys.* 95 (1991) 2854.
- [168] D.L. Allara, A.N. Parikh, F. Rondelez, *Langmuir* 11 (1995) 2357.
- [169] T. Vallant, J. Kattner, H. Brunner, U. Mayer, H. Hoffmann, *Langmuir* 15 (1999) 5339.
- [170] K. Bierbaum, M. Kinzler, C. Wöll, M. Grunze, G. Hähner, S. Heid, F. Effenberger, *Langmuir* 11 (1995) 512.
- [171] S. Heid, F. Effenberger, K. Bierbaum, M. Grunze, *Langmuir* 12 (1996) 2118.
- [172] P. Harder, K. Bierbaum, C. Wöll, M. Grunze, S. Heid, F. Effenberger, *Langmuir* 13 (1997) 445.
- [173] M.G. Samant, C.A. Brown, J.G. Gordon II, *Langmuir* 8 (1992) 1615.
- [174] M.H. Dishner, J.C. Hemminger, F.J. Feher, *Langmuir* 13 (1997) 4788.
- [175] F.K. Huang, R.C. Horton, D.C. Myles, R.L. Garrell, *Langmuir* 14 (1998) 4802.
- [176] M.R. Linford, P. Fenter, P.M. Eisenberger, C.E.D. Chidsey, *J. Am. Chem. Soc.* 117 (1995) 3145.
- [177] M.M. Sung, G.J. Kluth, O.W. Yauw, R. Maboudian, *Langmuir* 13 (1997) 6164.
- [178] F. Effenberger, G. Götz, B. Bidlingmaier, M. Wezstein, *Angew. Chem. Int. Ed.* 37 (1995) 3145.
- [179] R. Boukherroub, S. Morin, F. Bensebaa, D.D.M. Wayner, *Langmuir* 15 (1999) 3831.
- [180] A.B. Sieval, V. Vleeming, H. Zuilhof, E.J.R. Sudhölter, *Langmuir* 15 (1999) 8288.
- [181] M.M. Sung, G.J. Kluth, R. Maboudian, *J. Vac. Sci. Technol. A* 17 (1999) 540.
- [182] J.P. Folkers, C.B. Gorman, P.E. Laibinis, S. Buchholz, G.M. Whitesides, R.G. Nuzzo, *Langmuir* 11 (1995) 813.
- [183] J.G. Van Alsten, *Langmuir* 15 (1999) 7605.
- [184] P. Fenter, N. Sturchio, *Geochim. Cosmochim. Acta* 63 (1999) 3145.
- [185] K.J. Strandburg, *Rev. Mod. Phys.* 60 (1988) 161.
- [186] F. Schreiber, M.C. Gerstenberg, S.R. Forrest, G. Scoles, H. Dosch (in preparation).
- [187] G.E. Poirier, M.J. Tarlov, H.E. Rushmeier, *Langmuir* 10 (1994) 3383.
- [188] B. Kuchta, R.D. Etters, *Phys. Rev. B* 54 (1996) 12057.
- [189] J. Hautman, M.L. Klein, *J. Chem. Phys.* 93 (1990) 7483.
- [190] L.H. Dubois, B.R. Zegarski, R.G. Nuzzo, *J. Electron Spectros. Relat. Phenom.* 54/55 (1990) 1143.

- [191] F. Bensebaa, T.H. Ellis, A. Badia, R.B. Lennox, *J. Vac. Sci. Technol. A* 13 (1995) 1331.
- [192] A. Badia, W. Gao, S. Singh, L. Demers, L. Cuccia, L. Reven, *Langmuir* 12 (1996) 1262.
- [193] W. Gao, L. Dickinson, C. Grozinger, F.G. Morin, L. Reven, *Langmuir* 13 (1997) 115.
- [194] S.R. Cohen, R. Naaman, J. Sagiv, *J. Phys. Chem.* 90 (1986) 3054.
- [195] M. Calistri-Yeh, E.J. Kramer, R. Sharma, W. Zhao, M.H. Rafailovich, J. Sokolov, J.D. Brock, *Langmuir* 12 (1996) 2747.
- [196] D.W. Britt, V. Hlady, *J. Colloid Interface Sci.* 178 (1996) 775.
- [197] G.J. Kluth, M.M. Sung, R. Maboudian, *Langmuir* 13 (1997) 3775.
- [198] G.J. Kluth, M. Sander, M.M. Sung, R. Maboudian, *J. Vac. Sci. Technol. A* 16 (1998) 932.
- [199] K.K. Berggren, A. Bard, J.L. Wilbur, J.D. Gillaspay, A.G. Helg, J.J. McClelland, S.L. Rolston, W.D. Phillips, M.P. Prentiss, G.M. Whitesides, *Science* 269 (1995) 1255.
- [200] S.B. Hill, C.A. Haich, F.B. Dunning, G.K. Walters, J.J. McClelland, R.J. Celotta, H.G. Craighead, J. Han, D.M. Tanenbaum, *J. Vac. Sci. Technol. B* 17 (1999) 1087.
- [201] P. Engels, S. Salewski, H. Levsen, K. Sengstock, W. Ertmer, *Appl. Phys. B* 69 (1999) 407.
- [202] R.D. Piner, J. Zhu, F. Xu, S. Hong, C.A. Mirkin, *Science* 283 (1999) 661.
- [203] S. Hong, J. Zhu, C.A. Mirkin, *Science* 286 (1999) 523.
- [204] S. Xu, S. Miller, P.E. Laibinis, G.-Y. Liu, *Langmuir* 15 (1999) 7244.
- [205] A. Kumar, G.M. Whitesides, *Appl. Phys. Lett.* 63 (1999) 2002.
- [206] E. Delamarche, H. Schmid, A. Bietsch, N.B. Larsen, H. Rothuizen, B. Michel, H. Biebuyck, *J. Phys. Chem. B* 102 (1998) 3324.
- [207] N.L. Abbott, J.P. Folkers, G.M. Whitesides, *Science* 257 (1992) 1380.
- [208] T. Komeda, K. Namba, Y. Nishioka, *J. Vac. Sci. Technol. A* 16 (1998) 1680.
- [209] S.J. Stranick, A.N. Parikh, Y.-T. Tao, D.L. Allara, P.S. Weiss, *J. Phys. Chem.* 98 (1994) 7636.
- [210] J.P. Folkers, P.E. Laibinis, G.M. Whitesides, J. Deutch, *J. Phys. Chem.* 98 (1994) 563.
- [211] J.P. Folkers, P.E. Laibinis, G.M. Whitesides, *Langmuir* 8 (1992) 1330.
- [212] S.V. Atre, B. Liedberg, D.L. Allara, *Langmuir* 11 (1995) 3882.
- [213] K. Tamada, M. Hara, H. Sasabe, W. Knoll, *Langmuir* 13 (1997) 1558.
- [214] J.I. Siepmann, I.R. McDonald, *Mol. Phys.* 75 (1997) 255.
- [215] L.A. Bumm, J.J. Arnold, M.T. Cygan, T.D. Dunbar, T.P. Burgin, L.J. II, D.L. Allara, J.M. Tour, P.S. Weiss, *Science* 271 (1996) 1705.
- [216] G. Leatherman, E.N. Durantini, D. Gust, T.A. Moore, A.L. Moore, S. Stone, Z. Zhou, P. Rez, Y.Z. Liu, S.M. Lindsay, *J. Phys. Chem. B* 103 (1999) 4006.
- [217] C.D. Bain, E.B. Troughton, Y.-T. Tao, J. Evall, G.M. Whitesides, R.G. Nuzzo, *J. Am. Chem. Soc.* 111 (1989) 321.
- [218] C.D. Bain, J. Evall, G.M. Whitesides, *J. Am. Chem. Soc.* 111 (1989) 7155.
- [219] I. Engquist, I. Lundström, B. Liedberg, *J. Phys. Chem.* 99 (1995) 12257.
- [220] W.J. Miller, N.L. Abbott, *Langmuir* 13 (1997) 7106.
- [221] J. Hautman, M.L. Klein, *Phys. Rev. Lett.* 67 (1991) 1753.
- [222] Y.F. Miura, M. Takenaga, T. Koini, M. Graupe, N. Garg, R.L. Graham Jr., T.R. Lee, *Langmuir* 14 (1998) 5821.
- [223] I. Engquist, Ph.D. Thesis, Linköping University, Linköping, 1996.
- [224] I. Engquist, B. Liedberg, *J. Phys. Chem.* 100 (1996) 20089.
- [225] C.E.D. Chidsey, G.-Y. Liu, G. Scoles, J. Wang, *Langmuir* 6 (1990) 1804.
- [226] K.L. Prime, G.M. Whitesides, *Science* 252 (1991) 1164.
- [227] L. Häußling, W. Knoll, H. Ringsdorf, F.-J. Schmitt, J. Yang, *Makromol. Chem. Macromol. Symp.* 46 (1991) 145.
- [228] R. Singhvi, A. Kumar, G.P. Lopez, G.N. Stephanopoulos, D.I.C. Wang, G.M. Whitesides, D.E. Ingber, *Science* 264 (1994) 696.
- [229] M.J. Wirth, R.W.P. Fairbank, H.O. Fatunmbi, *Science* 275 (1997) 44.
- [230] J. Lahiri, L. Isaacs, B. Grzybowski, J.D. Carbeck, G.M. Whitesides, *Langmuir* 15 (1999) 7186.
- [231] N. Higashi, M. Takahashi, M. Niwa, *Langmuir* 16 (2000) 1793.
- [232] R.M. Nyquist, A.S. Eberhardt, L.A. Silks III, Z. Li, X. Yang, B.I. Swanson, *Langmuir* 16 (1998) 1793.
- [233] P. Harder, M. Grunze, R. Dahint, G.M. Whitesides, P.E. Laibinis, *J. Phys. Chem. B* 10 (1998) 2426.

- [234] R.L.C. Wang, H.J. Kreuzer, M. Grunze, *J. Phys. Chem. B* 101 (1997) 9767.
- [235] S. Petrash, N.B. Sheller, W. Dando, M.D. Foster, *Langmuir* 13 (1997) 1881.
- [236] P. Wagner, S. Nock, J.A. Spudich, W.D. Volkmuth, S. Chu, R.I. Cicero, C.P. Wade, M.R. Linford, C.E.D. Chidsey, *J. Struct. Biol.* 119 (1997) 189.
- [237] G. Nelles, M. Weisser, R. Back, P. Wohlfahrt, G. Wenz, S. Mittler-Neher, *J. Am. Chem. Soc.* 118 (1996) 5039.
- [238] M. Weisser, G. Nelles, R. Back, P. Wohlfahrt, G. Wenz, S. Mittler-Neher, *J. Phys. Chem.* 100 (1996) 17893.
- [239] D.A. Hutt, G.J. Leggett, *Langmuir* 13 (1998) 2740.
- [240] S. Pan, D.G. Castner, B.D. Ratner, *Langmuir* 14 (1998) 3545.
- [241] G.E. Poirier, T.M. Herne, C.C. Miller, M.J. Tarlov, *J. Am. Chem. Soc.* 121 (1999) 9703.
- [242] T.P. Niesen, M.R. De Guire, *J. Electroceram.* (in press).
- [243] M. Agarwal, M.R. DeGuire, A.H. Heuer, *J. Am. Ceram. Soc.* 80 (1997) 2967.
- [244] T.P. Niesen, J. Wolff, J. Bill, T. Wagner, F. Aldinger, in: P. Vincencini (Ed.), *Adv. Sci. Technol., Techn. Publ., Florence, Italy* 20 (1999) 21.
- [245] B.C. Bunker, P.C. Rieke, B.J. Tarasevich, A.A. Campbell, G.E. Fryxell, G.L. Graff, L. Song, J. Liu, J.W. Virden, G.L. McVay, *Science* 264 (1994) 48.
- [246] K. Bandyopadhyay, K. Vijayamohan, *Langmuir* 14 (1998) 6924.
- [247] J. Aizenberg, A.J. Black, G.M. Whitesides, *Nature* 398 (1999) 495.
- [248] V.L. Colvin, A.N. Goldstein, A.P. Alivisatos, *J. Am. Chem. Soc.* 114 (1992) 5221.
- [249] O. Cavalleri, A.M. Bittner, H. Kind, K. Kern, T. Greber, *Phys. Chem.* 208 (1999) 107.
- [250] H. Hagenström, M.A. Schneeweiss, D.M. Kolb, *Langmuir* 15 (1999) 7802.
- [251] K. Kuhnke, R. Becker, K. Kern, *Surf. Sci.* 377–379 (1997) 1056.
- [252] K. Kuhnke, R. Becker, M. Eppe, K. Kern, *Phys. Rev. Lett.* 79 (1997) 3246.
- [253] F. Schreiber, M.C. Gerstenberg, B. Edinger, B. Toperverg, S.R. Forrest, G. Scoles, H. Dosch, *Physica B* 283 (2000) 75.
- [254] M.C. Gerstenberg, F. Schreiber, T.Y.B. Leung, G. Bracco, S.R. Forrest, G. Scoles, *Phys. Rev. B* 61 (2000) 7678.
- [255] R. Staub, M. Toerker, T. Fritz, T. Schmitz-Hübsch, F. Sellam, K. Leo, *Surf. Sci.* 445 (2000) 368.
- [256] V.K. Gupta, N.L. Abbott, *Science* 276 (1997) 1533.
- [257] A.L. Plant, *Langmuir* 9 (1993) 2764.
- [258] Z. Liu, C. Zhao, M. Tang, S. Cai, *J. Phys. Chem.* 100 (1996) 1733.
- [259] D.B. Wurm, S.T. Brittain, Y.-T. Kim, *Langmuir* 12 (1996) 3756.
- [260] G. Decher, J.D. Hong, *Ber. Bunsenges. Phys. Chem.* 95 (1991) 1430.
- [261] G. Decher, *Science* 277 (1997) 1232.
- [262] R. Maoz, S. Matlis, E. DiMasi, B.M. Ocko, J. Sagiv, *Nature* 384 (1996) 150.
- [263] R. Jordan, A. Ulman, *J. Am. Chem. Soc.* 120 (1998) 243.
- [264] I. Luzinov, D. Julthongpiput, A. Liebmann-Vinson, T. Cregger, M.D. Foster, V.V. Tsukurk, *Langmuir* 16 (2000) 504.
- [265] A.S. Eberhardt, T.Y.B. Leung, P. Fenter, F. Schreiber, P. Eisenberger, G. Scoles (unpublished).
- [266] A.S. Eberhardt, Ph.D. Thesis, Princeton University, Princeton, 1996.
- [267] M.R. Anderson, M.N. Evaniak, M. Zhang, *Langmuir* 12 (1996) 2327.
- [268] D.G. Castner, K. Hinds, D.W. Grainger, *Langmuir* 12 (1996) 5083.
- [269] W. Pan, C.J. Durning, N.J. Turro, *Langmuir* 12 (1996) 4469.
- [270] F. Bensebaa, R. Voicu, L. Huron, T.H. Ellis, E. Kruus, *Langmuir* 13 (1997) 5335.
- [271] D.S. Karpovich, G.J. Blanchard, *Langmuir* 10 (1994) 3315.
- [272] M. Buck, M. Grunze, F. Eisert, J. Fischer, F. Träger, *J. Vac. Sci. Technol. A* 10 (1992) 926.
- [273] R.F. DeBono, G.D. Loucks, D.D. Manna, U.J. Krull, *Can. J. Chem.* 74 (1996) 677.
- [274] S. Xu, S. Cruchon-Dupeyrat, J.C. Garno, G.-Y. Liu, G.K. Jennings, T.-H. Yong, P.E. Laibinis, *J. Chem. Phys.* 108 (1998) 5002.
- [275] R. Yamada, K. Uosaki, *Langmuir* 13 (1997) 5218.
- [276] R. Yamada, K. Uosaki, *Langmuir* 14 (1998) 855.
- [277] M. Himmelhaus, F. Eisert, M. Buck, M. Grunze, *J. Phys. Chem. B* 104 (2000) 576.

- [278] G. Hähner, Ch. Wöll, M. Buck, M. Grunze, *Langmuir* 9 (1993) 1955.
- [279] T. Ishida, S. Tsuneda, N.N.M. Hara, H. Sasabe, W. Knoll, *Langmuir* 13 (1997) 4638.
- [280] M. Kawasaki, T. Sato, T. Tanaka, K. Takao, *Langmuir* 16 (2000) 1719.
- [281] E. Barrena, C. Ocal, M. Salmeron, *J. Chem. Phys.* 111 (1999) 9797.
- [282] H.J. Kreuzer, *Surf. Sci. Lett.* 344 (1995) L1264.
- [283] S. Hong, J. Zhu, C.A. Mirkin, *Langmuir* 15 (1999) 7897.
- [284] H. Ron, H. Cohen, S. Matlis, M. Rappaport, I. Rubinstein, *J. Phys. Chem. B* 102 (1998) 9861.
- [285] Y. Barness, O. Gershevitz, M. Sekar, C.N. Sukenik, *Langmuir* 16 (2000) 247.
- [286] K. Bierbaum, M. Grunze, A.A. Baski, L.F. Chi, W. Schrepp, H. Fuchs, *Langmuir* 11 (1995) 2143.
- [287] R. Banga, J. Yarwood, A.M. Morgan, B. Evans, J. Kells, *Langmuir* 11 (1995) 4393.
- [288] A.G. Richter, M.K. Durbin, C.-J. Yu, P. Dutta, *Langmuir* 14 (1998) 5980.
- [289] A.G. Richter, C.-J. Yu, A. Datta, J. Kmetko, P. Dutta, *Phys. Rev. E* 61 (2000) 607.
- [290] J.B. Brzoska, N. Shahidzadeh, F. Rondelez, *Nature* 360 (1992) 719.
- [291] A.N. Parikh, D.L. Allara, I.B. Azouz, F. Rondelez, *J. Phys. Chem.* 98 (1994) 7577.
- [292] C. Carraro, O.W. Yauw, M.M. Sung, R. Maboudian, *J. Phys. Chem. B* 102 (1998) 4441.
- [293] T. Vallant, J. Kattner, H. Brunner, U. Mayer, H. Hoffmann, *J. Phys. Chem.* 102 (1998) 7190.
- [294] R.R. Rye, G.C. Nelson, M.T. Dugger, *Langmuir* 13 (1997) 2965.
- [295] X. Zhao, R. Kopelman, *J. Phys. Chem.* 100 (1996) 11014.
- [296] H. Brunner, T. Vallant, U. Mayer, H. Hoffmann, B. Basnar, M. Vallant, G. Friedbacher, *Langmuir* 15 (1999) 1899.
- [297] P. Silberzan, L. Léger, D. Ausserré, J.J. Benattar, *Langmuir* 7 (1991) 1647.
- [298] C.P. Tripp, M.L. Hair, *Langmuir* 8 (1992) 1120.
- [299] D.K. Schwartz, S. Steinberg, J. Israelachvili, J.A.N. Zasadzinski, *Phys. Rev. Lett.* 69 (1992) 3354.
- [300] J.T. Woodward, A. Ulman, D.K. Schwartz, *Langmuir* 12 (1996) 3626.
- [301] R. Resch, M. Grasserbauer, G. Friedbacher, T. Vallant, H. Brunner, U. Mayer, H. Hoffmann, *Appl. Surf. Sci.* 140 (1999) 168.
- [302] J.T. Woodward, D.K. Schwartz, *J. Phys. Chem.* 118 (1996) 7861.
- [303] I. Doudevski, W.A. Hayes, D.K. Schwartz, *Phys. Rev. Lett.* 81 (1998) 4927.
- [304] I. Doudevski, D.K. Schwartz, *Phys. Rev. B* 60 (1999) 14.
- [305] M. Toerker, R. Staub, T. Fritz, T. Schmitz-Hübsch, F. Sellam, K. Leo, *Surf. Sci.* 445 (2000) 100.
- [306] R. Gerlach, G. Polanski, H.-G. Rubahn, *Thin Solid Films* 318 (1998) 270.
- [307] R. Summers, NASA Technical Note TN D-5285, 1969.
- [308] W.H. Weinberg, in: M. Grunze, H.J. Kreuzer (Eds.), *Kinetics of Interface Reactions*, Springer, Berlin, 1987.
- [309] F. Schreiber, A. Levi (unpublished).
- [310] M.W.J. Beulen, B.-H. Huisman, P.A. van der Heijden, F.C.J.M. van Veggel, M.G. Simons, E.M.E.F. Biemond, P.J. de Lange, D.N. Reinhoudt, *Langmuir* 12 (1996) 6170.
- [311] H. Takiguchi, K. Sato, T. Ishida, K. Abe, K. Yase, K. Tamada, *Langmuir* 16 (2000) 1703.
- [312] G. Witte, C. Wöll, private communication.
- [313] J.F. Nagle, H.L. Scott, *Physics Today* 31 (1978) 38.
- [314] D.A. King, *Surf. Sci.* 47 (1975) 384.
- [315] P.A. Redhead, *Vacuum* 12 (1962) 203.
- [316] C.-J. Zhong, M.D. Porter, *J. Am. Chem. Soc.* 116 (1994) 11616.
- [317] B.A. Sexton, A.E. Hughes, *Surf. Sci.* 140 (1984) 227.
- [318] A.V. Teplyakov, A.B. Gurevich, M.X. Yang, B.E. Bent, J.G. Chen, *Surf. Sci.* 396 (1998) 340.
- [319] N. Karl, C. Günther, *Cryst. Res. Technol.* 34 (1999) 243.
- [320] A.C. Levi, *Surf. Sci.* 426 (1999) 308.
- [321] J. Libuda, G. Scoles, *J. Phys. Chem. B* 103 (1999) 9933.
- [322] S. Xu, P.E. Laibinis, G.-Y. Liu, *J. Am. Chem. Soc.* 120 (1998) 9356.
- [323] M. Copel, M.C. Reuter, E. Kaxiras, R.M. Tromp, *Phys. Rev. Lett.* 63 (1989) 632.
- [324] H.A. van der Vegt, H.M. van Pinxteren, M. Lohmeier, E. Vlieg, J.M.C. Thornton, *Phys. Rev. Lett.* 68 (1992) 3335.
- [325] F. Schreiber, T.Y.B. Leung, P. Fenter, G. Scoles (unpublished).

- [326] J. Hautman, M.L. Klein, *J. Chem. Phys.* 91 (1989) 4994.
- [327] W. Mar, M.L. Klein, *Langmuir* 10 (1994) 188.
- [328] R. Bhatia, B.J. Garrison, *Langmuir* 13 (1997) 765.
- [329] A.J. Pertsin, M. Grunze, *J. Chem. Phys.* 106 (1997) 7343.
- [330] R. Bhatia, B.J. Garrison, *Langmuir* 13 (1997) 4038.
- [331] H. Sellers, A. Ulman, Y. Shnidman, J.E. Eilers, *J. Am. Chem. Soc.* 115 (1993) 9389.
- [332] K.M. Beardmore, J.D. Kress, N. Grønbench-Jensen, A.R. Bishop, *Chem. Phys. Lett.* 286 (1998) 40.
- [333] H. Häkkinen, R.N. Barnett, U. Landman, *Phys. Rev. Lett.* 82 (1999) 3264.
- [334] H. Grönbeck, A. Curioni, W. Andreoni, *J. Am. Chem. Soc.* 122 (2000) 3839–3842.
- [335] H. Morgner, *Langmuir* 13 (1997) 3990.
- [336] G.K. Jennings, P.E. Laibinis, *Colloids Surf. A* 116 (1996) 105.
- [337] M. Ishibashia, M. Itoh, H. Nishihara, K. Aramaki, *Electrochim. Acta* 41 (1996) 241.
- [338] F.P. Zamborini, R.M. Crookes, *Langmuir* 14 (1998) 3279.
- [339] Y. Feng, W.-K. Teo, K.-S. Siow, Z. Gso, K.-L. Tan, A.-K. Hsieh, *J. Electrochem. Soc.* 144 (1997) 55.
- [340] X. Xiao, J. Hu, D.H. Charych, M. Salmeron, *Langmuir* 12 (1996) 235.
- [341] H.I. Kim, M. Graupe, O. Oloba, T. Koini, S. Imaduddin, T.R. Lee, S.S. Perry, *Langmuir* 15 (1999) 3179.
- [342] R.W. Carpick, M. Salmeron, *Chem. Rev.* 97 (1997) 1163.
- [343] E. Barrera, S. Kopta, D.F. Ogletree, D.H. Charych, M. Salmeron, *Phys. Rev. Lett.* 82 (1999) 2880.
- [344] S. Kim, G.Y. Choi, A. Ulman, C. Fleischer, *Langmuir* 13 (1997) 6850.
- [345] S. Kidoaki, T. Matsuda, *Langmuir* 15 (1999) 7639.
- [346] H.O. Finklea, in: A.J. Bard, I. Rubinstein (Eds.), *Electroanalytical Chemistry*, Marcel Dekker, New York, 1996.
- [347] G.B. Sigal, C. Bamdad, A. Barberis, J. Strominger, G.M. Whitesides, *Anal. Chem.* 68 (1996) 490.
- [348] C.E.D. Chidsey, *Science* 251 (1991) 919.
- [349] S.B. Sachs, S.P. Dudek, R.S. Hsung, L.R. Sita, J.F. Smalley, M.D. Newton, S.W. Feldberg, C.E.D. Chidsey, *J. Am. Chem. Soc.* 119 (1997) 10563.
- [350] L.A. Bumm, J.J. Arnold, T.D. Dunbar, D.L. Allara, P.S. Weiss, *J. Phys. Chem.* 103 (1999) 8122.
- [351] D. Vuillaume, C. Boulas, J. Collet, G. Allan, C. Delerue, *Phys. Rev. B* 58 (1998) 16491.
- [352] I.H. Campbell, J.D. Kress, R.L. Martin, D.L. Smith, N.N. Barashkov, J.P. Ferraris, *Appl. Phys. Lett.* 71 (1997) 3528.
- [353] C.A. Mirkin, M.A. Ratner, *Ann. Rev. Phys. Chem.* 43 (1992) 719.
- [354] A. Kahn, *Prog. Surf. Sci.* (to appear).
- [355] F. Schreiber, P. Fenter (unpublished).
- [356] M.C. Vargas, P. Gionozzi, A. Sellonir, G. Scoles, *J. Am. Chem. Soc.* (submitted).
- [357] S.M. Driver, D.P. Woodruff, *Langmuir*. 16 (2000) 6693–6700.